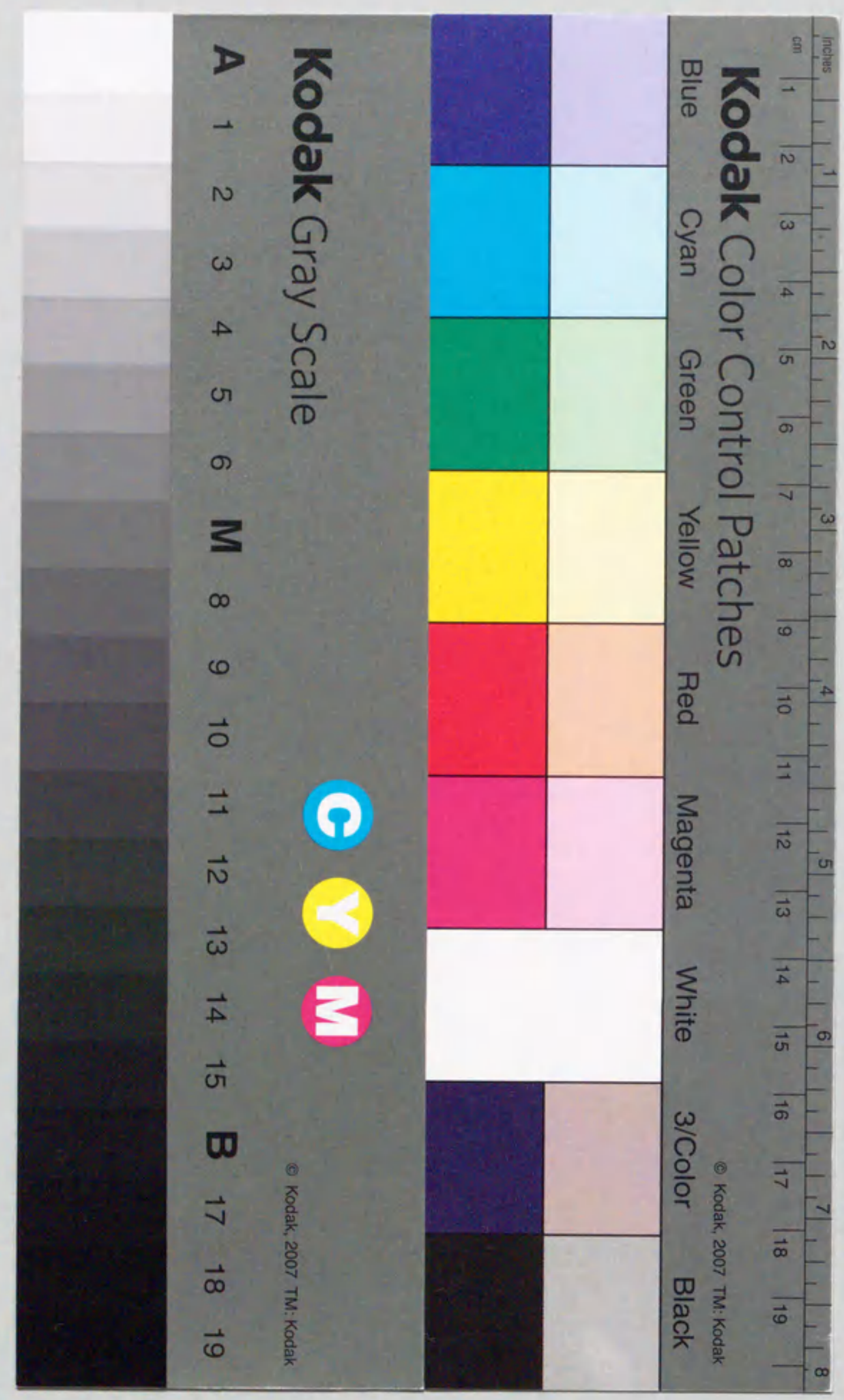


報告番号 甲第 4056 号

*Studies on the Development and Application of  
Permanent Magnet Electron Cyclotron  
Resonance Plasma Sources*

Shoji Den



①

***Studies on the Development and Application of  
Permanent Magnet Electron Cyclotron Resonance  
Plasma Sources***

(永久磁石を用いた電子サイクロトロン共鳴プラズマ源  
の開発と応用に関する研究)

**Shoji Den**

**1998**

**Nagoya University**

## TABLE OF CONTENTS

<b>Chapter 1. Introduction</b>	<b>1</b>
1.1 Low-pressure High-density Plasma Processing	1
1.2 Problems in Previous Studies on ECR Plasma Processing	8
1.2.1 Problems Associated with Present ECR Plasma Sources	8
1.2.2 Problems Associated with the Measurement of Radical Densities	11
1.2.3 Problems Associated with Selective SiO <sub>2</sub> /Si Etching	14
1.3 Purpose and Composition of This Work	15
References	18
<b>Chapter 2. Development of Plasma Source Technology for 8-inch Wafer Processing</b>	<b>20</b>
2.1 Introduction	20
2.2 Design of a High Density and Uniform ECR Plasma with Permanent Magnet	21
2.2.1 Configuration	21
2.2.2 Characteristics	24
2.3 Summary	31
References	33
<b>Chapter 3. Comparison of Fluorocarbon Radical Kinetics in Large-area Permanent Magnet and Electromagnet Electron Cyclotron Resonance Plasma Sources</b>	<b>34</b>
3.1 Introduction	34
3.2 Experimental	35
3.2.1 Experimental Set-up	35
3.2.2 Infrared Diode Laser Absorption Spectroscopy for Measurement of CF <sub>x</sub> Radical Densities	35
3.2.3 Actinometry for Measurement of F Atom Density	37
3.3 Results	39
3.3.1 CF <sub>x</sub> Radical and F Atom Densities in CF <sub>4</sub> Plasma	39
3.3.2 CF <sub>x</sub> Radical and F Atom Densities in C <sub>4</sub> F <sub>8</sub> Plasma	43
3.3.3 Life Time of CF and CF <sub>2</sub> Radicals	47
3.4 Discussions	49
3.4.1 Dissociation Kinetics in Low-temperature High-density ECR Plasma	49
3.4.2 Control of CF <sub>x</sub> /F Density Ratios	53
3.5 Summary	55
References	57

<b>Chapter 4. Improvement of the Large-area Permanent Magnet Electron Cyclotron Resonance Plasma Source and Scale-up for 12-inch Wafer Processing</b>	<b>58</b>
4.1 Introduction	58
4.2 Development of an Advanced Permanent Magnet Electron Cyclotron Resonance Plasma Source for 12-inch Wafer Processing	59
4.2.1 Configuration	59
4.2.2 Characteristics	62
4.3 Summary	67
References	68

<b>Chapter 5. Effect of Carbon Atoms on Selective SiO<sub>2</sub>/Si Etching with a Large-area Permanent Magnet Electron Cyclotron Resonance Plasma Source</b>	<b>69</b>
5.1 Introduction	69
5.2 Experimental	70
5.2.1 Experimental Set-up	70
5.2.2 Hollow Cathode Lamp Absorption Spectroscopy for Measurement of C Atom Density	72
5.3 Diagnostics of CF <sub>x</sub> Radicals and Fluorine Atom Density in C <sub>4</sub> F <sub>8</sub> Plasma	72
5.4 Measurement of Carbon Atom Density in a C <sub>4</sub> F <sub>8</sub> ECR Etching Plasma.	75
5.5 Etch Rate and Selectivity of SiO <sub>2</sub> and Si in C <sub>4</sub> F <sub>8</sub> /CH <sub>4</sub> ECR Plasma.	78
5.6 Summary	81
References	83

<b>Chapter 6. Development and Characterization of a Compact Microwave Plasma Radical Source</b>	<b>84</b>
6.1 Introduction	84
6.2 Configuration	85
6.3 Characterization	87
6.4 Summary	96
References	98

<b>Chapter 7. Conclusions</b>	<b>100</b>
7.1 Overall Summary	100
7.2 Future Prospects	103
References	109

<b>Acknowledgments</b>	<b>109</b>
------------------------	------------

<b>List of Papers</b>	<b>111</b>
1. Original Papers	111
2. International Conferences	112
Other Related Publications	113

## Chapter 1. Introduction

### 1.1 Low-pressure High-density Plasma Processing

By the year 2000, the world electronics market is projected to reach 120 trillion yen.[1] To meet this demand, technological breakthroughs are indispensable in ultra large scale integrated(ULSI) circuits. The semiconductor industry is expected to have an annual growth rate of 13% over the next five years. By the year 2000, metal-oxide-semiconductor(MOS) devices will make up 88% of all devices sold. Figure 1.1 shows the growth in the number of components per MOSFET dynamic random access memory (DRAM) and bipolar transistor. The figures for bipolar, MESFET and MODFET chips are also shown. The number of components has almost doubled every year since 1975. We are fast approaching 100 million components per chip. Over the last 20 years, the microelectronics industry, in particular, the fabrication of integrated circuits has been driving the development of processing techniques and equipment. As seen in Fig. 1.1, the number of transistors contained in DRAM chips has been increasing twofold every year. Present DRAM chips contain 16 million transistors, pilot production of 64 Megabit DRAMs is underway and plans for 256 Megabit and 1 Gigabit DRAMs are under consideration. This trend is driven by the need for increased functionality at lower costs.

These advances in the chip production have been achieved mainly by the ability to produce transistors of smaller dimensions. The continued reduction of the device-feature length (a) is shown in Figure 1.2 along with (b) junction depth, and (c) gate oxide thickness of MOSFET devices. Over the last 40 years, the feature size has been reduced by a factor of two almost every six years. The minimum feature size (design rule) in 1960 was around 50  $\mu\text{m}$ , in the 1990's it is 0.35  $\mu\text{m}$  and is expected to be around 0.2  $\mu\text{m}$  at the beginning of the next millennium. The first problem for both the chip and equipment makers is to develop new tools which can provide the control necessary to achieve these feature sizes with the highest possible yield.

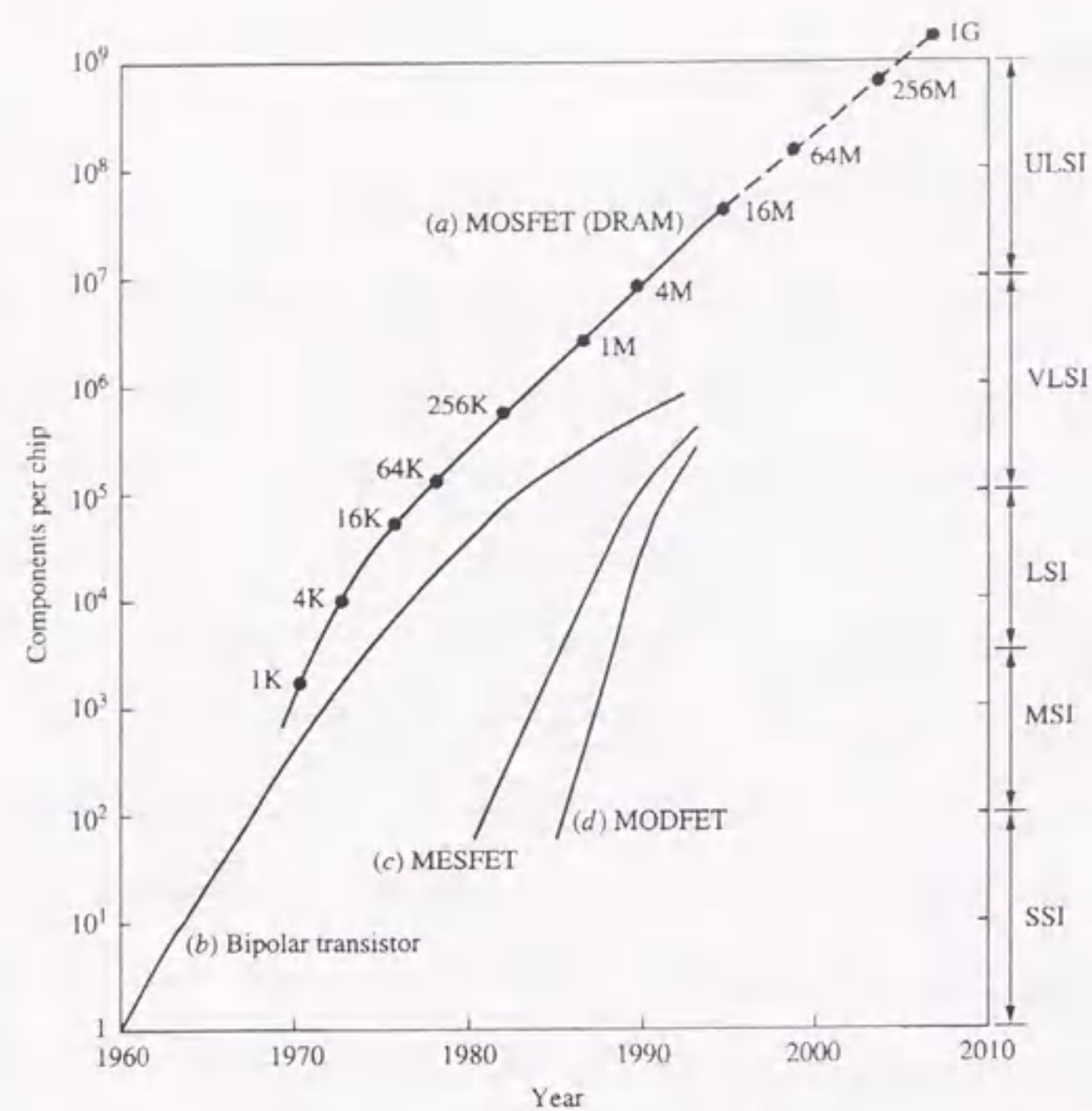


Fig. 1.1 (a) Exponential growth of the number of components per MOS IC chip. (b), (c) and (d) Components per chip versus year for bipolar, MESFET, and MODFET ICs, respectively. [Ref. 1]

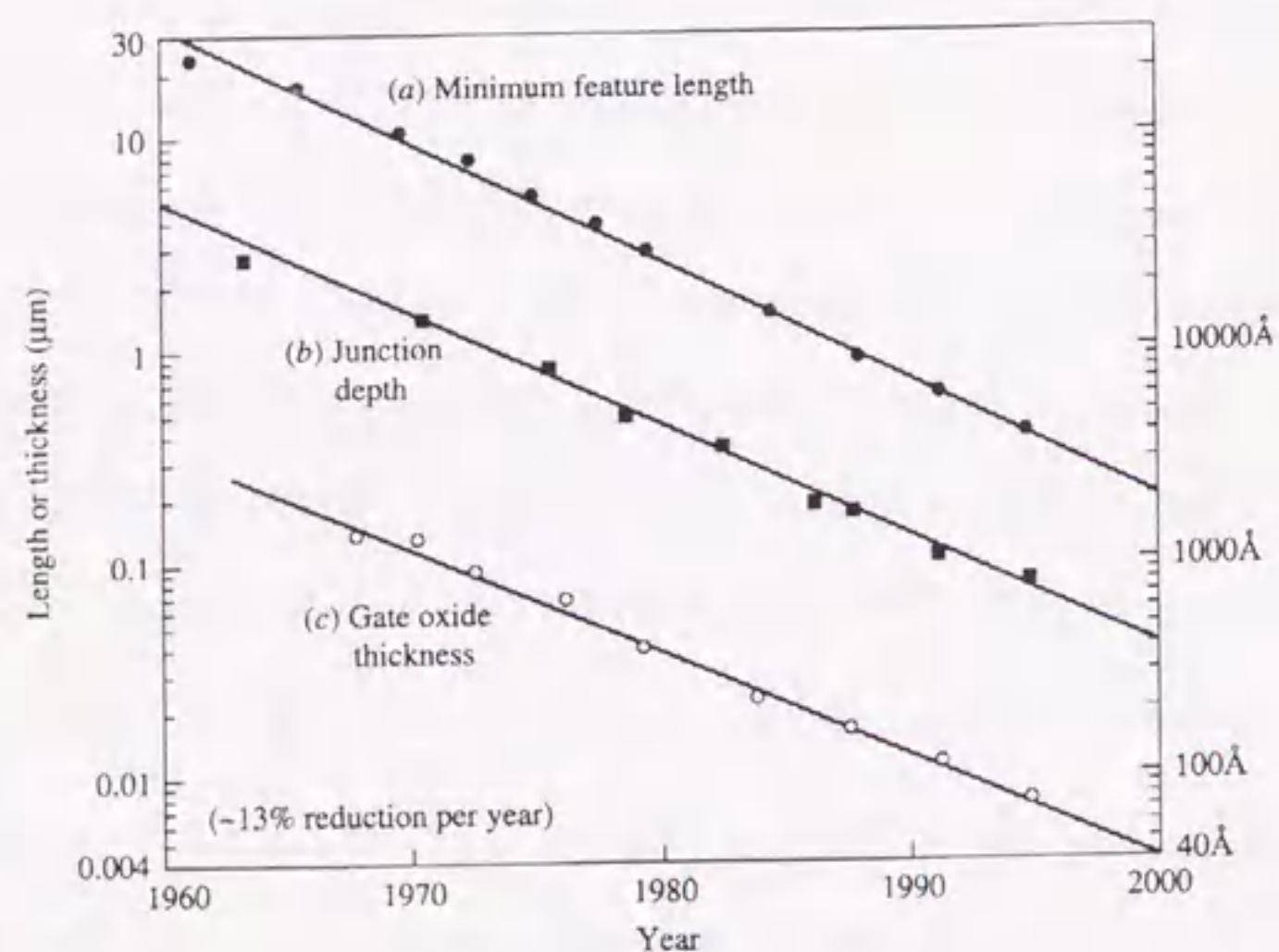


Fig. 1.2 Exponential decrease of (a) minimum feature size, (b) junction depth, and (c) gate oxide thickness of MOSFET. [Ref. 1]

Increased functionality at lower costs is also being achieved, through the use of larger Si wafers. The wafer size used in production today is 8-inches in diameter and 12-inch pilot lines are in operation. As the wafer size increases, so does the cost of the wafer and after processing the value of the wafer will increase 50-fold. Therefore, the second problem which exists for equipment manufacturers is how to scale-up the equipment and provide the same process yield.

In the fabrication of ULSI MOS circuits, the use of plasma has demonstrated many advantages over conventional wet chemical processing. Plasma material processing is now an integral part in integrated circuit manufacturing. Processing of semiconductor devices consist mainly of three types of processing steps:

1. Deposition, where dielectric layers for insulation, passivation and protection or metal layers for contacts are deposited by plasma assisted processing.
2. Lithography, which patterns a mask to define the specific features and sizes of the circuit elements on the substrates.
3. Etching, in which a plasma process etches the unmasked area of the semiconductor or the dielectric or metal layer.

Over thirty percent of all ULSI processing steps are now plasma-driven with some of these steps being possible only through the use of plasma. Sub-0.25μm feature size technology has been achieved in part due to the continued development and improved characterization of advanced plasma systems. The design rules used for sub 0.25 μm fabrication of ULSI circuits are placing an ever increasing need to understand the mechanisms involved in plasma etch processing.

To date, parallel plate capacitively driven radio frequency (rf) discharges have been commonly used for plasma etch processing (see Fig. 1.3). However, such rf sources are limited by the fact that the ion flux bombarding the driven electrode and the ion energy cannot be controlled independently. For a wafer placed on the driven electrode, this can result in damage or loss of feature size control. Moreover, the lack of controllability means that there is only a very small process window available for most applications.

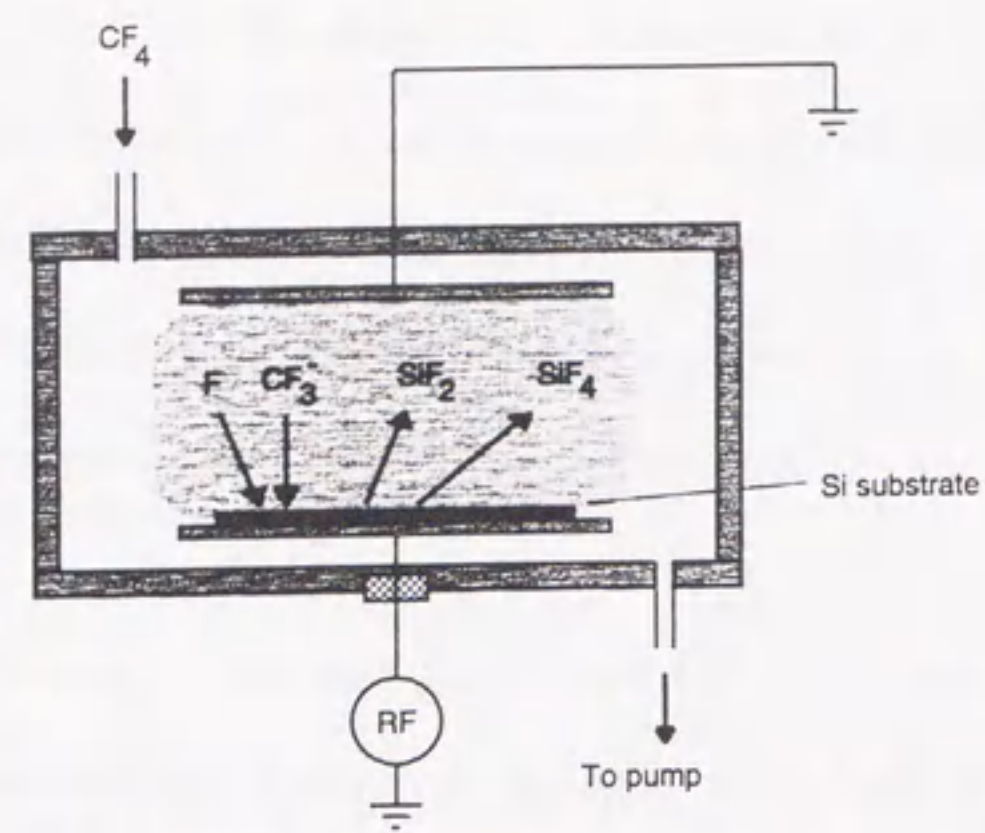


Fig.1.3 Schematic of a reactive ion etching system

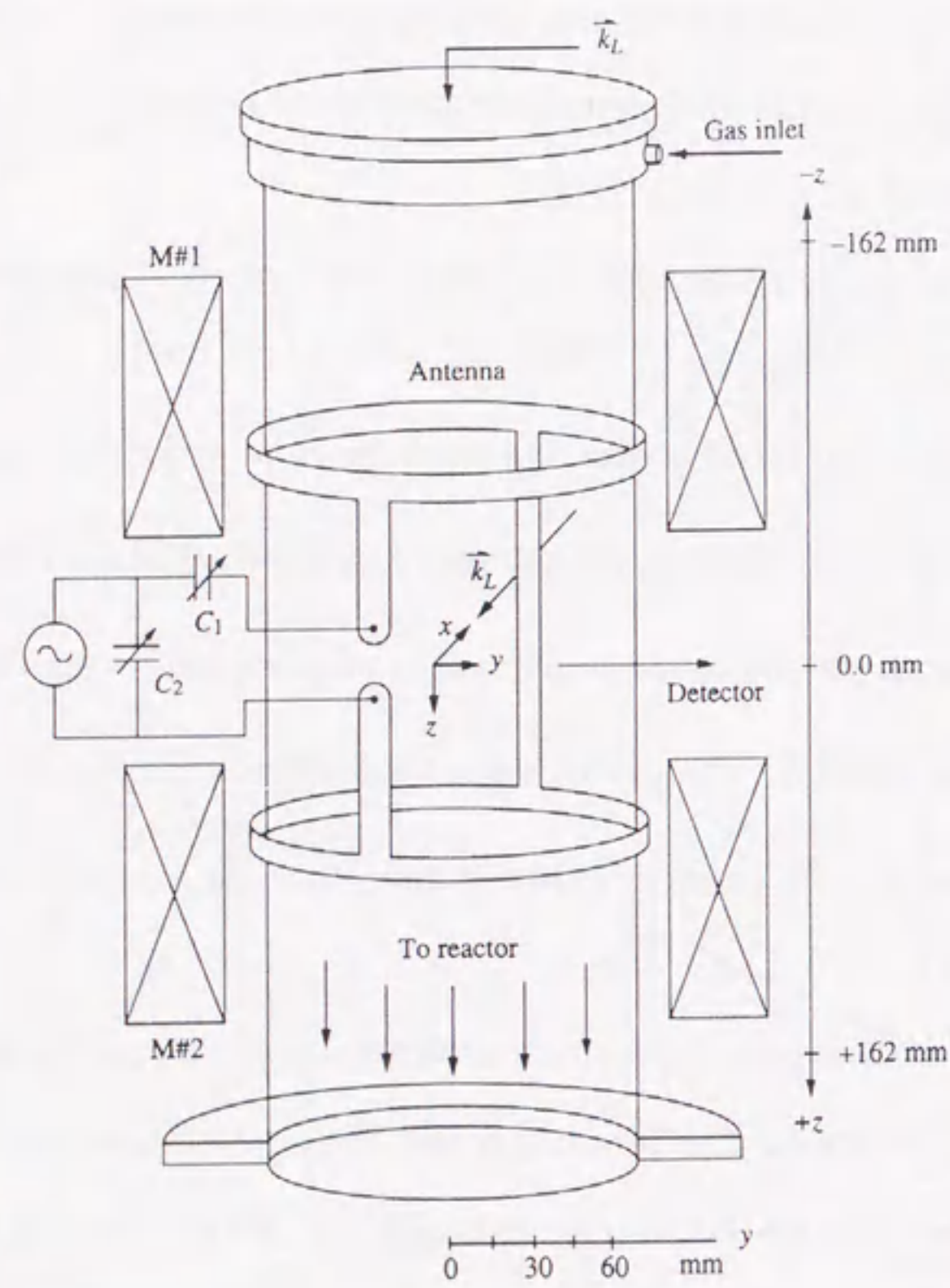
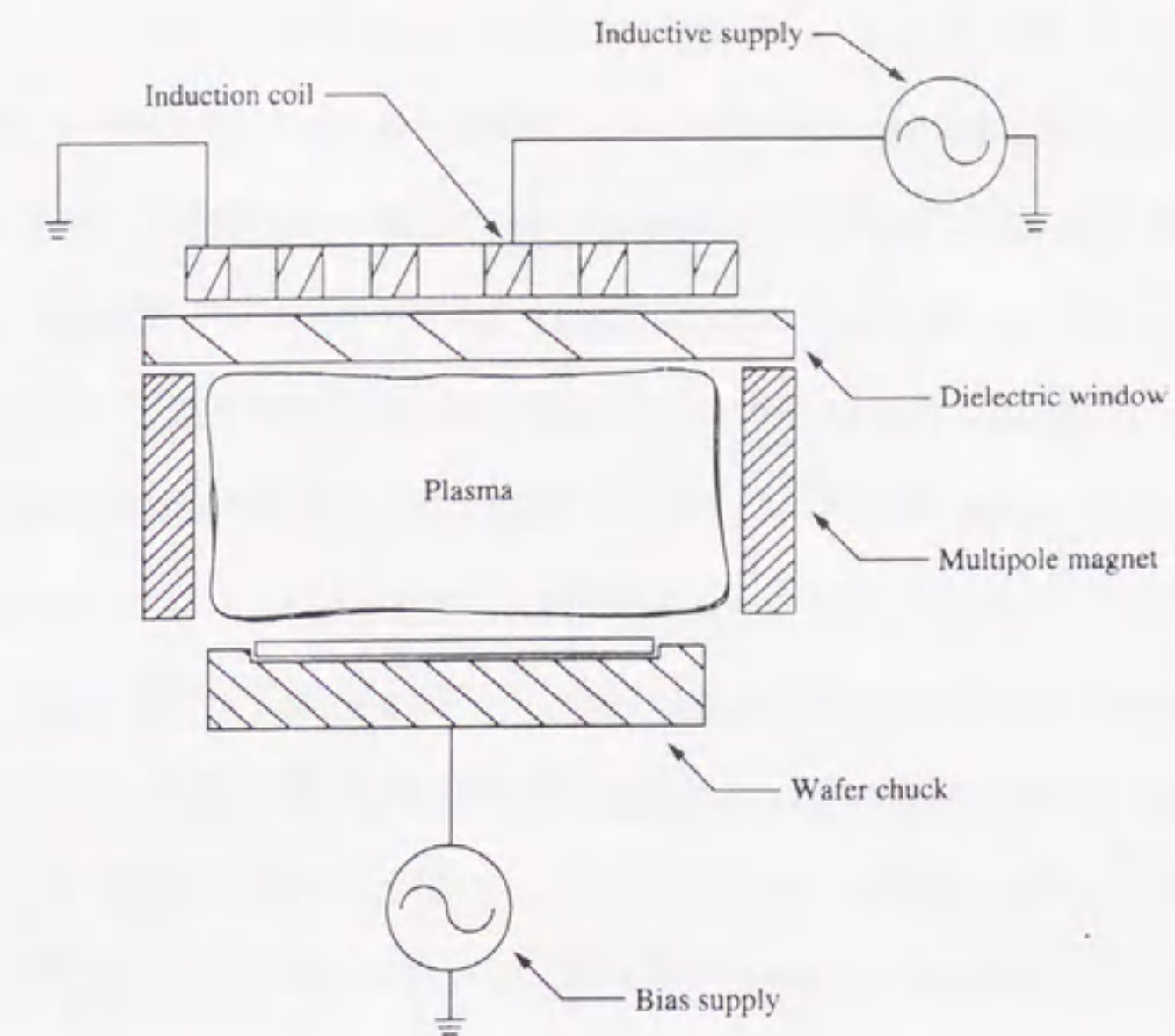
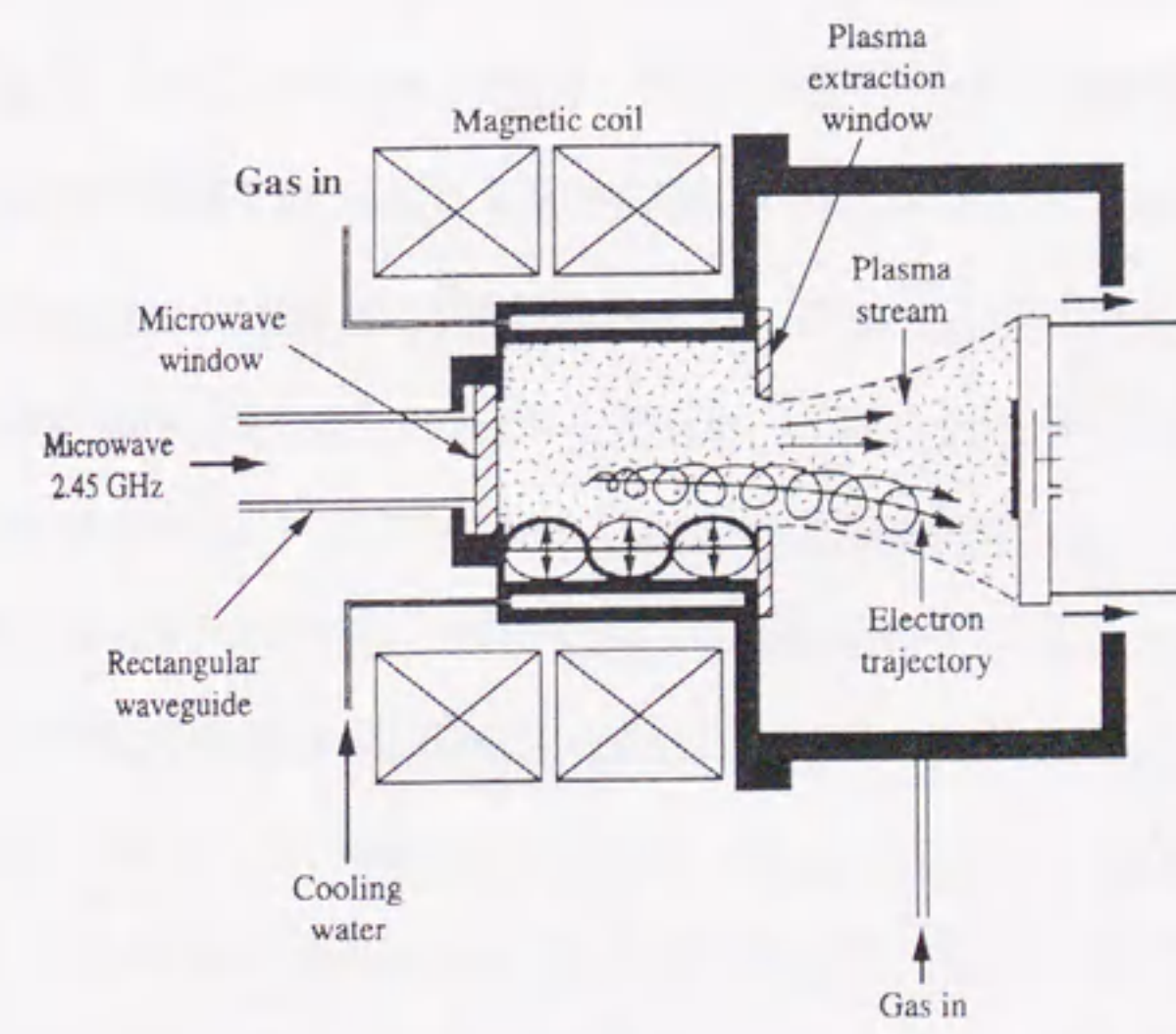


Fig.1.4 (a)



(b)



(c)

Fig. 1.4 (a) Schematic of a helicon reactor with a double loop antenna, (b) an inductively coupled plasma reactor and (c) an ECR etch reactor with mirror magnetic field around the wafer.

The low ion flux in these sources has also meant that batch processing was necessary to maintain throughput. Batch processing however, produces poor wafer-to-wafer reproducibility. Higher ion and neutral fluxes are required for single wafer processing. Magnetically enhanced rf sources have also been developed to try and improve performance, but comparatively poor uniformity limits their applicability to next-generation device fabrication.

To meet the feature size, selectivity and damage control for next-generation fabrication, the mean ion energy and the ion energy distribution should be controllable independently of the ion and neutral fluxes. Future manufacturing of the metal-oxide-semiconductor field-effect-transistors (MOSFET) which is the basic component of DRAMs, is based on the ability to realize high selectivity anisotropic etching of finer contact holes in large diameter Si wafers. As the diameter of Si wafer increases, it is necessary to increase the density of the plasma in order to maintain a high etch rate. High etch rates will subsequently increase the productivity of the ULSI devices, hence plasma sources which can provide etch rates of up to  $1\mu\text{m}/\text{min}$  need to be developed. Anisotropic etching is attributed to the normal incidence of ions bombarding the surface after acceleration through the sheath. Ions in a low pressure plasma impinge on the surface at normal incidence without collisions. Therefore, low-pressure plasma etching is a promising technique to perform anisotropic etching. Low pressure operation is one means of ensuring a highly anisotropic etch, but a lower plasma operational pressure is associated with higher electron temperatures ( $T_e$ ). Therefore, it causes a different plasma chemistry compared to that at higher pressures. In achieving such a low pressure etch process, a wide variety of high density plasma sources are being employed.[2-5]

Figure 1.4 shows a schematic diagram of the different configurations used in the industry today. Figure 1.4(a) shows a helicon plasma source which can be used to generate high-density plasma.[2] A transverse electromagnetic radio-frequency (rf) wave of 13.56 MHz excited by a single or double loop antenna located outside the a quartz cavity, is coupled with a steady longitudinal magnetic field ( $\sim 100\text{G}$ ). Propagation of a helicon wave

depends on the magnitude of the magnetic field and the dimensions of the cavity. If the wavelength of the wave is the same as the antenna length then coupling will be resonant. Plasma diffuses into the process chamber to the wafer which is independently biased with a second rf generator.

The plasma in an inductively coupled discharge is created by applying rf power to a nonresonant inductive coil as shown in Fig. 1.4(b).[3] The wafer is located several skin-depths away from the coil, so as not to be affected by the electromagnetic field generated by the coil. The plasma density is high ( $\sim 10^{12}\text{cm}^{-3}$ ) since the plasma is generated at only a few mean free paths away from the wafer. High etch rates can therefore be achieved. Plasma confinement is provided by multipole magnets and the wafer is also independently biased with a second rf generator.

In ECR plasma[4-6], the microwave is coupled to the electron cyclotron frequency in a static magnetic field and efficiently transfers the energy to electrons, which ionize gas molecules. Resonance of electrons occurs when the electron cyclotron frequency is equal to the excitation frequency of 2.45GHz. This occurs for a magnetic field surface of 0.0875T within the discharge. Electrons are accelerated in this volume to produce a high degree of ionization which can be controlled by varying discharge parameters such as input microwave power, discharge pressure and flow rates. A typical microwave ECR plasma system is shown in the schematic diagram of Fig.1.4(c). Microwaves propagating in a rectangular waveguide are converted to a circular mode and launched to the discharge area via a dielectric window. The discharge area is usually circular with gas inlet ports and dielectric lined walls. A magnetic field for resonance is provided by either electromagnets or permanent magnets. The induced magnetic field also plays the role to confine the plasma within the discharge area and to guide charged particles into the downstream region. Although simple in construction, the performance of ECR plasma sources is judged by how effectively the plasma parameters, in particular the ion energy distribution, can be controlled. Magnetic field effects are therefore, one of the main concerns in developing ECR plasma sources. Some of the main advantages of ECR plasma are as follows;



1. Very high ionization efficiency resulting in a high density plasma
2. A dynamic operating pressure range
3. Low intrinsic ion energy that can be easily controlled
4. Suitable for use with reactive gases

Another feature of high density ECR plasma sources is that the power is coupled to the plasma by noncapacitive methods, through the dielectric window. This noncapacitive coupling of the power produces low sheath voltages with subsequent low ion energies ( $< 30\text{eV}$ ). For an overall review of this area of plasma production the reader is referred to excellent reviews by Asmussen,[7] Margot *et. al.*,[8] and more recently Lieberman *et. al.*,[9] The high density and relatively low energy charged particles associated with ECR plasma are presently being used in various areas of today's device processing. Such areas include reactive-ion-beam etching[10-14] which uses reactive gases such as chlorine in damage-and contamination-free etching, substrate surface cleaning[15-19] in which hydrogen plasma is used for substrate cleaning prior to growth processes such as plasma-enhanced chemical beam epitaxy (PECBE), and thin film deposition.[20-25] However, despite the advantages of ECR sources and wide range of applications in which they are used, conventional ECR sources do have problems.

## 1.2 Problems in Previous Studies on ECR Plasma Processing

### 1.2.1 Problems Associated with Present ECR Plasma Sources

Various present ECR system configurations are shown in Fig. 1.5.[9] A high aspect ratio system with the source plasma far from the wafer and with microwave injection along magnetic field is shown in Fig. 1.5(a). Expansion of the plasma from the resonance zone to the wafer reduces the ion flux and increases the ion impact energy at the wafer. A low aspect ratio system where only a single high-field coil magnet is used and where the resonance zone may be only 10~20 cm from the wafer is shown in Fig. 1.5(b). Uniformity is controlled at least in part by shaping the axial magnetic field. As shown in Fig. 1.5(c), uniformity can be improved and density is increased by adding multipole permanent magnets around the

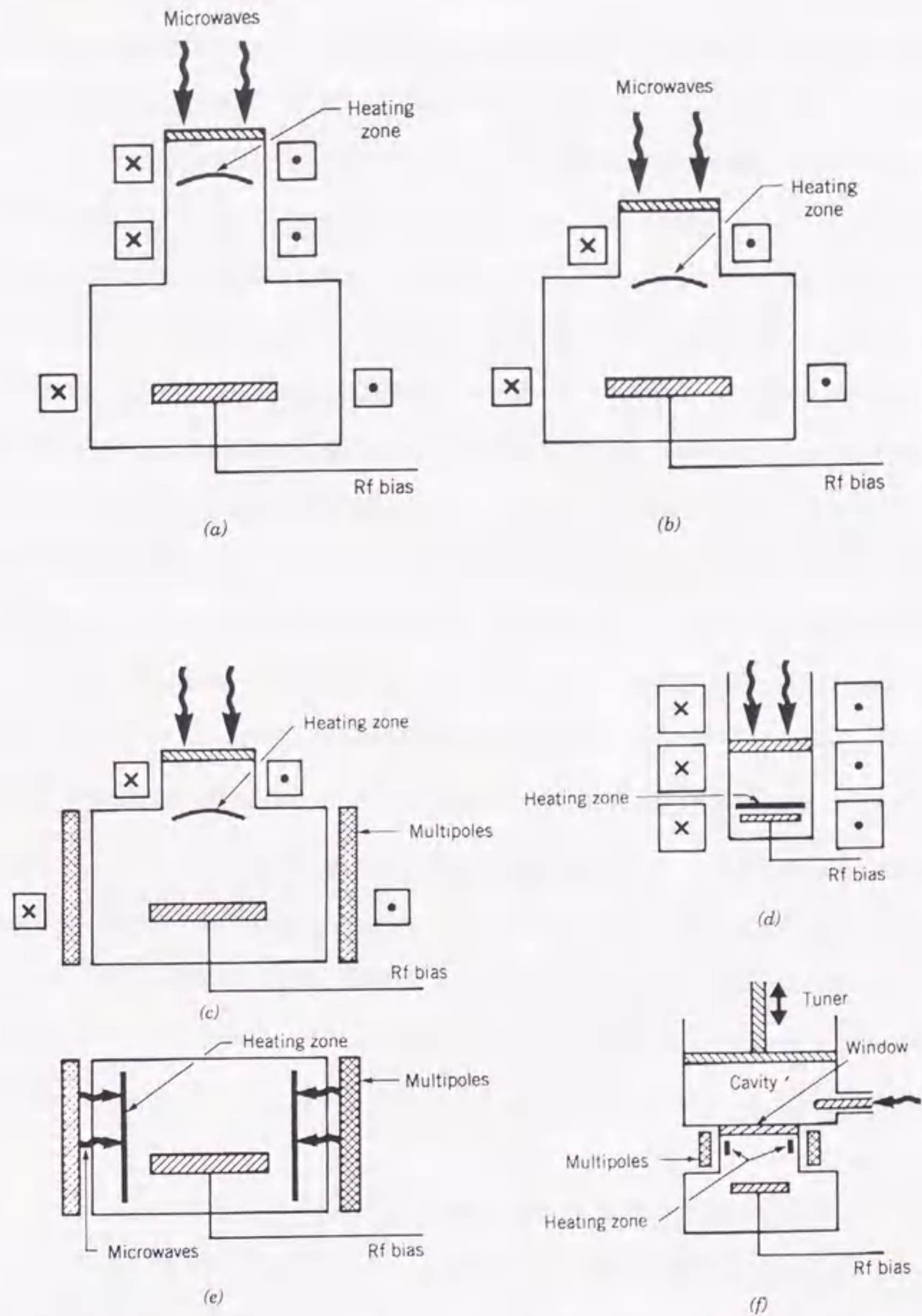


Fig. 1.5 Common ECR configurations: (a) high aspect ratio; (b) low aspect ratio; (c) low aspect ratio with multipoles; (d) close-coupled; (e) distributed (DECR); (f) microwave cavity excited. (From "Design of High-Density Sources for Materials Processing" from the work "Physics of Thin Films," Vol.18, by Academic Press, Inc., Publisher in Press)

circumference of the process chamber, but this system becomes complex. Another approach to achieving adequate uniformity and density is to combine the source and process chambers that is to place the resonance zone close to the wafer which is leading to a low aspect ratio *close-coupled* configuration as shown in Fig. 1.5(d). In this system, it is difficult to scale-up because the electromagnetic coil around the circumference of the process chamber becomes large and heavy. In the multipole distributed ECR system shown in Fig. 1.5(e), microwave power is injected perpendicular to the strong multipole magnetic field produced by permanent magnets. As four or more microwave applicators are arranged the circumference of the process chamber to achieve adequate uniformity, this system is complex in the structure of microwave introduction. A microwave cavity excited system is shown in Fig. 1.5(f). The coaxial feed is tuned using a sliding short on the top and a stub tuner from the side in the system. The linear resonance zones are generated by a set of 8~12 strong permanent magnets arranged around the circumference of the source chamber as shown. In this system, uniformity depends on the standing mode of microwave.

The fact that ECR plasma can be produced at low pressures region (0.01-1 Pa) with high plasma density ( $>10^{10} \text{ cm}^{-3}$ ) suggests that etching with ECR plasma is one of the more promising technologies for etching the next generation of ULSI circuits. However, producing high density plasma at low pressures in conventional ECR plasma sources is limited by the phenomenon of cutoff. If one sends a microwave beam with a given frequency  $\omega$  through a plasma, the wavelength  $2\pi/k$  in the plasma will take on the value given by

$$\omega^2 = \omega_p^2 + c^2 k^2 \quad (1.1)$$

This is the dispersion relation for an electromagnetic wave propagating in a plasma for the simple case where no magnetic field is present. As the plasma density increases, then  $\omega_p^2$  will increase,  $k^2$  will decrease and hence the wavelength becomes longer and longer. Finally a density is reached where  $k^2$  is zero and eqn. 1.1 cannot be satisfied for any real value of  $k$  and the wave will not propagate. The density at which this occurs is known as the cutoff density. To overcome this limitation, magnetic field effects are used. Launching of the microwave perpendicular to a magnetic field gives rise to a condition of resonance of the

microwave frequency and the plasma electron frequency. Under such conditions preferential absorption of the microwave power occurs and plasma densities in excess of the cutoff density can be realized.

Another challenge facing ECR plasma sources is one of basic equipment design. The main factors governing the acceptance of plasma processing equipment in the industry today are that the equipment should be,

1. Reliable in producing the same etch characteristics on each wafer,
2. Free of contaminants and damage,
3. A low cost of ownership,
4. Easy to operate and maintain.

With these criteria in mind, we have designed permanent magnet ECR plasma sources from which the conventional electromagnetic coil is moved away; this provides us with a tool which is cost effective, easy to operate and can provide superior etch processing. The criteria which need to be met for future device etch processes are

1. High selectivity,
2. Good anisotropy,
3. High etch rates,
4. Good feature uniformity across the wafer,
5. Reduced bulk and surface damage.

### 1.2.2 Problems Associated with the Measurement of Radical Densities

In the design and development of production worthy plasma etching equipment, it is essential that the plasma is characterized. Plasma sources have been evaluated by many techniques. For example, there are the very basic measurements of plasma parameters such as the electron density ( $n_e$ ), the electron temperature ( $T_e$ ) and plasma potential ( $V_p$ ) to the performance characteristics such as stability, purity and lifetime. Another and very important type of characterization is process performance, i.e., how well does the plasma source perform the designated etching. Although there are many diagnostics available for

characterization, it is difficult to obtain reliable and accurate results due complicated systems in etch plasma, that uses complex gases, sometimes a mixture of gases. Furthermore, the state of the reactor walls are continuously changing as the deposition and etch processes progress.

Fluorocarbon gas plasmas are generally employed in the selective etching of silicon dioxide over silicon or silicon nitride [26-27]. It is well known that the selective etching is performed in competition with fluorocarbon polymer deposition on the surface. Furthermore, the fluorocarbon radicals are considered to affect etch properties such as selectivity, etch rate, pattern profile and microscopic uniformity. It can be seen therefore, that characterization of these species in the plasma is very important to develop production worthy plasma etch equipment. Fluorocarbon radicals such as  $Cf_x(x=1-3)$  in the plasma have been measured by various techniques in many plasma sources using various kinds of feed gases. For example, optical emission spectroscopy (OES) has been used for long time in the qualitative diagnostic of plasma physics and chemistry. CF and  $CF_2$  radicals have been measured by using actinometric techniques[28,29] and laser induced fluorescence (LIF) [30-32]. The former enables us to measure the relative densities of some fluorocarbon radicals. However, it is difficult to calculate absolute densities using this technique because of the lack of suitable actinometers and the complex excitation processes which frequently occur in the plasma. In the case of F atom density by using Argon gas as an actinometer, the absolute density can be calculated as described in Chapter 2. The latter is a highly sensitive technique that measures radicals which have emissive lines. The  $CF_3$  radical, however, is not measurable using this spectroscopic technique.

Infrared diode laser absorption spectroscopy (IRLAS) is a very powerful diagnostic technique for the non-intrusive in-situ measurement of radicals in plasma [27,33-36]. Recently, Maruyama et al. have succeeded in measuring the absolute density of the CF radical in the rf discharge plasma employing  $CHF_3$  by using IRLAS for the first time [34]. Furthermore, IRLAS enables us to measure the absolute densities of  $CF_3$  radicals [32,33]. Takahashi has also applied this technique to analyze the radicals in ECR plasma [37]. In order to develop an ECR plasma source that can meet the challenges of high precision

etching, it is necessary to measure the  $CF_x(x=1-3)$  radicals in the plasma and to clarify the gas phase kinetics of these radicals. Fluorocarbon radicals properties are dependent on factors such as the composition of gases, gas pressure, discharge power and equipment design. It is, therefore, necessary to understand these properties and the effects on the etch process, and also control the  $CF_x(x=1-3)$  radical densities in order to make most use of the important precursors in the high selective etching.

By using appearance mass spectroscopy (AMS),  $CF_x(x=1-3)$  have been measured in the capacitively and inductively coupled plasmas employing  $CF_4$  by Hikosaka et al.. However, there is the possibility that the sampling orifice of appearance mass device disturbs the plasma so that the mass spectroscopy is considered not always suitable for in-situ radical measurements in the reactive plasma.

While various evidence has been put forward in support of both CF and  $CF_2$  radical species as being the main precursor of fluorocarbon films for etching, some debated point still remains. This is compounded by the fact that carbon atoms from the plasma chemistry and resist polymers may also play a significant role, but to date very little data has been presented. It is necessary to obtain the carbon atom characteristics of the plasma and their relation to the etch process. Recently, an estimate of the carbon atom density was obtained using a hollow cathode spectroscopy by H. Ito et al. as described in Chapter 5.

In order to summarize measurement methods of fluorocarbon radical densities described above, characteristics and problems of them are shown in Table 1.1.

Table 1.1 Characteristics and problems of main measurement methods of fluorocarbon radical densities

<b>Methods</b>	<b>Characteristics</b>	<b>Problems</b>
<i>IRLAS</i>	non-intrusive, wide range	(some assumptions)
<i>Actinometry</i>	without difficulty	relative density (CF, $CF_2$ )
<i>LIF</i>	high sensitivity	can not measure $CF_3$
<i>AMS</i>	wide range	intrusive
<i>OES</i>	easy	only qualitative

### 1.2.3 Problems Associated with Selective SiO<sub>2</sub>/Si Etching

The selective removal of one material from another is an important part of IC processing. In the case of SiO<sub>2</sub> selectivity over Si, it is necessary to remove the SiO<sub>2</sub> from the underlying Si without removing any significant amount of the Si. The depth of dopant layers used for device operation is usually within 100 nm of the wafer surface and should remain unaltered after the etching process. Plasma etching proceeds through a combination of physical and chemical effects. Physical interaction between the plasma and material produces a damaged layer that is then removed through chemical reactions. Therefore, this type of selective etching requires controllable physical interactions and selective chemical reactions. In other words, the former are controllable ion energies to induce damage to the etch layer only and not damaging the underlying layer, and the latter are chemical reactions that will etch only the SiO<sub>2</sub> layer but not the underlying Si.

Etch profiles are also extremely important in ULSI fabrication, and control of the surface etch process is necessary, if a directional etch is to be achieved. The precise etch mechanisms are still not understood, but it is clear that, ions damage the etch surface that is then more reactive to the neutral etchants, and ions produce etch-products which inhibit etching. The ions in the plasma must be anisotropic (i.e. traveling in a direction perpendicular to the wafer). Ions accelerated in the sheath sometime collide with neutrals that results in sidewall etching. To prevent sidewall etching, low-pressure (fewer collisions) plasma processing is required. Plasma etching is usually a competitive process between the etching of SiO<sub>2</sub> and deposition of etch products on the sidewalls of the trench. Therefore, with the continuous shrinking of pattern sizes, control of sidewall deposition is required to avoid differences between the mask size and the actual etch pattern size.

Microscopic uniformity problems in ULSI fine pattern etching occur because etch rates and profiles are dependent on feature size and pattern density. Two main problems exist, the first is aspect ratio-dependent etching (ARDE) which means that larger aspect ratio trenches are etched more slowly than those of small aspect ratio. The second is microloading

resulting from depletion of reactants due the increase in unmasked area of high density circuits.

Future MOS etch processes require a SiO<sub>2</sub>/Si etching selectivity of 100, SiO<sub>2</sub> etching rate of 1 μm/min and an aspect ratio of 100. However, as pointed out above, there are several problems associated with high density plasma etching employing fluorocarbon gases. In this thesis, we are concerned with, first the ability to control the fluorine atom to fluorocarbon radical ratio to obtain a high etching selectivity, and second with the understanding of transients in chamber wall conditions and the effect on high precision etching. The first problem is caused by a high ratio of fluorine atoms to fluorocarbon radicals. However, until the absolute densities of all the species are measured, this remains a much debated point. It has been suggested that high SiO<sub>2</sub>/Si selective etching could be achieved by the selective formation of carbon-rich fluorocarbon film on Si surface of the bottom of the contact hole. The second problem is also closely related to the composition of fluorocarbon radicals in the plasma, because the plasma composition changes with variations in the chamber wall conditions.

Therefore, in order to obtain a high precision etch, it is necessary to develop controllable plasma sources, to identify the key precursors responsible for the carbon-rich fluorocarbon film formation and to study the mechanism of film formation in fluorocarbon high density plasma.

### 1.3 Purpose and Composition of This Work

There are three main objectives of this work in order to achieve superior etching features in next-generation devices. The first is to develop and improve a controllable large-area ECR plasma source through scientific evaluation of the plasma parameters. The second is to quantitatively characterize the radical species in SiO<sub>2</sub>/Si selective etching plasma for identifying the key precursors responsible for the selectivity and clarifying the mechanism of selective etching process. The last is to control the plasma process using these newly-developed high-density ECR plasma source. In meeting these objectives, as diagnostics of

fluorocarbon radicals in etching plasma are indispensable, infrared diode laser absorption spectroscopy (IRLAS) was used as a very powerful technique.

In this thesis, it is reported that two large-area ECR and a compact microwave plasma sources using permanent magnet have been developed, characterized and applied to the etching of Si and SiO<sub>2</sub>. These sources are described here along with details of the plasma characteristics evaluated by IRLAS, Langmuir probe diagnostics, emission spectroscopy, hollow cathode lamp absorption spectroscopy and titration. Every effort has been made to demonstrate how the ECR plasma characteristics can be related directly to the etching process. A brief outline of each chapter is given below.

In Chapter 2, design of a large area ECR plasma(300D-ECR) using permanent magnets and applying whistler-mode launching of the microwave is described. Plasma produced with this modified source was evaluated by Langmuir probe diagnostics. A uniform plasma  $\pm 3.5\%$  is produced over 20 cm and  $\pm 1.8\%$  over 16cm. The plasma space potential is  $17\text{ V} \pm 1\%$  over 20 cm. The maximum ion current density was measured to be  $11.5\text{ mA/cm}^2$ . No contaminants from the discharge were detected and under 100 h continuous testing no damage occurred. The source is applicable to large area plasma etching processes for ULSI device production.

In Chapter 3, diagnostics of fluorocarbon radicals and fluorine (F) atom species in the size-scalable large-area permanent magnet (300D-ECR) and a conventional electromagnet ECR (C-ECR) etching plasma employing CF<sub>4</sub> and C<sub>4</sub>F<sub>8</sub> gases are reported. Non-intrusive infrared diode laser absorption spectroscopy and actinometric measurement techniques are used in evaluating the performance of the permanent magnet ECR plasma source and in studying the kinetic processes associated with etching plasma chemistry. Successful measurements of the absolute CF and CF<sub>2</sub> radical and F atom densities have been achieved. In particular for C<sub>4</sub>F<sub>8</sub> plasma, enhanced CF and CF<sub>2</sub> radical densities in the 300D-ECR plasma source which afford higher selectivity in the etching of SiO<sub>2</sub> on Si are discussed.

In Chapter 4, a large-area ECR source (Radial Strip-bar Antenna; RSA-ECR) improved by using a strip-bar antenna is described. In this system by launching the microwave near the high magnetic field of the permanent magnets, ECR plasma is produced. The source diameter is 35 cm. Plasma produced with this modified source was evaluated by Langmuir probe diagnostics. Parameters measured at the downstream position of 10 cm are an electron density of  $1.4 \times 10^{11}\text{ cm}^{-3}$ , electron temperature of 3 eV and a space potential with respect to the chamber walls of 20 V. Plasma uniformity of within  $\pm 3.8\%$  over 30 cm is achieved.

In Chapter 5, changes in the densities of fluorocarbon radicals and fluorine atoms in the RSA ECR etching plasma source employing C<sub>4</sub>F<sub>8</sub> gas with CH<sub>4</sub> addition have been investigated. Measurements using IRLAS and actinometric optical emission spectroscopy show that for a pure C<sub>4</sub>F<sub>8</sub> plasma, the dominant species is CF<sub>2</sub> radicals with a density of the order of  $10^{13}\text{ cm}^{-3}$ , followed by fluorine atoms, CF<sub>3</sub> and CF radicals which have a density an order of magnitude lower at  $10^{12}\text{ cm}^{-3}$ . The densities of the different fluorocarbon radical species were found to display different dependencies on increasing CH<sub>4</sub> gas addition. Hollow cathode absorption spectroscopy was used to estimate the carbon atom density, for the first time, in an etching plasma. The carbon atom density in the plasma increases linearly with CH<sub>4</sub> gas addition between 20 to 80 %. Analysis of actual SiO<sub>2</sub>/Si etching revealed that the etch selectivity and carbon atom to fluorine atom ratio follows a similar trend, indicating a direct correlation between the carbon atom density in the plasma and the etch selectivity.

In Chapter 6, a novel compact and versatile microwave plasma source is described. Plasma parameters are evaluated by emission spectroscopy and Langmuir probe diagnostics. In determining the absolute density of radical species, titration using NO<sub>2</sub> gas was employed to correlate the oxygen atom density with the plasma operating conditions. The effects of wall materials on the oxygen atom density are also investigated.

In Chapter 7, an overall summary of the results presented is given along with scope for future research.

## References

- [1] C. Y. Chang and S. M. Sze: ULSI Technology, McGraw-Hill, Signapore 1996.
- [2] A. J. Perry and R. W. Boswell: Appl. Phys. Lett. **55**, 148 (1989).
- [3] J. H. Keller, J. C. Forster and M. S. Barnes: J. Vac. Sci. Technol. A **11**, 2487 (1993).
- [4] S. Matsuo and M. Kiuchi: Jpn. J. Appl. Phys. **22**, L210 (1983).
- [5] N. Shida, T. Inoue, H. Kokai, Y. Sakamoto, W. Miyazawa, S. Den and Y. Hayashi: Jpn. J. Appl. Phys. **32**, L1635 (1993).
- [6] K. P. Giapis, N. Sadeghi, J. Margat, R. Gottscho, and T. C. Lee: J. Appl. Phys., **73**, 7188 (1993).
- [7] J. Asmussen: J. Vac. Sci. Technol. A **7** (1989) 883.
- [8] J. Margot and R.A. Gottscho: *Microwave Excited Plasmas*, Elsevier, Amsterdam, 1992.
- [9] M. A. Liberman and A. J. Lichtenberg: *Principles of plasma discharges and material processing*, John Wiley & Sons, Inc., New York, 1994.
- [10] K. Suzuki, S. Okudairo, N. Sadudo and I Kanomata: Jpn. J. Appl. Phys. **16** (1977) 1979.
- [11] C. Pomot, B. Mahi, B. Petit, Y. Arnal and J Pelletier: J. Vac. Sci. & Technol. B **4** (1986) 1.
- [12] O. Popov: J. Vac. Sci. & Technol. A **7** (1989) 894.
- [13] M. Matsuoka and K. Ono: Appl. Phys. Lett. **50**, (1987) 1864.
- [14] J. Hopwood, P. K.Reinhard, and J. Asmussen: J. Vac. Sci. & Technol. B **6** (1988) 1896.
- [15] A. Takamori, S. Sugata, K. Asakawa, E. Miyauchi and H. Hashimoto: Jpn. J. Appl. Phys. **26** (1987) L142.
- [16] Y. Tanaka, Y. Kunitsugu, I. Suemune, Y. Honda, Y. Kan and M. Yamanashi: Jpn. J. Appl. Phys. **64** (1988) 2778.
- [17] Z. Lu, M.T. Schmidt, R.M. Osgood, Jr., W.M. Holber and D.V. Podlesnik: J. Vac. Sci. & Technol. A **9** (3)(1991)1040.
- [18] P. O'Keeffe, S. Komuro, S. Den, T. Morikawa and Y. Aoyagi: Jpn. J. Appl. Phys. **31** (1992) 3301.
- [19] N. Kondo and Y. Namishi: Jpn. J. Appl. Phys. **28** (1989) L7.
- [20] S. Matsuo and M. Kiuchi: Jpn. J. Appl. Phys. **22** (1983) L210.
- [21] T. Ono, C. Takahashi and S. Matsuo: Jpn. J. Appl. Phys. **23** (1984) L534.
- [22] K. Kato and I. Kato: Jpn. J. Appl. Phys. **28** (1989) L343.
- [23] T. Watanabe, K. Azuma, M Nakatani, K. Suzuki, T. Sonobe and T. Shimada: Jap. J. Appl. Phys. **25**, (1987) 1805.
- [24] T. Watanabe, M. Tanaka, K. Azuma, M Nakatani, T. Sonobe and T. Shimada: Jap. J. Appl. Phys. **26**, (1987) 1215.
- [25] H. Fujita, H. Hanada, M. Nagano and H. Matsuo: Jap. J. Appl. Phys. **26**, (1987) 1112.
- [26] Y. Endo, C. Yamada and E. Hirota: J. Chem. Phys. **77** 3376 (1982).
- [27] M. Magane, N. Itabashi, N. Nishiwaki, T. Goto, C. Yamada and E. Hirota: Jpn. J. Appl. Phys. **29** L829 (1990).
- [28] J. W. Coburn: J. Appl. Phys. **50** 1419 (1979)
- [29] R. D'Agostino, S. De Benedictis and F. Cramarossa: Plasma Chem. Plasma Proc. **4** 1 (1984).
- [30] D. L. Flamm and V. M. Donnelly: Plasma Chem. Plasma Proc. **1** 317 (1981).
- [31] J. P. Booth, G. Hancock, N. D. Perry and M. J. Toogood: J. Appl. Phys. **66** 5251 (1989).
- [32] D. Edelson and D. L. Flamm: J. Appl. Phys. **56** 1522 (1984).
- [33] N. Itabashi, N. Nishiwaki, M. Magane, S. Naito, T. Goto, A. Matsuda, C. Yamada and E. Hirota: Jpn. J. Appl. Phys. **29** 505 (1990).
- [34] S. Naito, M. Ikeda, N. Ito, T. Hattori and T. Goto: Jpn. J. Appl. Phys. **32** 5721 (1993).
- [35] K. Maruyama, A. Sakai, and T. Goto: J. Phys. D **26** 199 (1993).
- [36] J. Wormhoudt: J. Vac. Sci. Technol. A **8** 1722 (1990).
- [37] K. Takahashi, M. Hori, K. Maruyama, S. Kishimoto and T. Goto: Jpn. J. Appl. Phys. **5** A L694 (1993).

## Chapter 2. Development of Plasma Source Technology for 8-inch Wafer Processing

### 2.1 Introduction

Today's ULSI technology requires 0.25 $\mu$ m processing over 8-inch wafers. ECR plasma sources are being investigated as one possible candidate for large diameter plasma etching. [1-4] The requirements imposed on the plasma source design for etching applications are as follows, (1) a plasma area larger than 20 cm in diameter, (2) uniformity of the plasma ion density, (3) a high ion current density, (4) low ion energies, (5) low contaminant levels and (6) a long operational life time.

In this chapter, the development and characterization of a ECR plasma source for 8-inch wafer processing is described. To meet the process requirements described above (1)–(6), the targets which should be established for development of a ECR plasma source are shown in Table 2.1. A large area ECR plasma source for 8-inch wafer is designed here by employing permanent magnets in order to reduce both the cost and space associated with electromagnetic coils.[5] To overcome the cut off density ( $7.0 \times 10^{10} \text{ cm}^{-3}$  for 2.45 GHz) associated with ECR plasma, whistler mode launching of the microwaves is used to produce an over dense plasma. Particular importance is placed on achieving good plasma uniformity since it has been reported that non-uniformity of plasma etching and deposition processes depend strongly on the non-uniformity of the ion current density in the plasma.[6]

Table 2.1 Targets and results of development of the ECR plasma source for 8-inch wafer processing.

	Targets	Results
Electron Temperature ; $T_e$	< 5 eV	3 eV
Electron Density ; $n_e$	> $10^{11} \text{ cm}^{-3}$	$4.3 \times 10^{11} \text{ cm}^{-3}$
Non-uniformity across 8-inch of ion current	< +/- 5 %	+/- 3.5 %
and space potential	< +/- 2 %	+/- 1 %
Space Potential	< 30 V	17 V
Operational life time	As long as possible	Over 100 hr
Contamination	Free	No detective

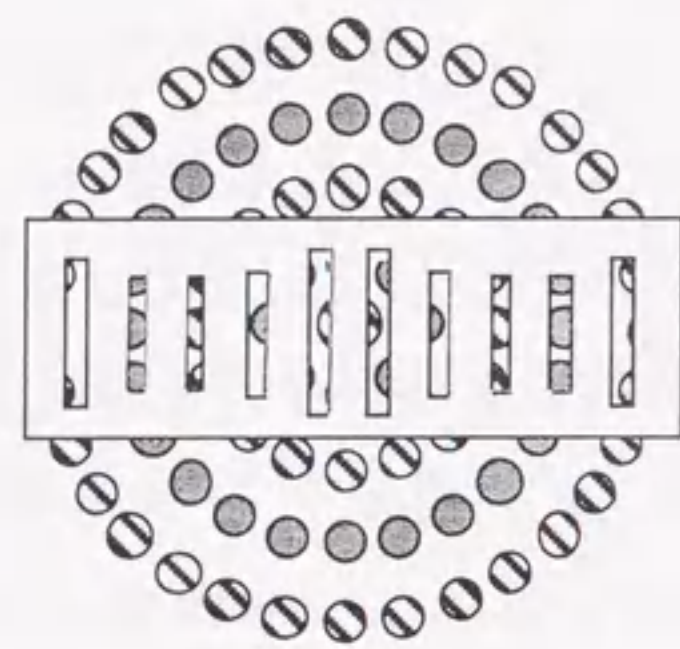
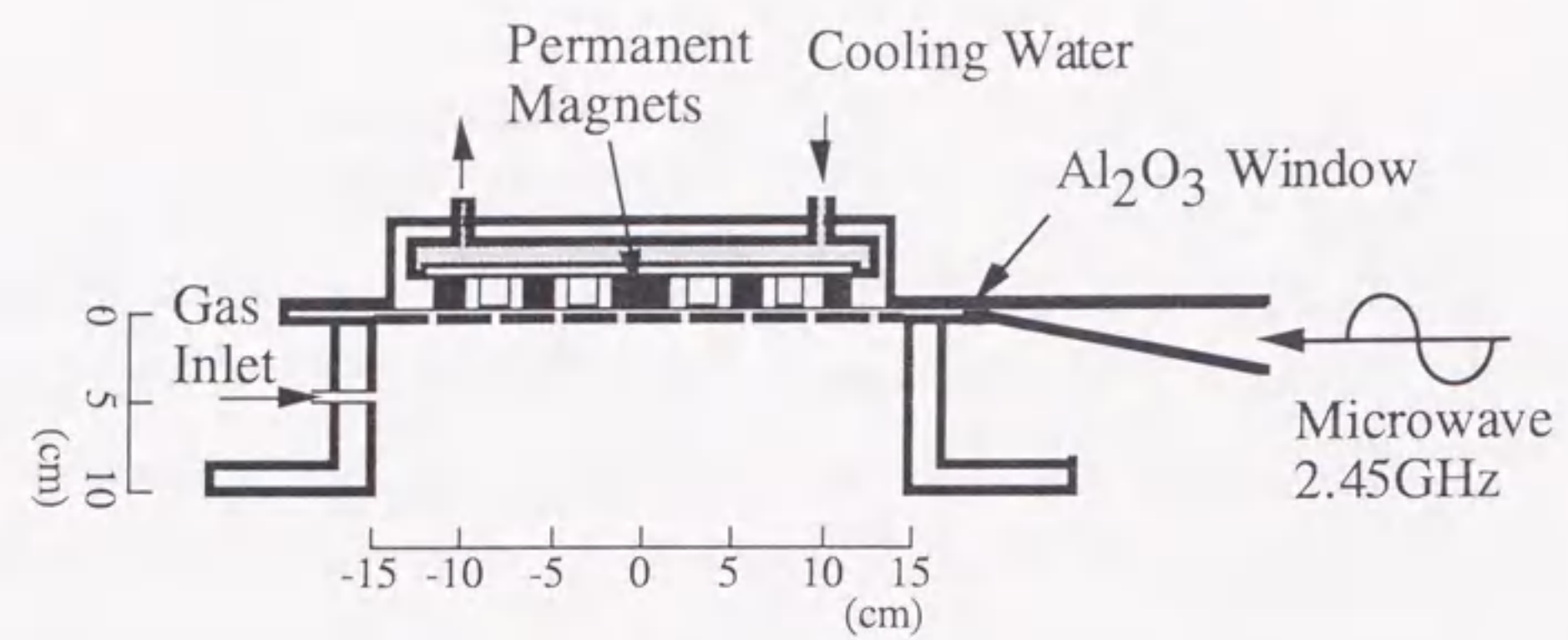
### 2.2 Design of a High Density and Uniform ECR Plasma with Permanent Magnet

#### 2.2.1 Configuration

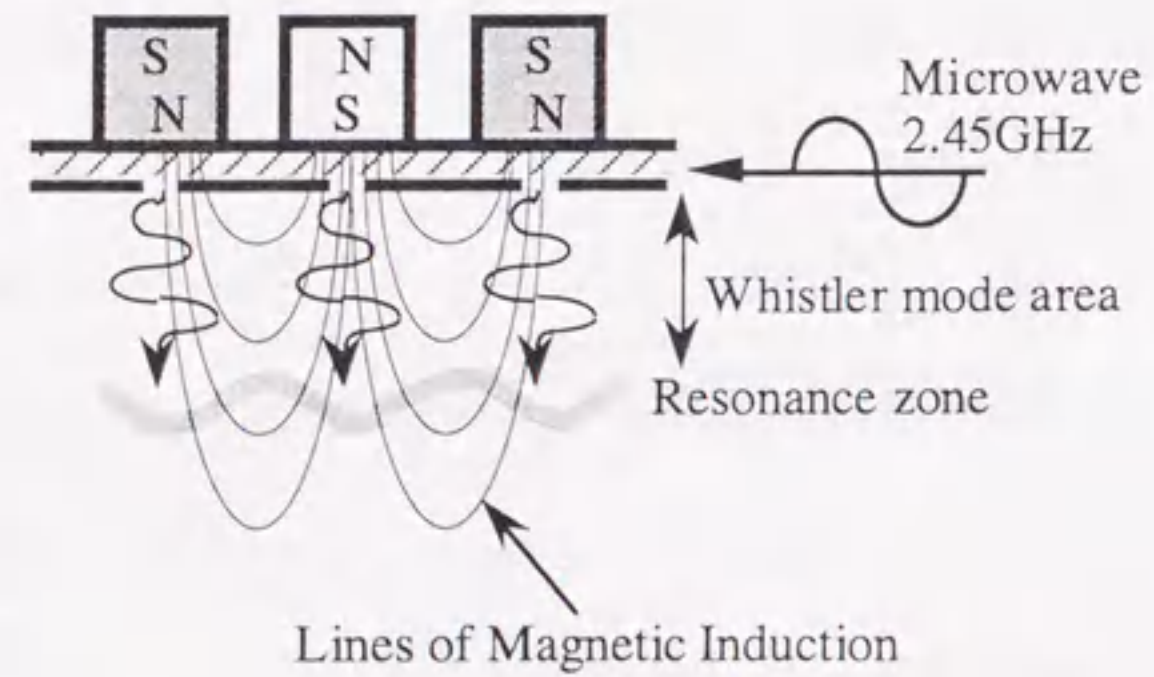
A schematic diagram of the developed ECR plasma source (Nichimen Electronic Technology Corporation, 300-D ECR) and the experimental setup is shown in Fig. 2.1(a) and to help understand the plasma generation process, an expanded view of the launcher is shown in Fig. 2.1(b). Figure 2.2 shows photographs of the experimental system, the magnet arrangement and a typical Argon (Ar) plasma discharge. The plasma chamber is made of aluminum (Al), with a diameter of 28 cm (see Fig.2.1 (a)). The resonance magnetic field for electron cyclotron resonance is generated by permanent magnets which are arranged in the upper wall or ceiling along concentric circles with successive opposite polarities. The magnets are made from neodymium iron boron and require strict water cooling. Microwave of 2.45 GHz is introduced by a slotted array antenna connected to a tapered rectangular waveguide. The slotted array antenna is arranged so that the slots are placed just under the magnets. The resonance zone is found at about 1.6 cm below the magnets. Between a slot and the resonance zone, the magnetic field is larger than that of resonance. The microwave radiated from the slotted array antenna transmits along the magnetic lines of force in the whistler mode as far as the right hand circularly polarized wave (R-wave) concerned, and is absorbed by electrons at this resonance zone (Fig. 2.1.(b)). The propagation constant of the R-wave for the cold and collision free plasma model is given by

$$k = k_0 \sqrt{1 - \left[ \frac{\omega_{pe}^2}{\omega(\omega - \Omega_{ce})} \right]} \quad (2.1)$$

where  $k_0$ ,  $\omega$ ,  $\omega_{pe}$  and  $\Omega_{ce}$  stand for the propagation constant for vacuum, the microwave, the plasma and the electron cyclotron frequencies, respectively. When the microwave is launched from a region where the magnetic field is larger than the resonance field, we always have real  $k$  even if  $\omega < \omega_{pe}$ . As a result, a plasma density larger than the cut off density can be generated.

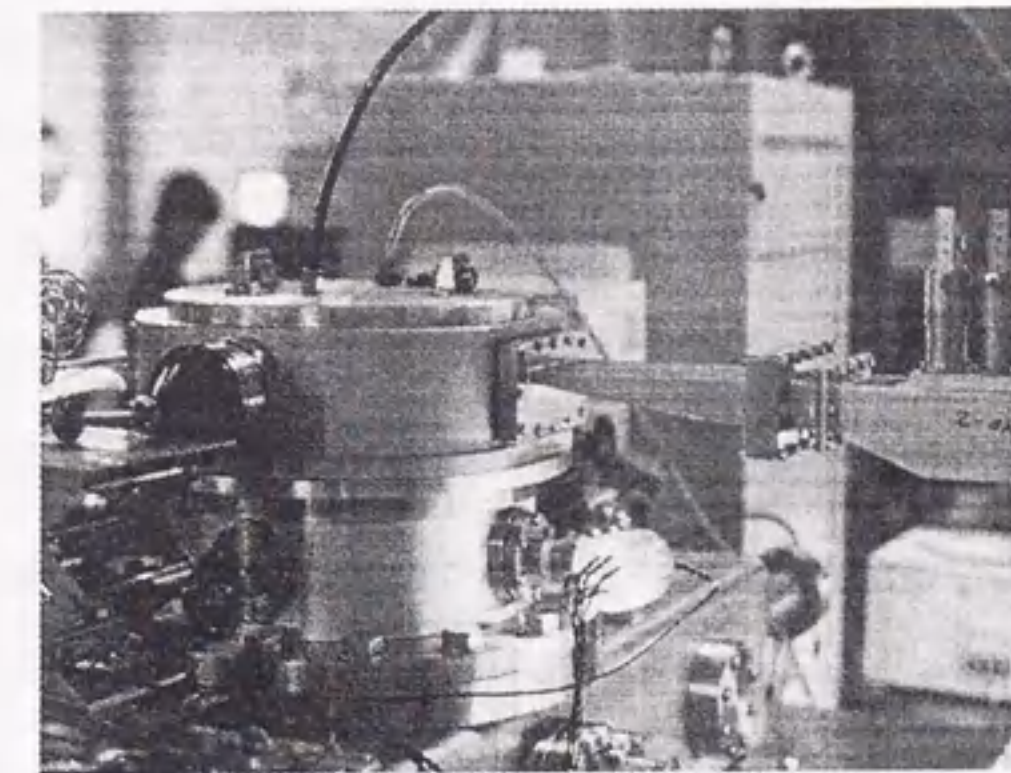


(a)

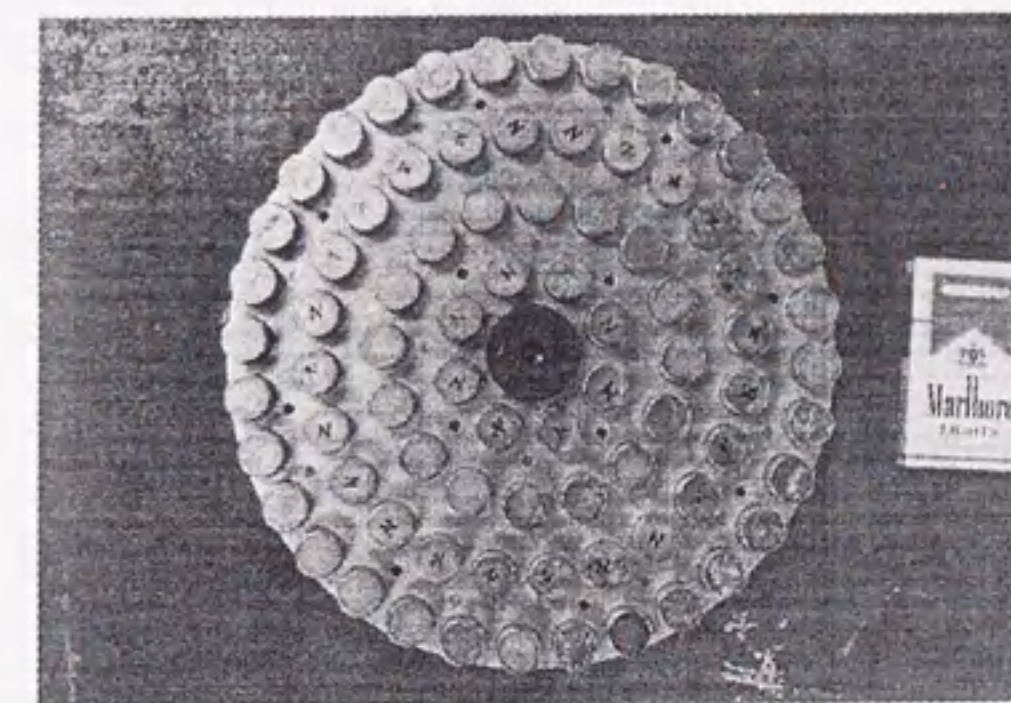


(b)

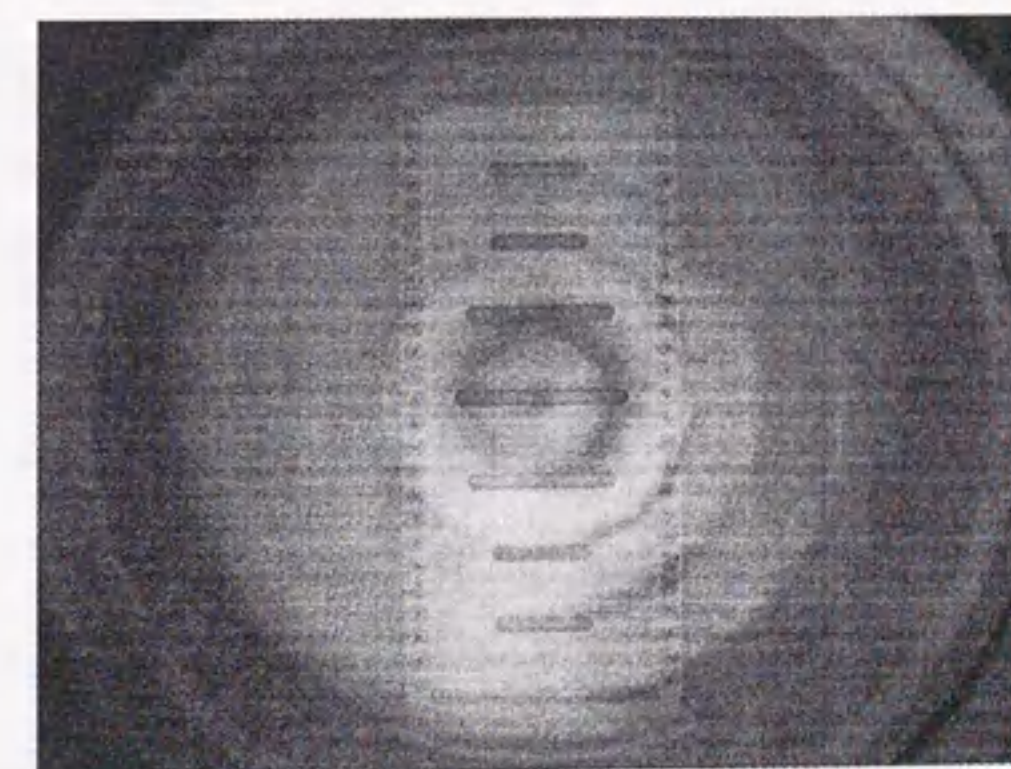
Fig. 2.1 (a) A schematic diagram of the 300D-ECR plasma source with permanent magnets. (b) Expanded schematic of the slot antenna and microwave launch mechanism.



(a)



(b)



(c)

Fig. 2.2 Photographs of (a) the experimental system, (b) the permanent magnets and (c) a typical Argon discharge.



By considering plasma particle drifts and confinement processes similar to those described by Geisler *et al.* [7], it is possible to give a qualitative explanation of the non-uniformity of the plasma. With reference to the magnetic configuration shown in Fig 2.1(a), magnetic mirror fields are formed by adjacent concentric rings. Microwaves introduced into the source radiate from the slots. Below a slot, electrons are generated by microwave absorption. Owing to the adiabatic invariance of the magnetic moment, electrons become trapped, bouncing back and forth in the magnetic mirror fields. These electrons experience drift motion due to curvature of the field. The direction of drift is determined by the magnetic configuration. The trapped electrons ionize neutral particles resulting in producing ions and electrons, thus generate a dense plasma below the waveguide. The lengths, widths and locations of the slot antenna are adjusted by try and error so that the emitted power in peripheral region is larger than that in central region. This design of slot antenna enables us to offer a radial plasma density distribution which has the maximum near the periphery (dumbbell type distribution) for axial positions near the magnets. Downstream away from the plasma-generation region, due to diffusion these inconsistencies are manifested as relatively uniform profiles.

The slot dimension is experimentally adjusted to produce the dumbbell shaped density distribution near the ceiling. Figure 2.1(a) shows the optimized slot array antenna which gives a uniform radial distribution at a distance of about 15 cm from the ceiling.

### 2.2.2 Characteristics

Plasma parameters were measured using a scanning Langmuir probe. Concerning the probe measurement, consideration is given to the influence of the microwave and the magnetic field on the characteristics as follows. Firstly, the plasma frequency of the produced plasma ranges 0.9 to 6.3 GHz and is of the same order of magnitude as the microwave frequency of 2.45 GHz. The sheath around the probe does not respond sufficiently to the microwave field, therefore, the electron temperature measurement is not influenced. Secondly, to avoid the influence of the magnetic field we estimated the density from the ion collection region. Ar gas was used throughout our experiments.

A Langmuir probe measurement is more commonly known as a simple technique to characterize the plasma and most extensively used, because it gives us relatively good quantitative information of physical plasma parameter such as electron temperature ( $T_e$ ), electron density ( $n_e$ ), the plasma potential ( $V_p$ ) and electron and ion energies. Although it is simple in construction (see Fig.2.3), interpretation of the results obtained is complicated. A typical **I-V** curve by the Langmuir probe is also shown in Fig.2.3. When the probe is biased ( $V_b$ ) so that current to the probe is zero, the bias is referred to as the floating potential  $V_f$ , i.e. the potential an isolated probe would float at in the plasma. As the probe bias is increased, the current collected becomes to be dominated by electron and tends to saturation at some potential  $V_p$ , that is, the plasma potential. The current is given by,

$$I_e(V_b) = I_e^{sat} \exp\left[\frac{-e(V_p - V_b)}{T_e}\right] \quad (2.1)$$

where

$$I_e^{sat} = S n_e e \sqrt{2\pi m_e} \quad (2.2)$$

and  $S$  is the probe collecting area.  $T_e$  can be obtained from the slope of semilog plot of  $I_e$  vs  $V_b$ , and in the case without magnetic field,  $n_e$  can be calculated from eqn.(2.2).

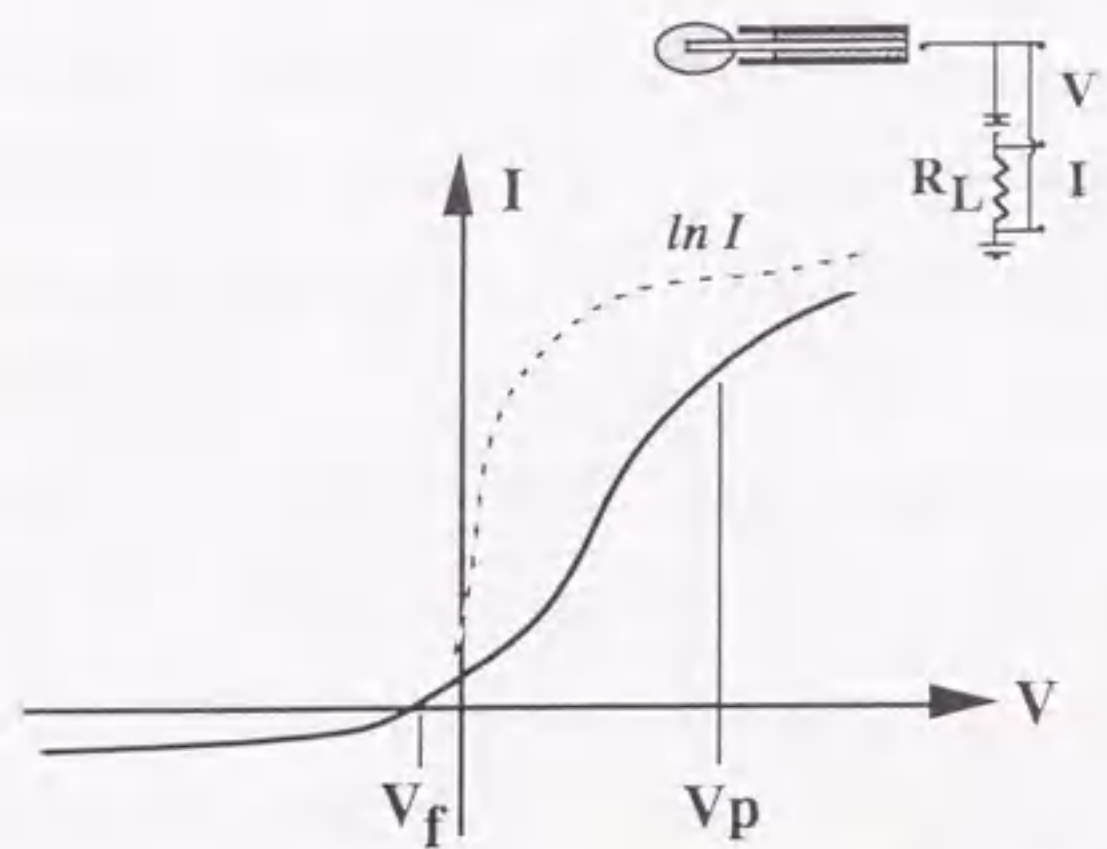


Fig.2.3 Typical I-V curve obtained from a Langmuir probe (inset).  
The floating potential ( $V_f$ ) and the plasma potential ( $V_p$ ) is marked.  
From the slope of  $\ln I$  vs  $V$ ,  $T_e$  can be calculated.

It is very complicated to obtain the electron density from the electron collection signal effected by magnetic field. The electron density can be calculated from the ion current density with good approximation by neglecting the magnetic field effect. The reason is explained as follows.

We measured the plasma parameters in downstream region where the magnetic field goes down to about 50 G. It is reasonable in the region that we suppose the electron temperature  $T_e$  and the ion temperature  $T_i$  for Argon plasma are typically 3 eV and 0.5 eV, respectively. Generally, the  $T_i$  is believed to be near the room temperature. However, we find low frequency waves in ECR plasmas whose electric fields accelerate ions and give energy to ions. This results in the ion heating. The electron and ion gyroradii ( $r_{ce}$ ,  $r_{ci}$ ) are given as follows,

$$r_{ce} = V_{ce} / \omega_{ce} = 1.2 \text{ mm}$$

$$r_{ci} = V_{ci} / \omega_{ci} = 129 \text{ mm}$$

where  $\omega_{ce}$ ,  $\omega_{ci}$ ,  $V_{ce}$  and  $V_{ci}$  are the cyclotron frequencies and particle velocities for the electron and ion, respectively. When these values are compared with the probe diameter  $D_p$

= 0.3 mm,  $r_{ce}$  is comparable and  $r_{ci}$  is much larger than  $D_p$ . Therefore, this result indicates the ion density is obtained from the ion collection signal with good approximation neglecting the magnetic field effect. The ion saturation current ( $I_0$ ) is given by

$$I_0 = \kappa n_e e (kT_e / m_i)^{1/2} S \quad (2.3),$$

where  $\kappa$  is a function of  $T_i/T_e$ . [8] Since  $T_e$  is known from the slope of semilog plot of  $I_e$  vs  $V_b$  described above,  $n_e$  can be calculated from Eqn.(2.3) using the  $I_0$  measured.

Measurements of Langmuir probe were made 20 cm downstream from plasma source. Based on the probe results, the electron density calculated from eqn.(2.3) versus pressure is plotted in Fig 2.4 as a function of microwave power. Measurements were made 20 cm downstream. Over the pressure range investigated 0.06 to 0.2 Pa, the density increases linearly with increasing pressure. The rate of density increases however, increases with increasing microwave power. At the power of 1000 W a maximum density of  $9.0 \times 10^{10} \text{ cm}^{-3}$  is recorded. Powers of up to 1500W can be accommodated with this source.

According to the design criteria described above, we should have a dumbbell shaped plasma ion density distribution near the resonance zone. In fact as is seen in Fig. 2.5, the ion current density has a dumbbell shape radial distribution at 5 cm from the ceiling. The electron density is  $4.3 \times 10^{11} \text{ cm}^{-3}$ , which is greater than the cut off density ( $7 \times 10^{10} \text{ cm}^{-3}$ ) for ECR plasma. This shows the effectiveness of the whistler mode launching. The plasma diffuses radially with increasing axial distance from the ceiling. As a result, the radial distribution changes from a dumbbell profile, to a flat profile and then to a parabolic one, as the observation point is shifted downward. A uniform distribution is found at about 15 cm from the ceiling, as shown in Fig. 2.5, where the pressure and the microwave power are 120 mPa and 200 W, respectively. The non-uniformity is within  $\pm 3.5\%$  over 20 cm and  $\pm 1.8\%$  over 16 cm. Figure 2.7 shows the plasma space potential uniformity, it is 17 V with the uniformity of  $\pm 1\%$  over a diameter of 20 cm.

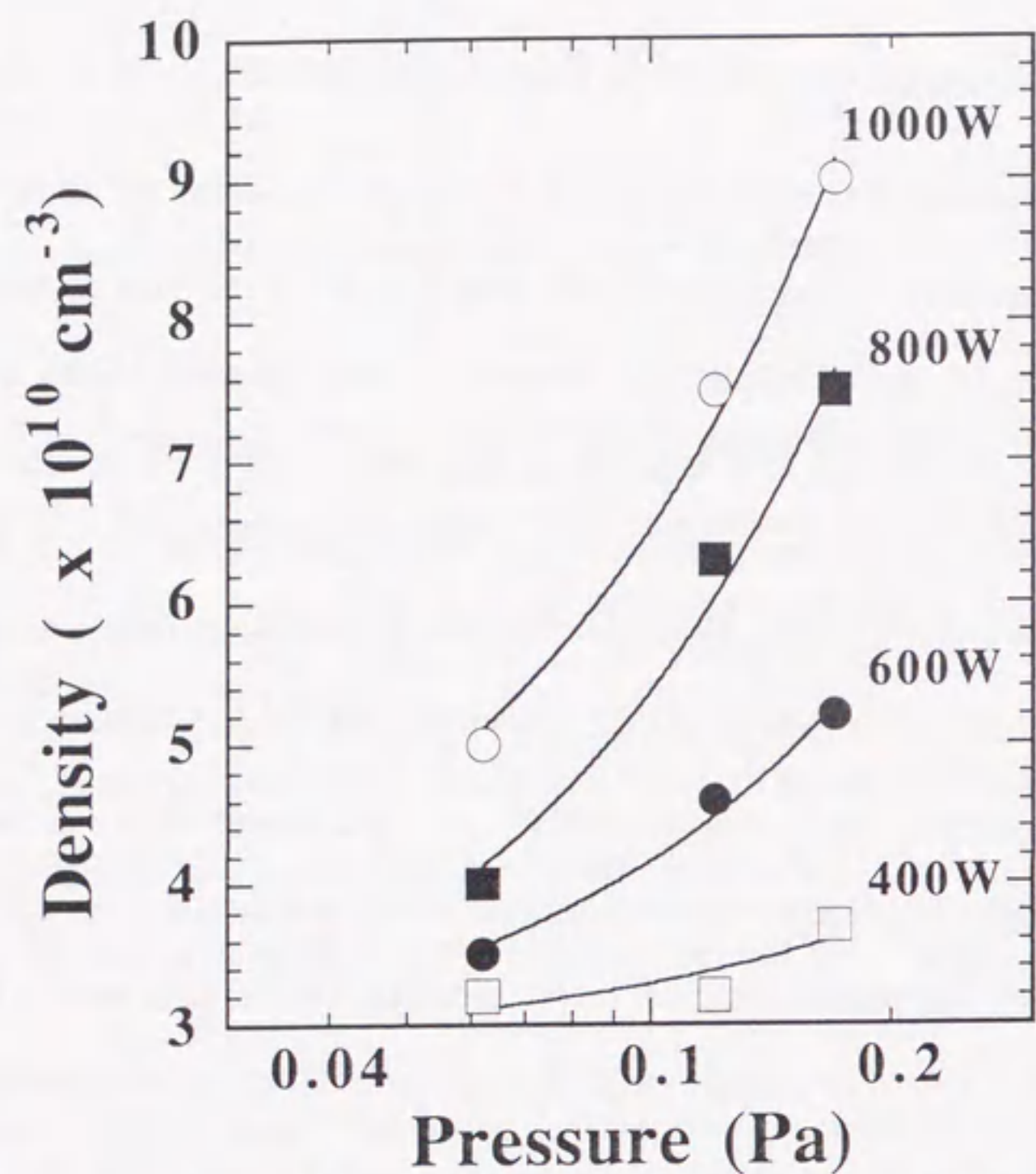


Fig. 2.4 The electron density versus pressure as a function of microwave power.

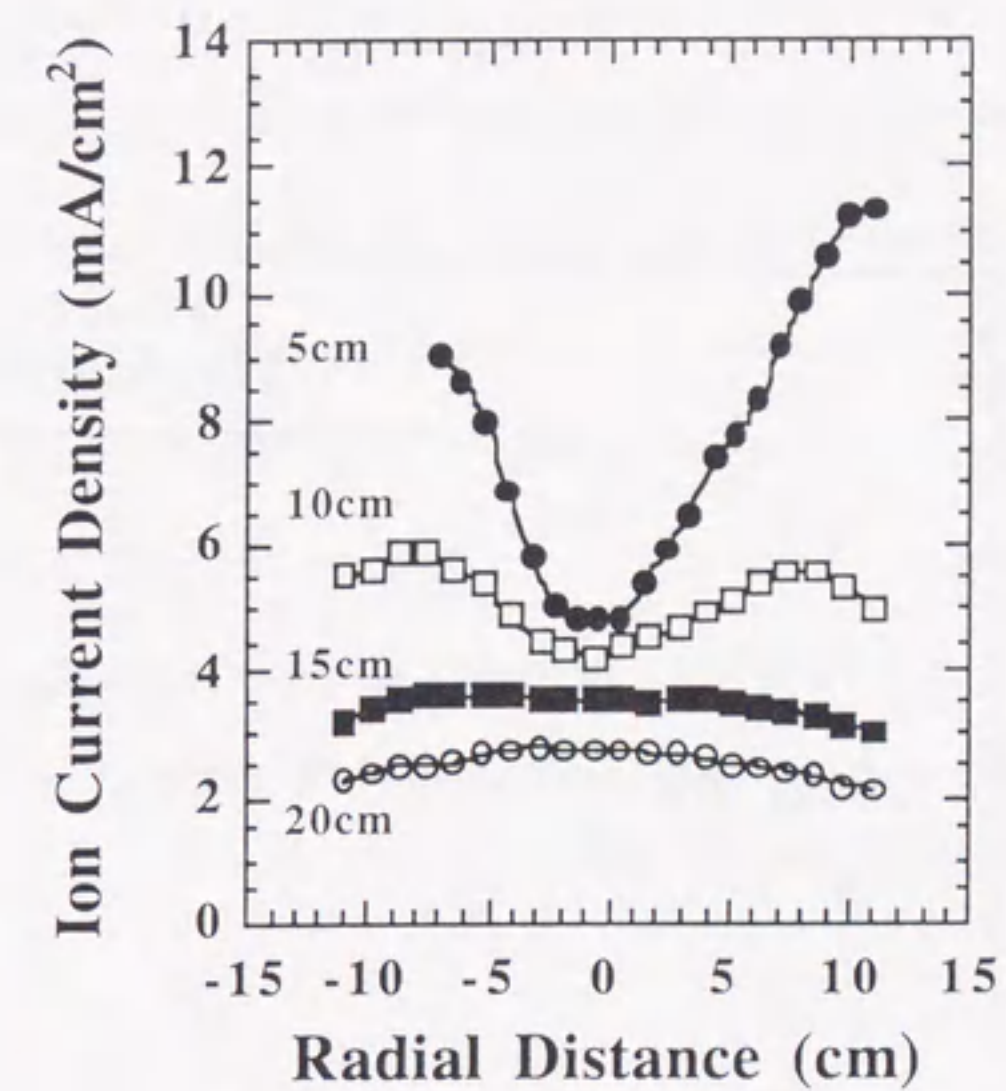


Fig. 2.5 Radial ion current density distribution. Parameters 5, 10, 15 and 20 cm refer to the axial distance. The pressure and microwave power are 120 mPa and 200 W, respectively.

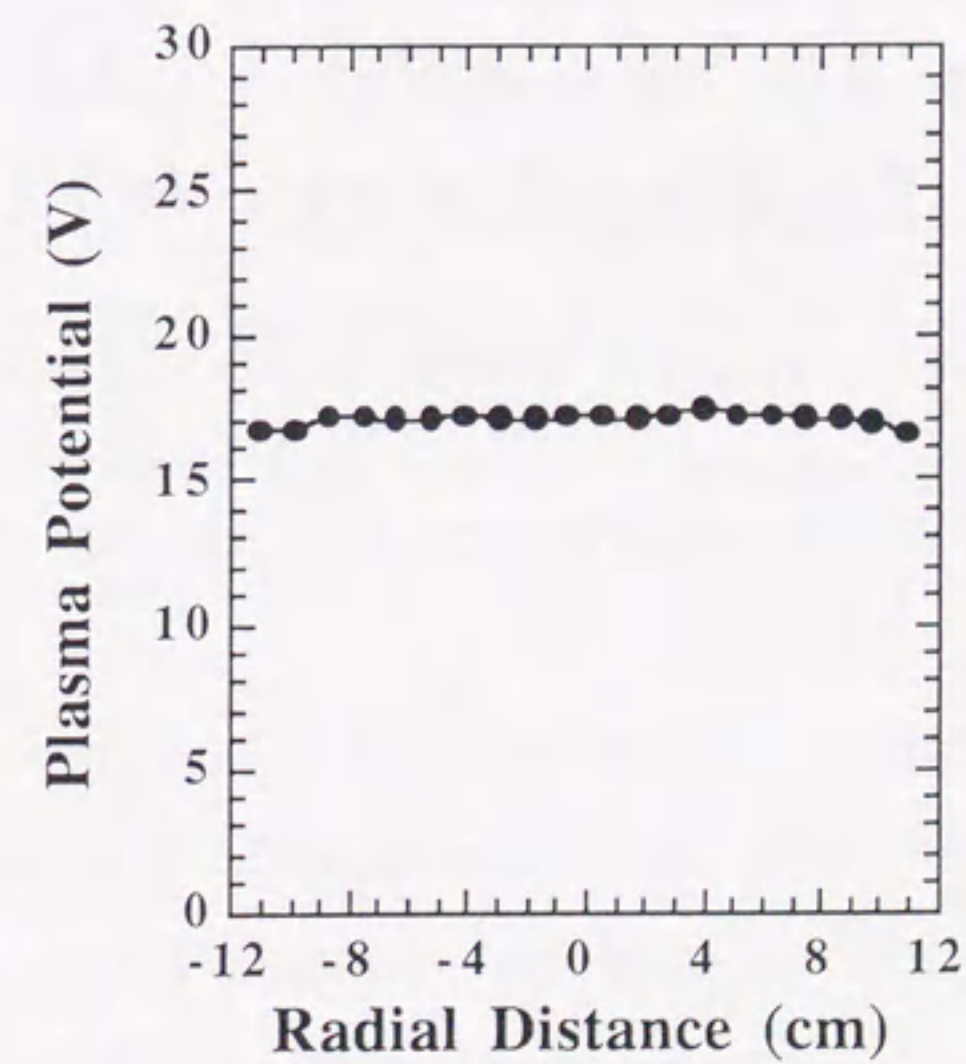


Fig. 2.6 Radial plasma potential distribution at an axial position of 15 cm. The pressure and microwave power are 120 mPa and 200 W, respectively.

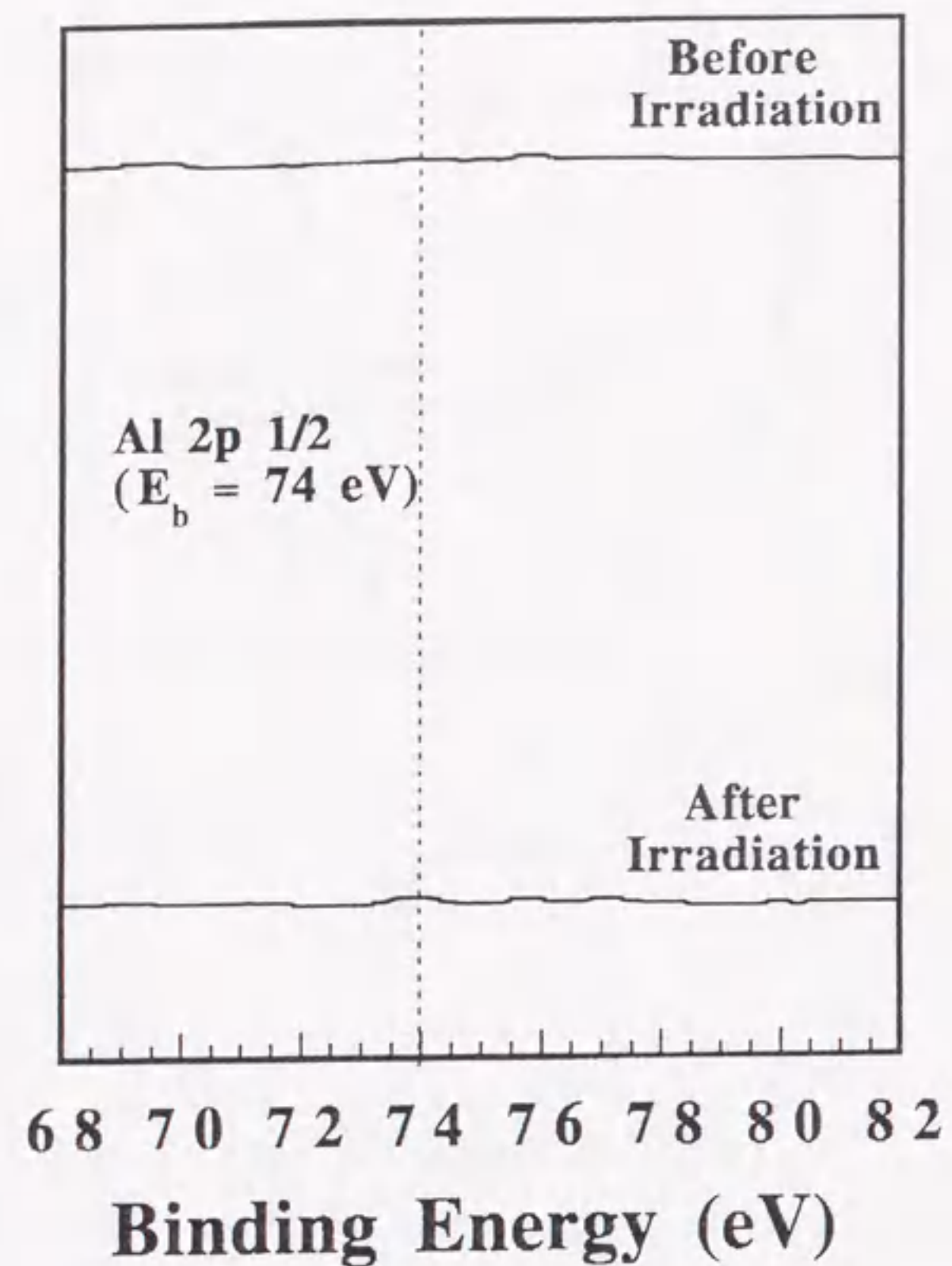


Fig. 2.7 X-ray photoelectron spectra showing the binding energy of the Al 2p electron before and after plasma irradiation of a Si wafer. No Al contamination is observed.

Contamination from plasma systems is a major cause for concern, hence, XPS (X-ray photoelectron spectroscopy) observation of a Si substrate irradiated by the plasma was used to check for impurities from the aluminum chamber walls. The sample was situated at a position where the electron density and temperature were approximately  $10^{11}$   $\text{cm}^{-3}$  and 3 eV respectively. The exposure time was approximately 90 minutes. With respect to the problem of impurities from the chamber wall it can be seen from the XPS spectra of the irradiated Si test piece, shown in Fig. 2.6 that no trace of Al (Al 2p $_{1/2}$ , binding energy 74 eV) was found. As a life time test, the source was operated continuously with microwave power of 600 W for 100 hr, and we found no damage to the system components.

### 2.3 Summary

An ECR plasma source of 20 cm in diameter has been developed. The magnetic field was generated by permanent magnets. Whistler mode launching of the microwaves is applied to introduce the microwave into the chamber, and a plasma density greater than the cut off density is successfully obtained;  $4.3 \times 10^{11}$   $\text{cm}^{-3}$ . The non-uniformity of ion current density is  $\sim 3.5\%$  over 20 cm and  $\sim 1.8\%$  over 16 cm. The plasma potential is around 17 V with the uniformity within  $\sim 1\%$  over 20 cm diameter. The maximum ion current density is approximately 11.5 mA/cm $^2$ . The impurities from the wall material (Al) have not been detected, by means of XPS. Concerning the life time, we found no damage after the continuous operation for 100 hr with microwave power of 600 W. This ECR plasma source is ULSI production worthy and is widely applicable to both etching and deposition processing.

In chapter one, early types of ECR plasma sources which use bulky coil magnets needed the huge electric power were described. In order to solve these problems, large-area ECR plasma sources with a simple structure employing a combination of permanent magnets and slot antenna were developed. Highly dense ECR plasma sources using a slot antenna where the uniform densities are realized are requested for next generation 12-inch plasma processing applications. However, there has been not yet reported on the plasma

source because the optimization of a slot antenna for 12-inch processing is very difficult and there is the serious problem where a slot antenna locally radiates microwave power and then generates the local breakdown.

### References

- [1] T. D. Mantei and T. E. Ryle: *J. Vac. Sci Technol. B* **9** (1991) 29.
- [2] R. Hidaka, T. Yamaguchi, N. Hirotsu, T. Ohshima, R. Koga, M. Tanaka and Y. Kawai : *Jpn. J. Appl. Phys.* **32** (1993) 174.
- [3] Y. Ushigusa, A. Hatta, K. Murayama, Y. Yasaka and R. Itatani: *Proc. 10th Symp. On Plasma Processing (Osaka, Japan)* ed. Y. Watanabe (Division of Plasma Electronics, The Japan Society of Applied Physics) 1992.
- [4] S. Iizuka, T. Ono, Y. Nakagawa and N. Sato: *Proc. 10th Symp. On Plasma Processing (Osaka, Japan)* ed. Y. Watanabe (Division of Plasma Electronics, The Japan Society of Applied Physics) 1992
- [5] N.Shida, T.Inoue, T.Kokai, Y.Sakamoto, W.Miyazawa, S.Den and Y.Hayashi: *Jpn. J. Appl. Phys.* **32**(1993) L1635-L1637.
- [6] J. E. Stevens, Y. C. Haung, R. L. Jarecki and J. L. Cecchi: *J. Vac. Sci Technol. A* **10** (1992) 1207.
- [7] M. Geisler, J. Kieser, E. Rauchle and R. Wilhelm: *J. Vac. Sci Technol. A* **8** (1990) 908.
- [8] Shinriki Teii: *PLASMA KISOKOUGAKU* published by UTIDA ROKAKUHO-PUBLISHING, CO., LTD.

### Chapter 3. Comparison of Fluorocarbon Radical Kinetics in Large-area Permanent Magnet and Electromagnet Electron Cyclotron Resonance Plasma Sources

#### 3.1 Introduction

The key requirement for today's etching processes is high selectivity of the different materials, and this has proven to be the parameter that is most difficult to control. Selectivity is determined by plasma-material interaction processes, and hence an understanding of the plasma chemistry and the kinetics involved is vital for achieving the required selectivity. For selective etching of silicon dioxide ( $\text{SiO}_2$ ) on silicon (Si), various parent gases such as  $\text{CHF}_3$ ,  $\text{CF}_4$ ,  $\text{C}_2\text{F}_6$  and  $\text{C}_4\text{F}_8$  have been employed.[1-4] Moreover, it has been suggested that control of the fluorocarbon radical densities and fluorine (F) atom density will lead to higher selectivity.[1] Experimentally, it has been found that there are vast differences in plasma chemistry resulting from differences in not only source gas but also the nature of the discharge source itself.[5-11] There are, therefore, two challenges which must be met if the required selectivity for the next-generation devices is to be attained. The first is in the design and development of a compatible ECR plasma source.[12,13] In particular, consideration should be given to confinement of electrons to produce a high-density plasma and diffusion characteristics in the downstream region to ensure a uniform low-energy plasma. Problems encountered in the case of conventional electromagnet ECR plasma sources, such as large losses to the chamber walls and high electron temperatures due to a divergent magnetic field, which have made it difficult to control etch selectivity at high etch rates need to be addressed. The second challenge is to study the plasma chemistry, especially the behavior of fluorocarbon radical species, and to quantify these radical species.

In this chapter, diagnostics of fluorocarbon radical species in a large-area permanent magnet (300D-ECR) and an electromagnetic coil (C-ECR) ECR etching plasma employing  $\text{CF}_4$  and  $\text{C}_4\text{F}_8$  gases are described.  $\text{C}_4\text{F}_8$  gas was chosen because high selectivity of  $\text{SiO}_2/\text{Si}$  is reported to be easily obtained using a high-density plasma with a low-pressure operating.

Non-intrusive infrared diode laser absorption spectroscopy (IRLAS) and actinometric measurement techniques are used in evaluating the performance of the permanent magnet ECR plasma source and in investigating the kinetic processes associated with etching plasma chemistry. In particular, for  $\text{C}_4\text{F}_8$  plasma, enhanced CF and  $\text{CF}_2$  radical densities which afford higher selectivity in the etching of  $\text{SiO}_2$  on Si are discussed.

#### 3.2 Experimental

##### 3.2.1 Experimental Set-up

Figure 3.1 shows a schematic diagram of the two experimental plasma sources investigated in this study. The 300D-ECR plasma source has been described in detail in the previous chapter. The C-ECR source is shown in Fig. 3.1(b). It consists of two electromagnetic coils arranged symmetrically around the plasma discharge chamber. The coils are movable in the axial direction, but for the experiments described here, they are positioned at a fixed 6 cm interval. The upper coil current was 150A and the lower 100 A. This arrangement provides a diverging magnetic field with the magnetic flux density decreasing gradually from the ECR zone that extracts the plasma into the process chamber. The process chamber is the same as that shown in Fig. 3.1(a). The ECR zone is positioned at 10 cm from the top of the plasma discharge chamber. The magnetic field at the substrate was measured to be 50 G. Plasma is excited by microwave of 2.45 GHz that is fed into the plasma discharge chamber through a dielectric window.

##### 3.2.2 Infrared Diode Laser Absorption Spectroscopy for Measurement of $\text{CF}_x$ Radical Densities

The details of the IRLAS measurement technique are given elsewhere.[7] Briefly, a tunable infrared laser diode is used as the source and a White-type multiple reflection cell is used to increase the absorption length of the IRLAS laser beam which has a spatial resolution of ~3-4 mm. The infrared laser is oscillated by sending the electric current to the p-n junction of the diode cooled by helium. The infrared laser beam is modulated at 400 Hz by a chopper

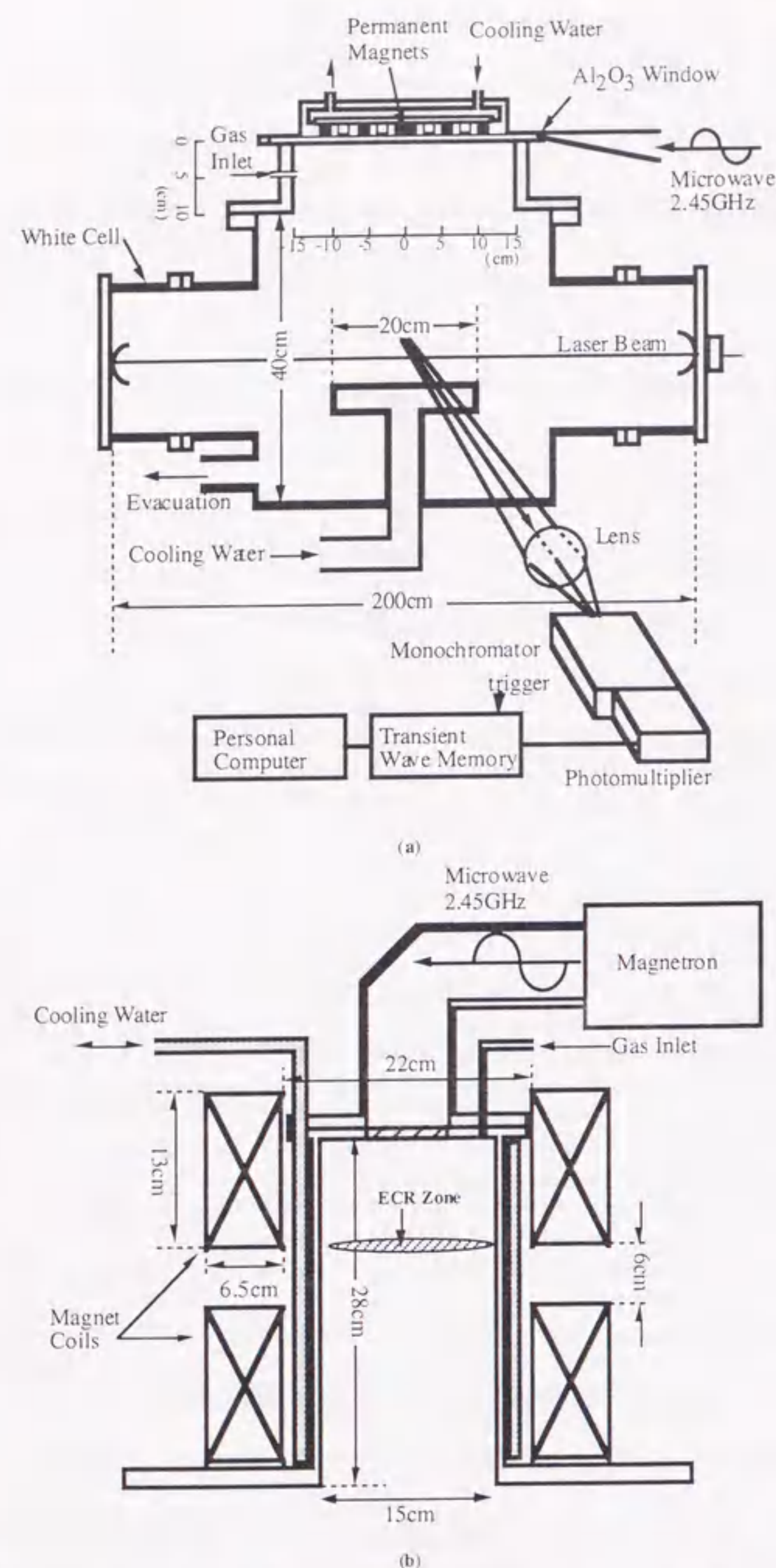


Fig. 3.1 Schematic diagram of the 300D-ECR plasma source and IRLAS measurement setup (a) and the conventional electromagnet ECR plasma source.

and the laser frequency was scanned by varying the current. The laser beam passes through a NaCl window into the discharge chamber. The laser beam made 12 and 40 passes when measuring the CF and CF<sub>2</sub> radicals, respectively. The laser beam intensity was detected by a mercury-cadmium-telluride (MCT) detector. The signal was detected by a phase-sensitive lock-in amplifier to improve the signal to noise ratio (S/N). The wavenumbers of the observed spectra were confirmed using the spectra of NO<sub>2</sub> as a reference gas. The absorption intensities were obtained by dividing the heights of the spectra by the intensities of the laser beam without absorption. The procedures used to calculate the CF<sub>x</sub> (x=1,2) radical densities are complex and have been described elsewhere.[7] Prior to measurement, the surfaces of the chamber were aged by exposure to fluorocarbon plasma for 2 hours. In all experiments, the pressure and gas flow rate were maintained constant at 0.4 Pa and 15 sccm, respectively. The measurement results discussed here were obtained at a position 20 cm downstream, that is a typical processing position.

### 3.2.3 Actinometry for Measurement of F Atom Density

Actinometric technique was first introduced by Coburn and Chen.[17] Actinometric techniques were used to estimate the F atom density in both CF<sub>4</sub> and C<sub>4</sub>F<sub>8</sub> plasma. The emission lines that were monitored were the 703.7 nm [3s(2P<sub>2</sub>)-3p(2P<sub>2</sub>)] transition of F\* and the 750.4 nm [4s'(1/2)<sup>0</sup>-4p'(1/2)] transition of Ar\*. Signals were measured using a monochromator and photomultiplier tube. The measured signals represent the spatially averaged signal from the bulk of the plasma. For each measurement, a transient emission waveform and the peak emission intensity correspond to the peak of this transient waveform were measured.

By adding a small amount of Ar as an actinometer to the plasma, it is possible to obtain an estimation as to the F atom density in the plasma. Argon is used because it has an electron excitation cross section similar to F atom. The measurement is valid by assuming that the F atom is created by single electron impact ionization from the ground state and

relaxed by photoemission. The F and Ar atom emission intensities ( $I_{F^*}$ ,  $I_{Ar^*}$ ) are given as follows,

$$I_{F^*} \propto k_F n_e [F] \quad (3.1)$$

$$I_{Ar^*} \propto k_{Ar} n_e [Ar] \quad (3.2)$$

where  $k_F$  and  $k_{Ar}$  are the excitation rate constants of F and Ar atoms, respectively,  $n_e$  is electron density, and  $[F]$  and  $[Ar]$  are the F and Ar atom densities, respectively. Jenq et al.[14] reported that the F atom density was estimated using the following relationship,

$$[F] = 0.56[Ar] (I_{F^*} / I_{Ar^*}), \quad (3.3)$$

where  $I_{F^*}$  and  $I_{Ar^*}$  are the peak emission intensities of F and Ar, respectively. In the experiments described here, addition of 5% Ar gas as an actinometer was used, and a total pressure was 0.4 Pa. Although many assumptions are made in the above equation, the error may be as large as a factor of two.[14] Therefore, it still enables us to estimate the F atom density enough precisely in an order of magnitude which is very useful in better understanding the dissociation kinetics described below.

For the measurement of ground-state F atom density, actinometry has been widely applied in rf discharge  $CF_4$  plasma.[17] The validity of actinometry in rf discharge  $CF_4$  plasma has been confirmed by Gottscho and Donnelly.[21] They have investigated the  $F^*$  and  $Ar^*$  emission line shape in the plasma and indicated that the  $F^*$  and  $Ar^*$  transitional temperatures were virtually identical. They concluded that  $F^*$  atom was created by single electron impact excitation from the ground-state F atom and so Ar can be used as an actinometer in determining F atom density.

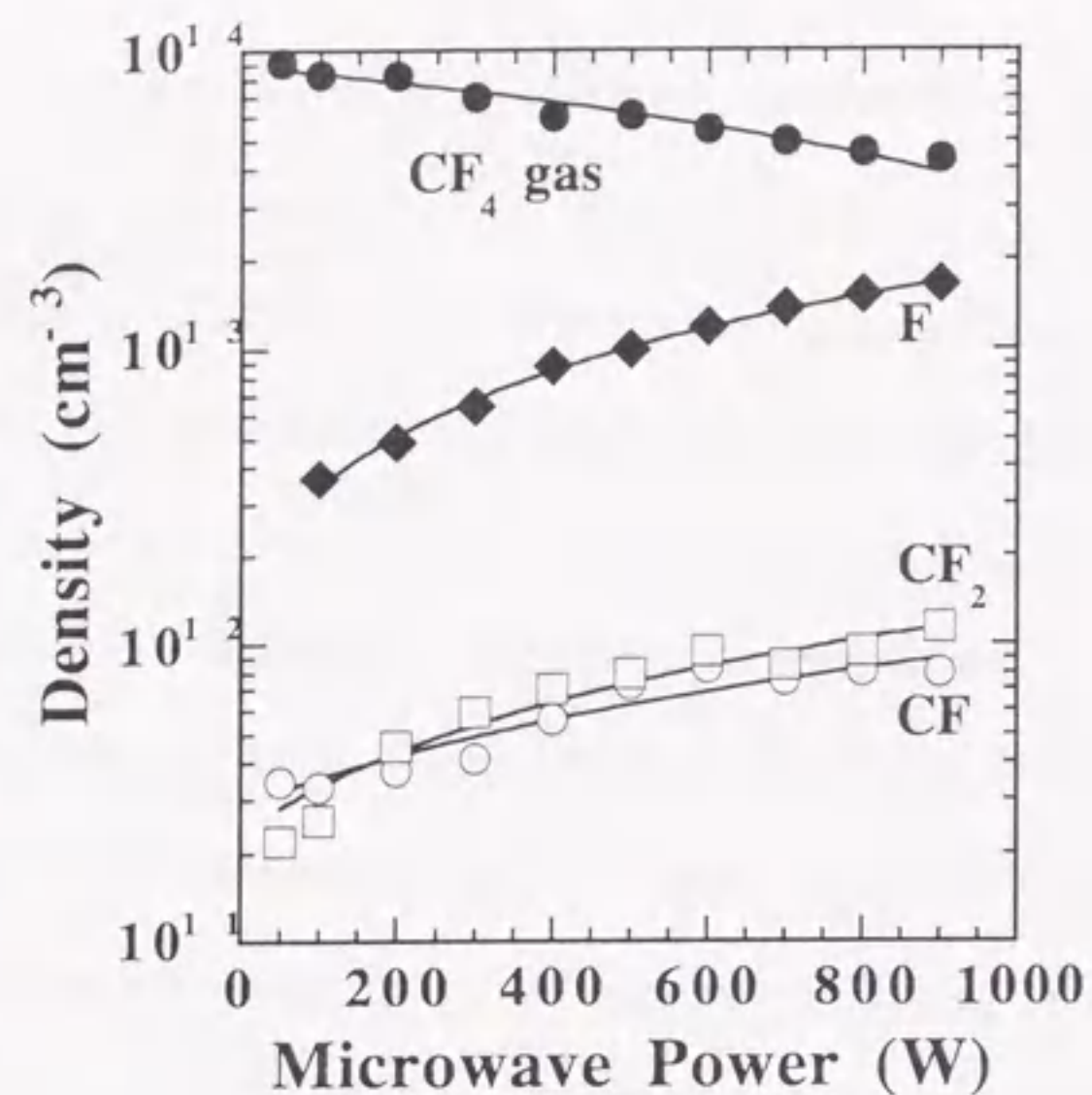
### 3.3 Results

#### 3.3.1 $CF_x$ Radical Densities and F Atom Density in $CF_4$ Plasma

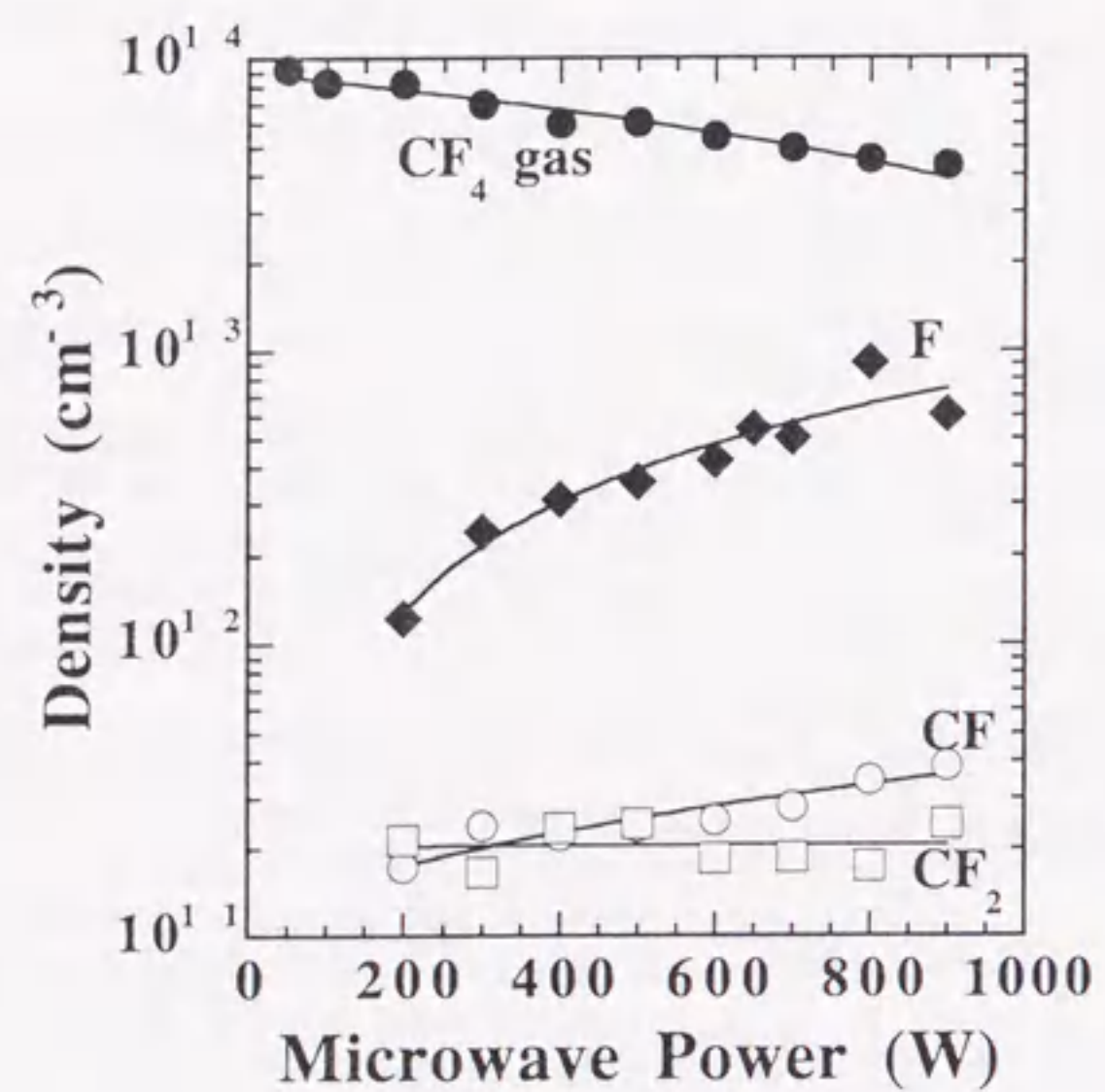
As a preliminary investigation of this permanent magnet ECR plasma source, diagnostics of fluorocarbon radicals in the now well studied  $CF_4$  plasma were undertaken. In Fig. 3.2, the F atom density calculated from eq. (3.3) and the  $CF_x$  ( $x=1,2$ ) radical densities measured by IRLAS are shown as a function of input microwave power. It can be seen from Fig. 3.2(a) that the dominant species in the 300D-ECR plasma is F atoms, with the densities of the  $CF_x$  ( $x=1,2$ ) radical species being an order of magnitude lower than that of the F atom density. Both the  $CF_2$  radical density and F atom density increase monotonically with increasing microwave power. This trend of increasing radical density with increasing power implies increasing dissociation of the parent  $CF_4$  gas, and is consistent with the dissociation of  $CF_4$  gas as shown in Fig. 3.2(a) and other reports in the literature.[16] The CF radical density increases with increasing microwave powers from 200 and 600W but tends towards saturation at both low and high microwave powers. Similar results were observed for the C-ECR plasma source. It can be seen from Fig. 3.2(b) that the dominant species is F atoms as the densities of the  $CF_x$  ( $x=1,2$ ) radical species being of an order of magnitude lower. The main difference is due to the low rate of change of the  $CF_x$  ( $x=1,2$ ) radical species in the case of the C-ECR plasma. The sum of F atom and  $CF_x$  ( $x=1,2$ ) radical densities is not agree with the dissociated parent  $CF_4$  gas density, because of another species produced in the plasma, and secondary reactions on the chamber wall.

For more detailed understanding of the dissociation processes which take place here, it is necessary to consider plasma creation and loss mechanisms along with plasma parameters such as  $n_e$ . If it is assumed that the main creation mechanism is that of electron impact dissociation and the main loss mechanism is recombination at the chamber wall,





(a)



(b)

Fig. 3.2 Absolute  $CF_x$  ( $x=1,2$ ) radical densities and F atom density in  $CF_4$  plasma as a function of input microwave power for (a) the 300D-ECR plasma source and (b) the C-ECR plasma source. The  $CF_4$  gas molecule density is also shown.

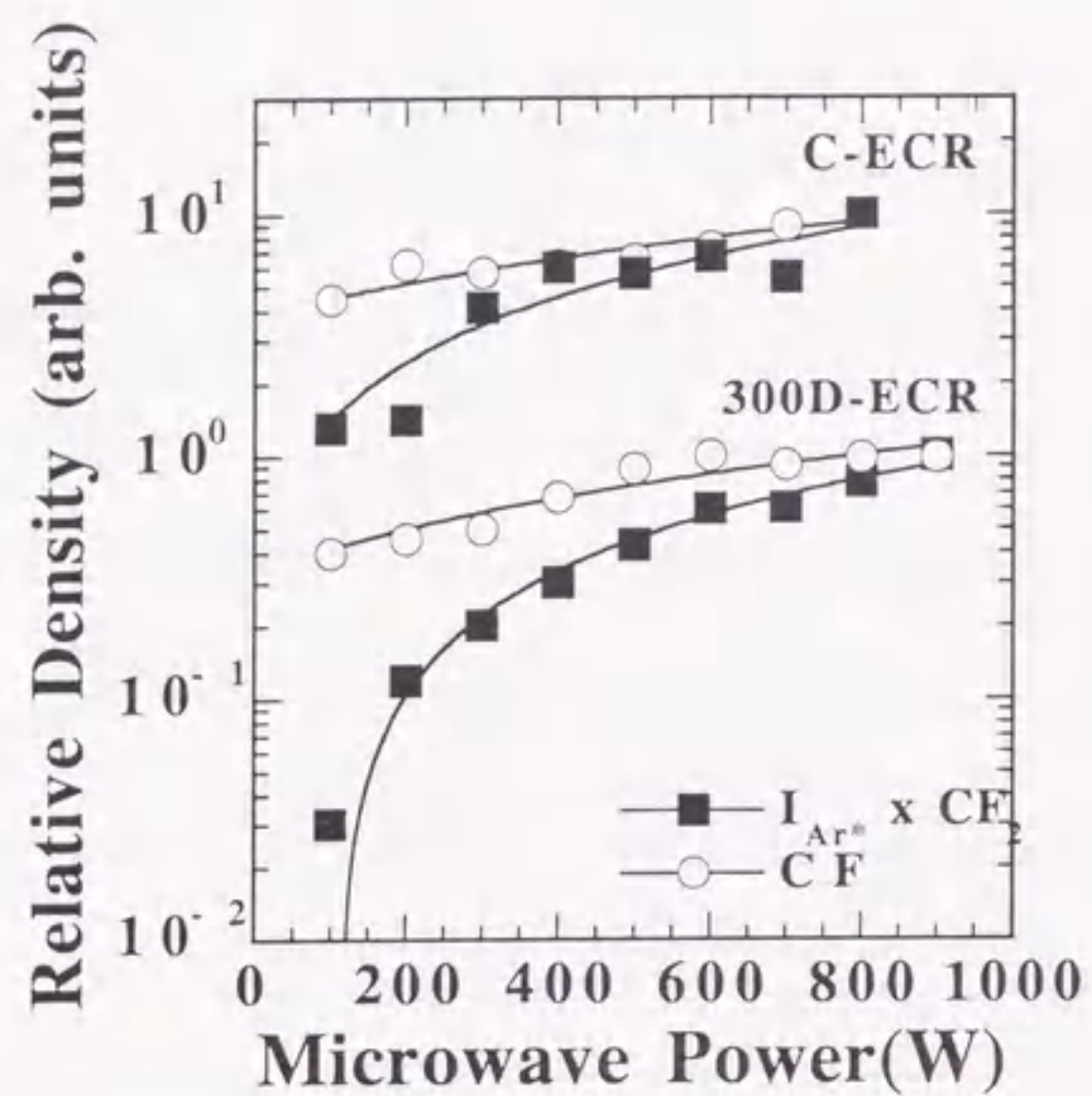
we can obtain the steady-state rate equation

$$kn_e[CF_4] = 1/\tau[CF_x] \quad x=1,2, \quad (3.4)$$

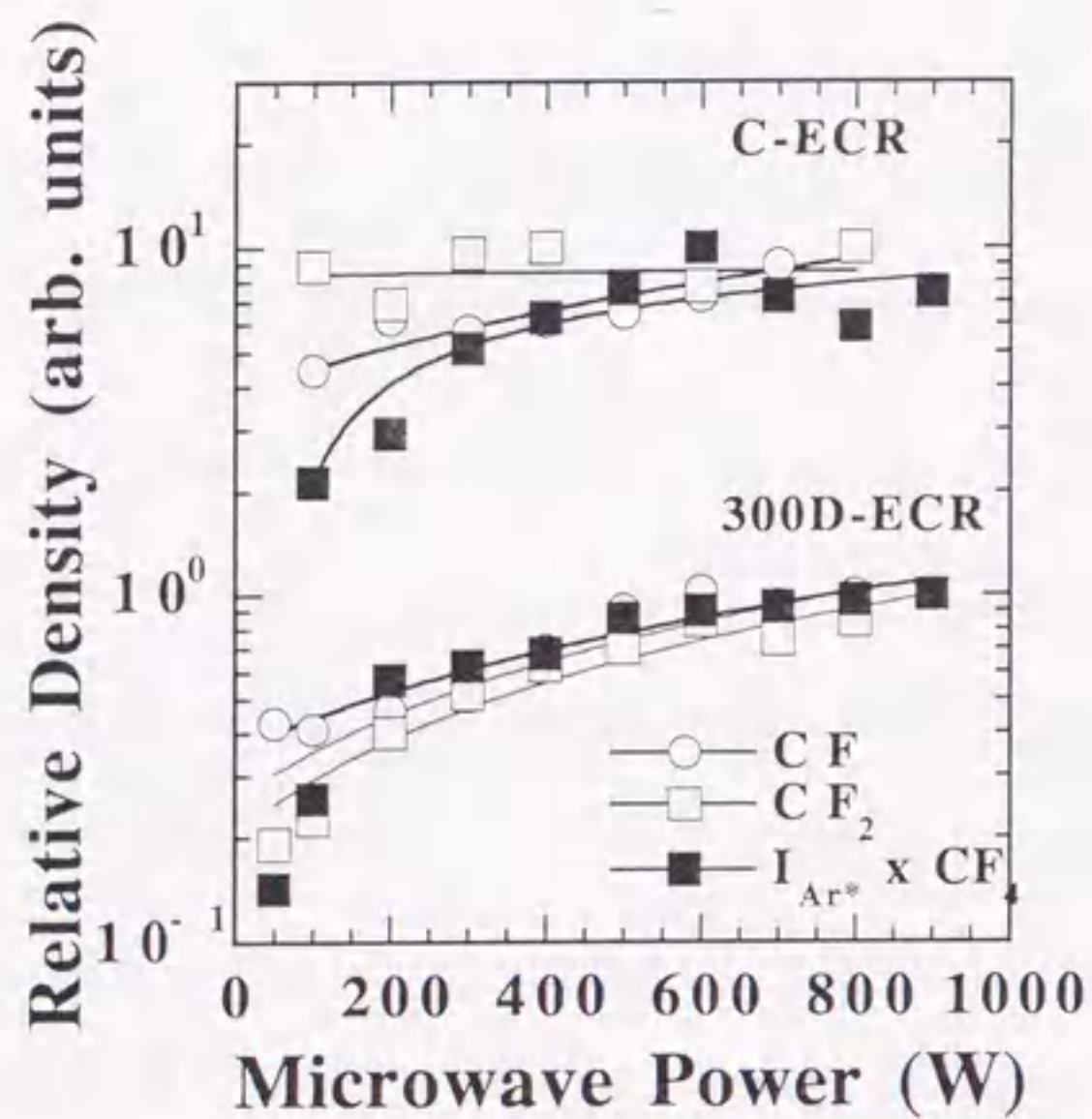
where  $k$  is the excitation rate constant and  $\tau$  is the radical species lifetime. Since  $\tau$  is a constant,[9] knowledge of the power dependence of  $kn_e$  will provide a means by which to study further the dissociation mechanisms. A qualitative estimation of  $kn_e$  can be obtained by measuring the optical emission intensity of an argon radical line ( $I_{Ar^*}$ ) in a  $CF_4$  plasma containing 5% Ar. [17] Then eq. (3.4) can be rewritten as

$$I_{Ar^*}[CF_4] \propto [CF_x] \quad x=1,2. \quad (3.5)$$

This method of qualitative analysis has been used in analysis of  $CHF_3$  time modulated electromagnet ECR plasma and is described in more detail by Takahashi *et al.* [8,9] They reported that CF radicals are generated mainly by the electron impact dissociation of  $CF_2$  radicals in the ECR  $CHF_3$  plasma. Therefore, for clarification of the dissociation mechanism responsible for the generation of CF radicals, eq. (3.5) was applied to the  $CF_2$  radical densities in Fig.3.2(a). The results are shown in Fig. 3.3(a), in which the relative CF and calculated  $CF(\propto I_{Ar^*}[CF_2])$  radical densities of both the 300D-ECR and C-ECR plasma sources are plotted. The densities are normalized to unity at 900 W and it can be seen that the power dependencies of the measured CF and calculated CF radical densities are quite different, implying that the main dissociation process responsible for the generation of CF radicals is not dissociation of  $CF_2$ . In Fig. 3(b), the relative CF and  $CF_2$  and  $I_{Ar^*}[CF_4]$  radical densities are plotted. It can be seen here that the power dependencies are very similar suggesting direct dissociation of the parent gas  $CF_4$  resulting in the production of CF and  $CF_2$  radical species.



(a)



(b)

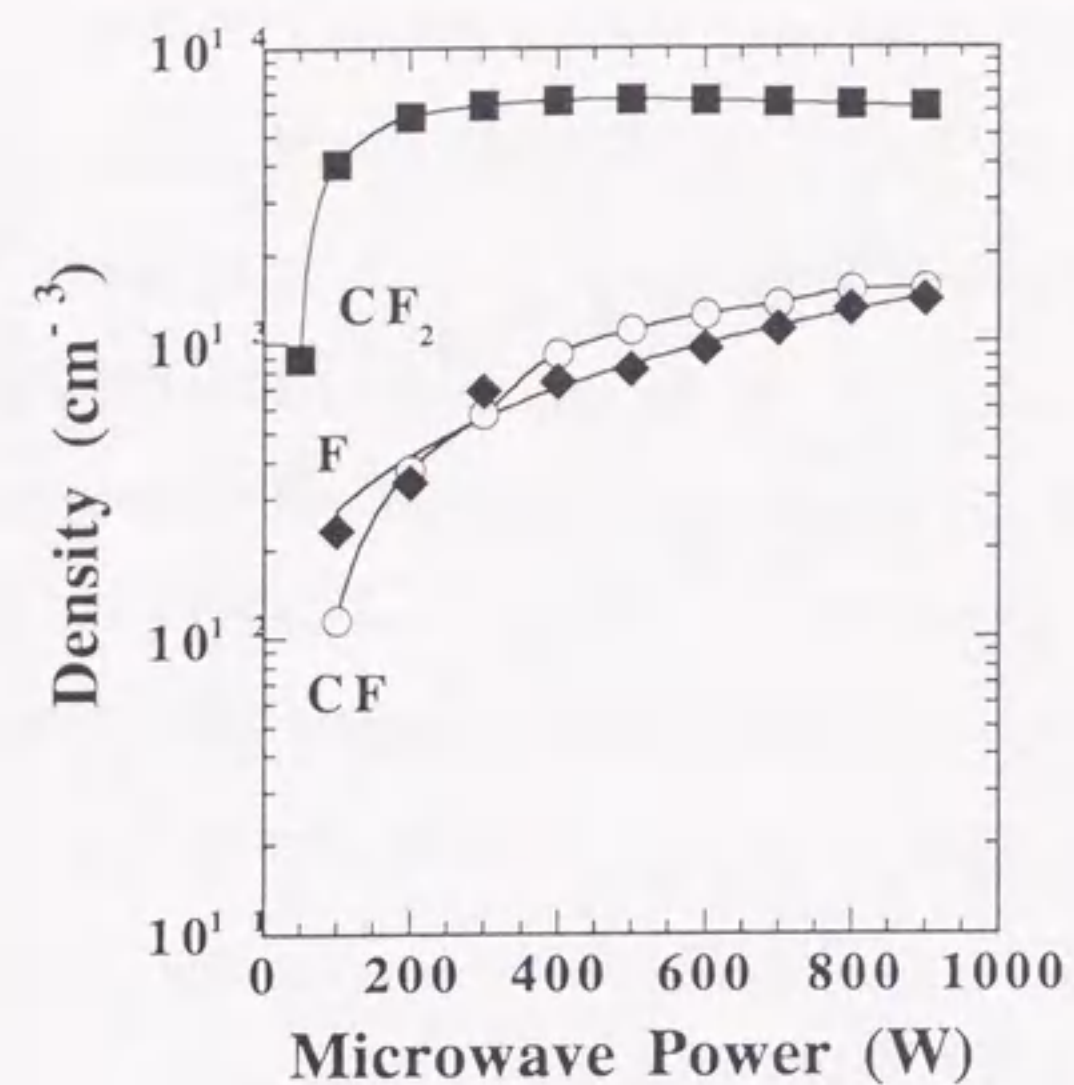
Fig. 3.3 Relative radical densities in  $CF_4$  plasma as a function of input microwave power for both the 300D-ECR and C-ECR plasma sources. The  $I_{Ar^*}CF_2$  intensity (a) and  $I_{Ar^*}CF_4$  intensity (b) are calculated using actinometric techniques with eq. (3.5).

### 3.3.2 $CF_x$ Radical Densities and F Atom Density in $C_4F_8$ Plasma

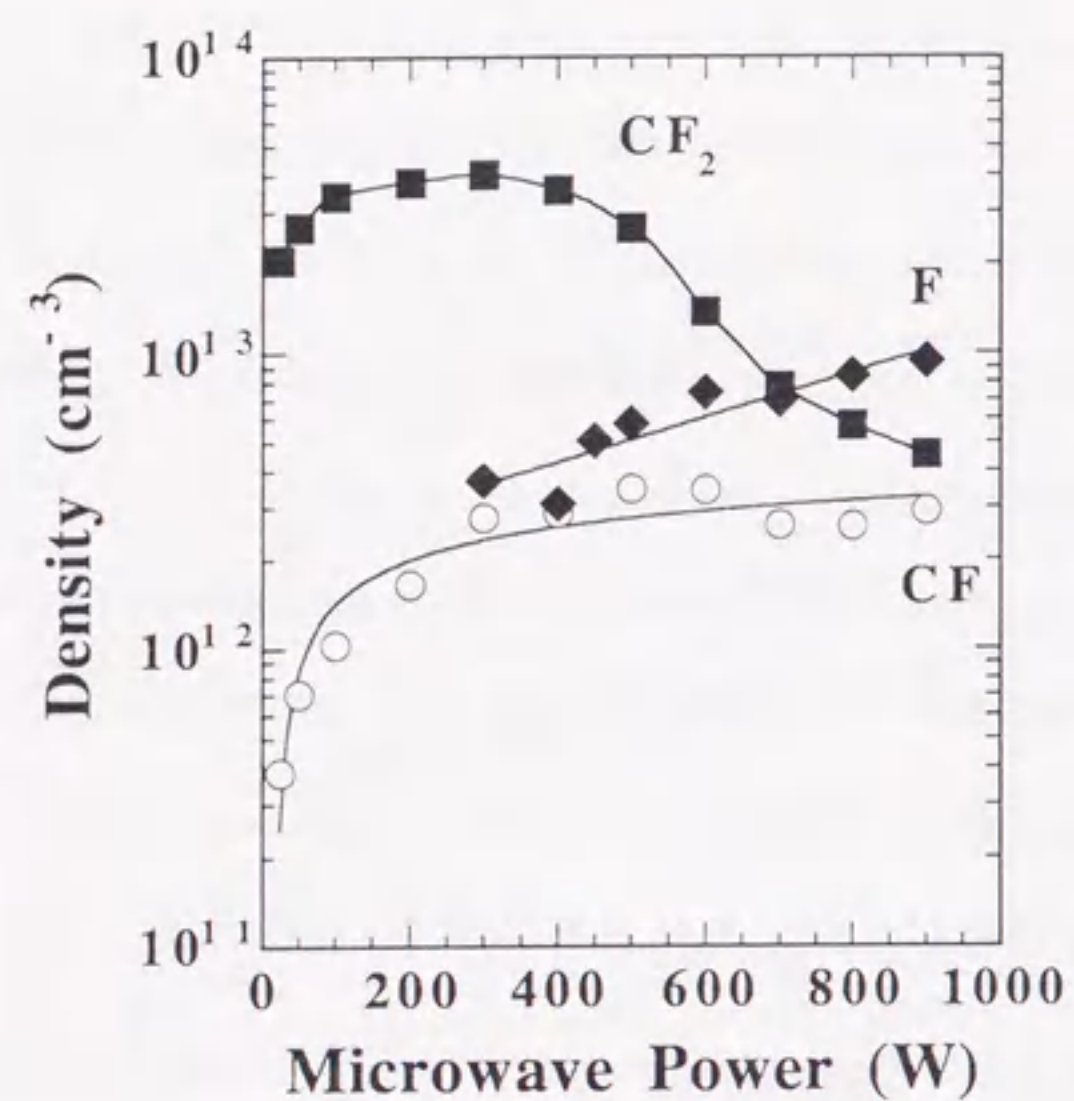
In Fig. 3.4 for both the 300D-ECR and C-ECR plasma sources, the  $CF_x$  ( $x=1,2$ ) radical densities and the F atom density for  $C_4F_8$  ECR plasma as a function of input microwave power are shown. In the case of the 300D-ECR plasma (Fig. 3.4(a)) the dominant species is  $CF_2$  radicals which exhibit an abrupt density increase with increasing microwave power up to 400 W. Both the CF radical and relative F atom densities are of an order of magnitude less than the  $CF_2$  radical density and display a rather monotonic increase with increasing microwave power. It should be noted that the F atom densities for both  $C_4F_8$  and  $CF_4$  ECR plasma at approximately  $10^{13} \text{ cm}^{-3}$  are similar. However, compared to  $CF_4$  plasma, the  $CF_2$  radical density and the CF radical density for  $C_4F_8$  plasma is greater by two orders of magnitude and by at least one order of magnitude, respectively.

The most interesting point to note about these results is that when compared to the C-ECR plasma source the microwave power dependencies of the densities of the CF and  $CF_2$  radicals in  $C_4F_8$  plasma are dramatically different. In the case of the C-ECR plasma, the dominant species at low power are also  $CF_2$  radicals. However, the  $CF_2$  radical density decreases with increasing microwave power above 400 W. The CF radical density displays an abrupt density increase with increasing microwave powers up to 400 W saturating at higher powers. The relative F atom density is an order of magnitude less than the  $CF_2$  radical density and display a rather monotonic increase with increasing microwave power. Similar to the 300D-ECR, the F atom densities for both  $C_4F_8$  and  $CF_4$  ECR plasma are approximately  $10^{13} \text{ cm}^{-3}$ . However, compared to  $CF_4$  plasma, the  $CF_2$  radical density and the CF radical density for  $C_4F_8$  plasma is greater by at least one order of magnitude.

For clarification of the dissociation mechanism responsible for the generation of CF radicals in  $C_4F_8$  plasma, eq. (3.5) was applied to the  $CF_2$  radical densities in Fig. 3.4. In the case of  $C_4F_8$  gas, absorption due to the  $C_4F_8$  molecules is difficult to determine due to overlap of absorption from unknown molecular products in the plasma. The results are



(a)



(b)

Fig. 3.4  $CF_x$  ( $x=1,2$ ) radical densities and F atom density in  $C_4F_8$  plasma as a function of input microwave power for (a) the 300D-ECR plasma source and (b) the C-ECR plasma source.

shown in Fig. 3.5, in which the relative CF and calculated CF ( $\propto I_{Ar^*}[CF_2]$ ) radical densities are plotted. The densities are normalized to unity at 900 W. It can be seen in Fig. 3.5 that for the 300D-ECR plasma, the power dependencies of the CF and calculated CF radical densities are quite similar, implying that the main dissociation process responsible for the generation of CF radicals is dissociation of  $CF_2$  radical. A similar proposal has been used to explain radical kinetics in  $C_3F_8$  plasma[19] and a conventional electromagnet  $C_4F_8$  ECR plasma.[10] It is assumed that the CF radical is formed through electron impact dissociation of the  $CF_2$  radicals as follows.



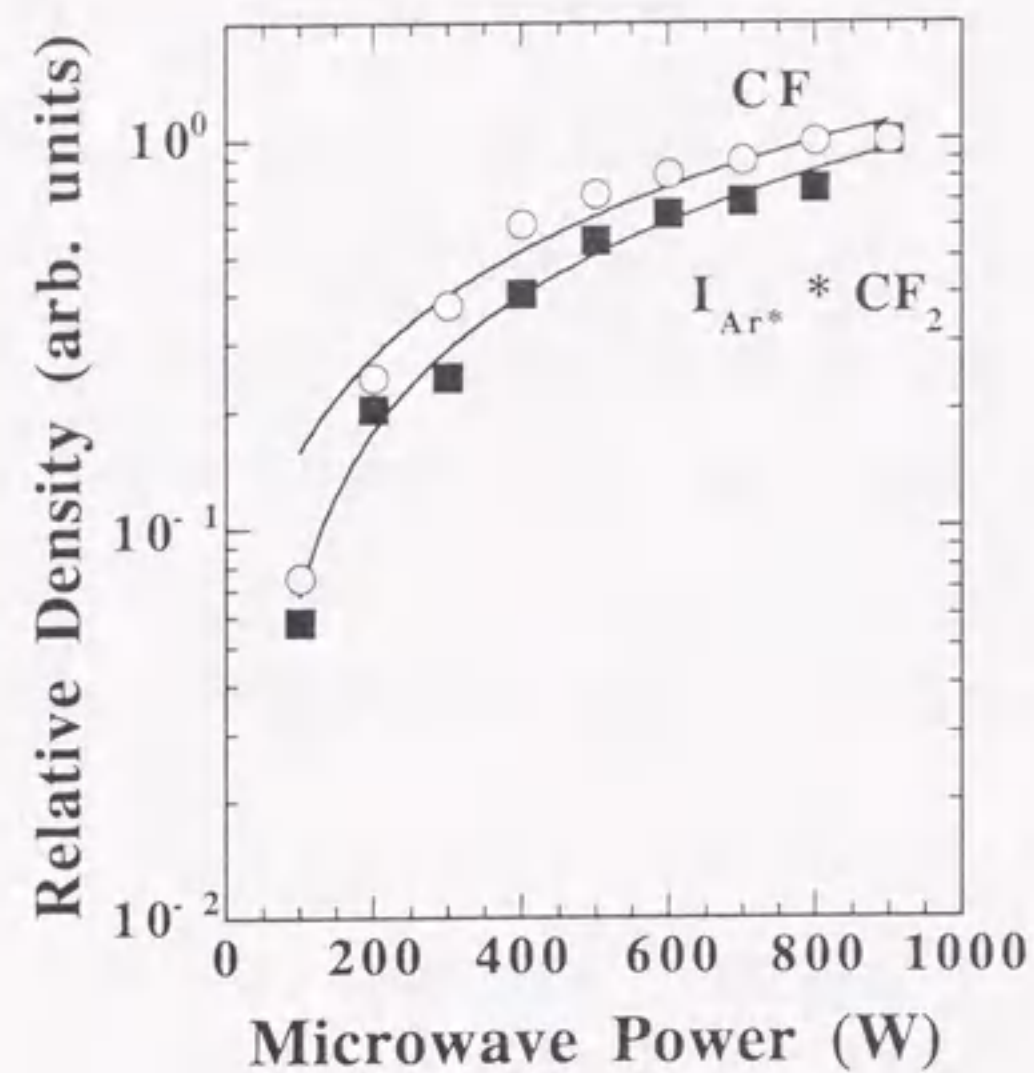
The balance equation of CF is given by

$$k_1 n_e [CF_2] = 1/\tau_{CF} [CF] \quad (3.7)$$

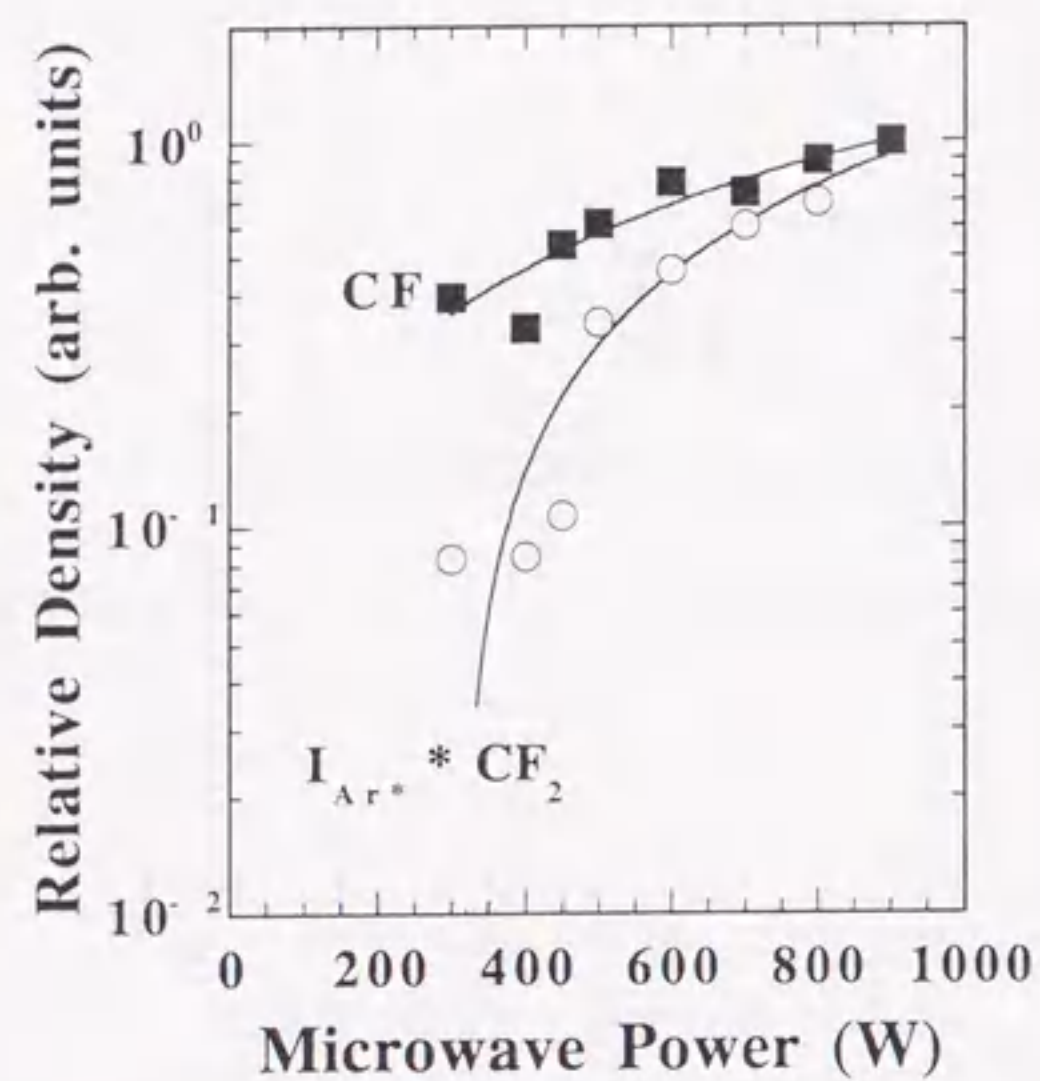
where  $k_1$  is the rate coefficient for reaction (3.6) and  $\tau_{CF}$  is the life time of CF radical. When  $k_1 n_e$  is assumed to be corresponding to  $k_{Ar^*} n_e$ , the CF radical density is given by

$$I_{Ar^*} [CF_2] \propto [CF]. \quad (3.8)$$

It can be seen in Fig. 3.5 that for the 300D-ECR plasma, dependencies of the CF and calculated CF radical densities by using (3.8) on power are quite similar. This fact indicates that the main process of the generation of CF radicals comes from the dissociation of  $CF_2$  radical. A similar proposal has been used to explain the radical kinetics in  $C_3F_8$  plasma[19] and  $C_4F_8$  ECR plasma with a conventional electromagnet.[10]



(a)



(b)

Fig. 3.5 Relative radical densities in  $C_4F_8$  plasma as a function of input microwave power for both the 300D-ECR and C-ECR plasma sources. The  $I_{Ar^*} * CF_2$  intensity is calculated from actinometric techniques using equation (3.8) described in the text.

These dissociation kinetics are different from those observed for  $CF_4$  gas where generation of both CF and  $CF_2$  was found to result from direct electron impact dissociation of the parent gas, that is,  $CF_4$ . These results are also different from those observed for the C-ECR  $C_4F_8$  plasma.

### 3.3.3 Life Time of CF and $CF_2$ Radicals

Figure 3.6 shows the time decay of the density of both CF and  $CF_2$  radicals in both the 300D-ECR and C-ECR  $C_4F_8$  plasma. The decay is measured by measuring the decrease in radical density after the plasma has been turned off, that is, in the afterglow. The decay curves are normalized to unity at time  $t=0$  s. The decay in all cases is exponential. The experimental data is fitted by a single exponential decay of the form  $I \propto \exp\{-t/\tau\}$ , where  $I$  and  $\tau$  are the radical density and radical lifetime, respectively. The solid lines in Fig. 3.6 are the calculated best fit lines based on the single exponential to the changes in radical density of both CF and  $CF_2$  radicals. From analysis of changes in the radical density, for both the 300D-ECR and C-ECR plasma sources, the density decay time of CF radicals is one order of magnitude shorter than that of  $CF_2$  radicals. For the 300D-ECR plasma source (Fig. 3.6(a)), the measured lifetimes of the CF and  $CF_2$  radicals are 0.05s and 0.5s, respectively. In the case of the C-ECR plasma source (Fig. 3.6(b)), the measured lifetimes of the CF and  $CF_2$  radicals are 0.03s and 0.17s, respectively. These order of decay times are consistent with other data in the literature,[7-9] and suggest that the electron trapping in magnetic mirror field of the 300D-ECR source is responsible for the longer lifetimes. The single exponential decay is characteristic of loss through reactor wall interaction processes.[18] It should be noted however, that for C-ECR plasma, both the CF and  $CF_2$  decay was faster than that of the 300D-ECR plasma, suggesting that radical lifetimes are dependent on reactor design.

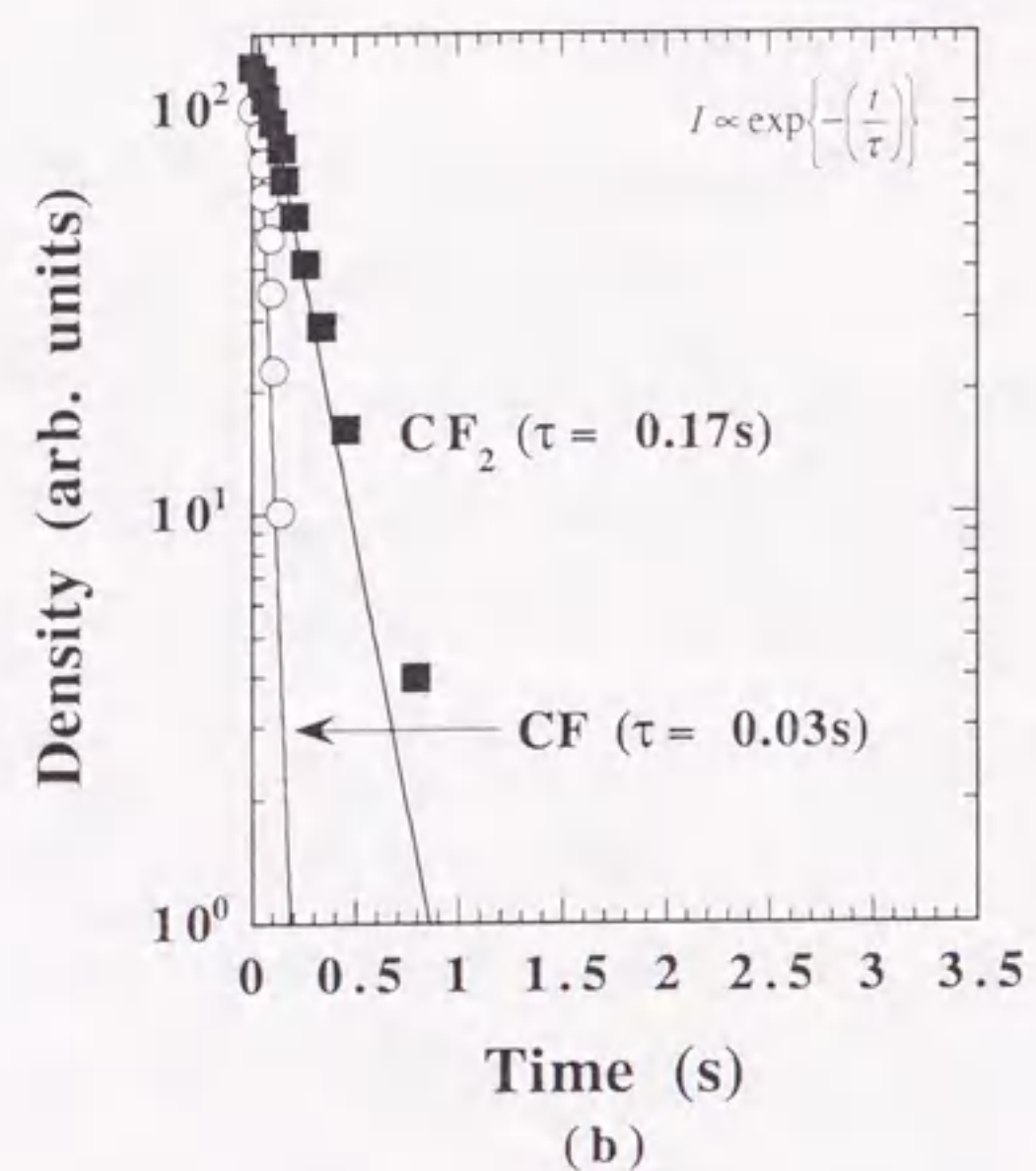
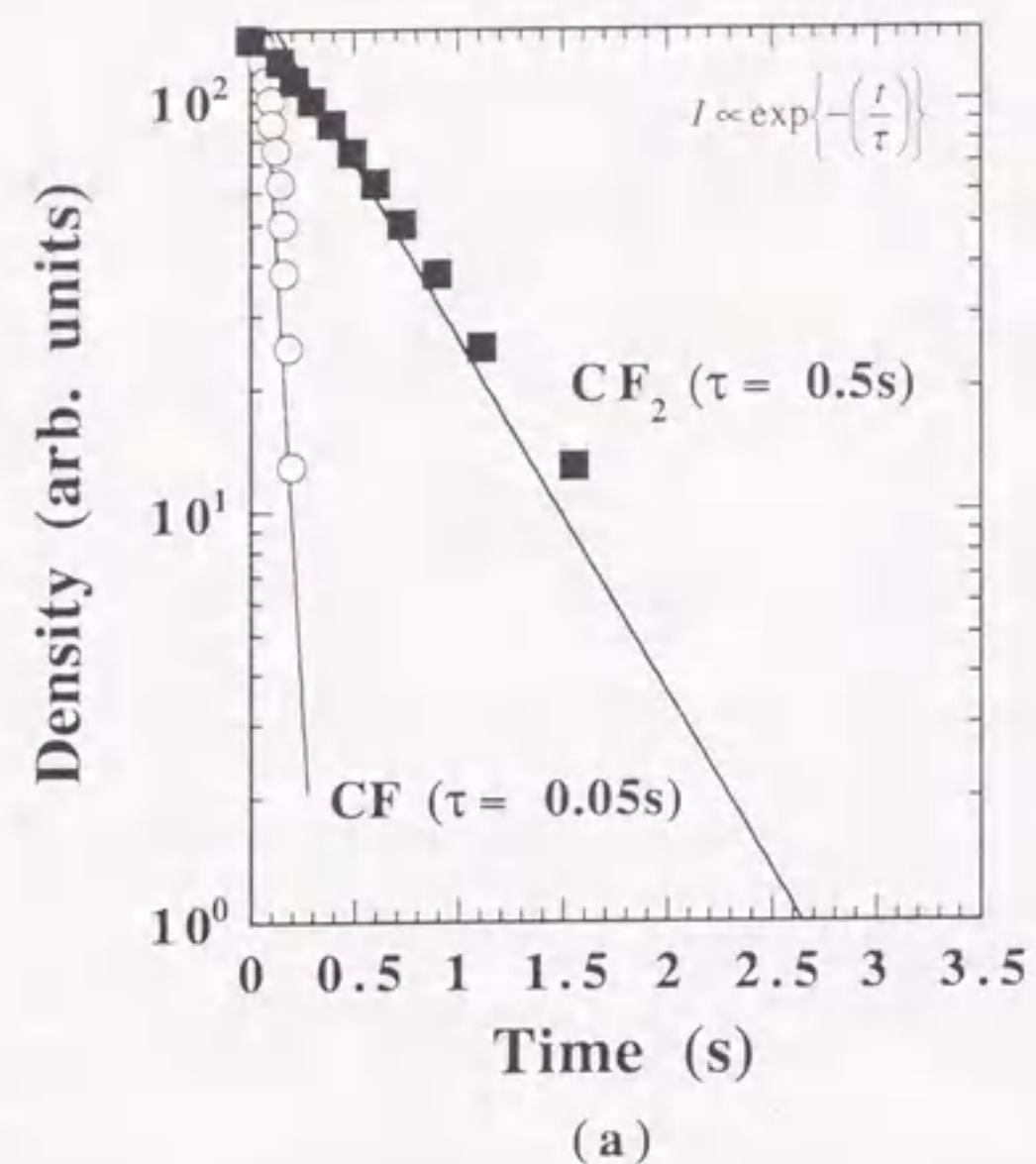


Fig. 3.6 Decay curves of the CF and CF<sub>2</sub> radical densities in the afterglow of C<sub>4</sub>F<sub>8</sub> plasma for (a) the 300D-ECR plasma source and (b) the C-ECR plasma source.

### 3.4 Discussions

#### 3.4.1 Dissociation Kinetics in Low-temperature High-density ECR Plasma

The above results can be qualitatively explained in terms of dissociation kinetics in low-temperature high-density ECR plasma. Generally the average  $T_e$  value associated with ECR plasma is less than the threshold energy for dissociation of CF<sub>4</sub> molecules. However, electrons have a distribution of energies and it is the high-energy tail of this distribution which produces the dissociation. In the case of the CF<sub>4</sub> ECR plasma results shown in Fig. 3.2, the CF<sub>x</sub> ( $x=1,2$ ) radical and F atom densities all increase linearly. The flux of CF<sub>x</sub> ( $x=1,2$ ) radicals in this case is simply determined by an increase in the electron density with increasing microwave power. This increase in the electron density with increasing microwave power is consistent with the linear increase in the intensity of the Ar\* emission line. As this argument is only qualitative, quantitative studies of electron kinetics are now under way to aid in the understanding of the details of these plasma production mechanisms in ECR fluorocarbon plasma. This trend was similar for both the 300D-ECR plasma source and the C-ECR plasma source.

In the case of C<sub>4</sub>F<sub>8</sub> ECR plasma results shown in Fig. 3.4, it was seen that the CF<sub>2</sub> radicals are dominant, which implies that the main dissociation mechanism in C<sub>4</sub>F<sub>8</sub> ECR plasma results in the formation of CF<sub>2</sub> radicals. Furthermore, in Fig. 3.5, it was seen that the CF radicals are produced mainly by dissociation of CF<sub>2</sub> radicals in the 300D-ECR plasma source. These results in 300D-ECR plasma are due to a low  $T_e$  value of the 300D-ECR plasma. From the thermochemical data, carbon to carbon (C-C) and carbon to fluorine (C-F) binding energies are estimated to be 3 eV and 4.8 eV, respectively. Since the C-C binding energy is much lower than the C-F binding energy, the C-C bond is preferentially dissociated by a low energy electron impact in 300D-ECR plasma and so a large amount of CF<sub>2</sub> radicals are produced from the electron impact dissociation of C<sub>4</sub>F<sub>8</sub> gas. Consequently, CF is produced with increase in collision probability of CF<sub>2</sub> with high energy electron. A similar model has been proposed to explain radical kinetics in C<sub>3</sub>F<sub>8</sub> plasma[19] and a

conventional electromagnet  $C_4F_8$  ECR plasma.[10] At high microwave power, the  $CF_2$  radical density saturates while the CF radical and F atom densities both increase. This is a result of increasing microwave power which results in increased dissociation of the C-F bonds.

The dissociation kinetics associated with the developed permanent magnet 300D-ECR plasma source developed in this study are explained qualitatively as follows.(see Fig.3.1 and Fig.2.1 in Chapter 2) The use of permanent magnets in alternating rings of polarity produces rings of closed magnetic fields of the basic mirror configuration. These localized mirror fields induce a thin sheet-like resonance zone 1.6 cm below the ceiling of the source, and act as a hot electron trap in which electrons are accelerated by curvature and gradient drift. This configuration with the parent gas being introduced just below the resonance zone produces a high-density plasma and an area where dissociation of the parent gas occurs at a high rate. Diffusion processes in the downstream region of this plasma source are controlled by particle diffusion due to an abrupt decrease of magnetic field. From these source characteristics, it can be seen that there are two main differences between the developed permanent magnet ECR source and conventional electromagnet ECR sources. The first is in the confinement mechanism in the discharge zone which produces a resonance zone very close to the point of microwave introduction. This allows for a very simple and compact source design with reduced losses to the surrounding source walls. The second difference is in the diffusion processes in the downstream region. In conventional electromagnet ECR plasma sources, the diverging magnetic field extracts and accelerates electrons in the downstream direction. Typically, the average electron temperature in our permanent magnet source is around 3 eV, which is considerably lower than values reported for conventional electromagnet ECR sources.[3] It is proposed that these differences in confinement and diffusion processes which result in a high-density plasma with low electron temperatures are responsible for the observed dissociation kinetics, in particular for  $C_4F_8$  ECR plasma. Due to low electron temperatures, an increase of the microwave power does not produce any appreciable dissociation of  $CF_2$  radicals, unlike in the case of conventional electromagnet

ECR plasma in which the divergence of the magnetic field in the downstream region results in a decrease of the  $CF_2$  radical density.

To summarize the above results, in Fig. 3.7 a schematic diagram depicting the main dissociation mechanisms associated with  $C_4F_8$  and  $CF_4$  ECR plasma is presented. In the case of  $C_4F_8$  ECR plasma, the large  $C_4F_8$  molecule is initially dissociated through breaking of the C-C bonds which have the lowest binding energy. From the experimental data, this dissociation results mainly in the production of  $CF_2$  which is then further dissociated into CF and F at higher microwave powers. Comparing the data from the 300D-ECR and C-ECR plasma sources and the binding energies shown in Fig. 3.7, it is reasonable to assume that, in the case of the 300D-ECR plasma source  $T_e$  is low. Moreover, increasing the microwave power does not produce any increase in  $T_e$  that would affect the dissociation process. On the other hand, it was seen that for the C-ECR plasma source, increase of the microwave power does produce different dissociation process that result in a decrease in the  $CF_2$  density at higher powers. The dissociation process of  $CF_4$  is more simple than that of  $C_4F_8$ , and from the results obtained, it is proposed that dissociation of the  $CF_4$  molecule proceeds with successive dissociation of  $CF_3$ ,  $CF_2$  and CF that results in an F density well in excess of the other species. On the basis of discussions above, it can be seen that both of the source design and gas chemistry are strongly connected resulting playing a very important role in developing plasma etch process, because there is a close relationship between dissociation kinetics of the parent gas and radicals, and the electron energy distribution in the plasma.

### Dissociation Mechanism

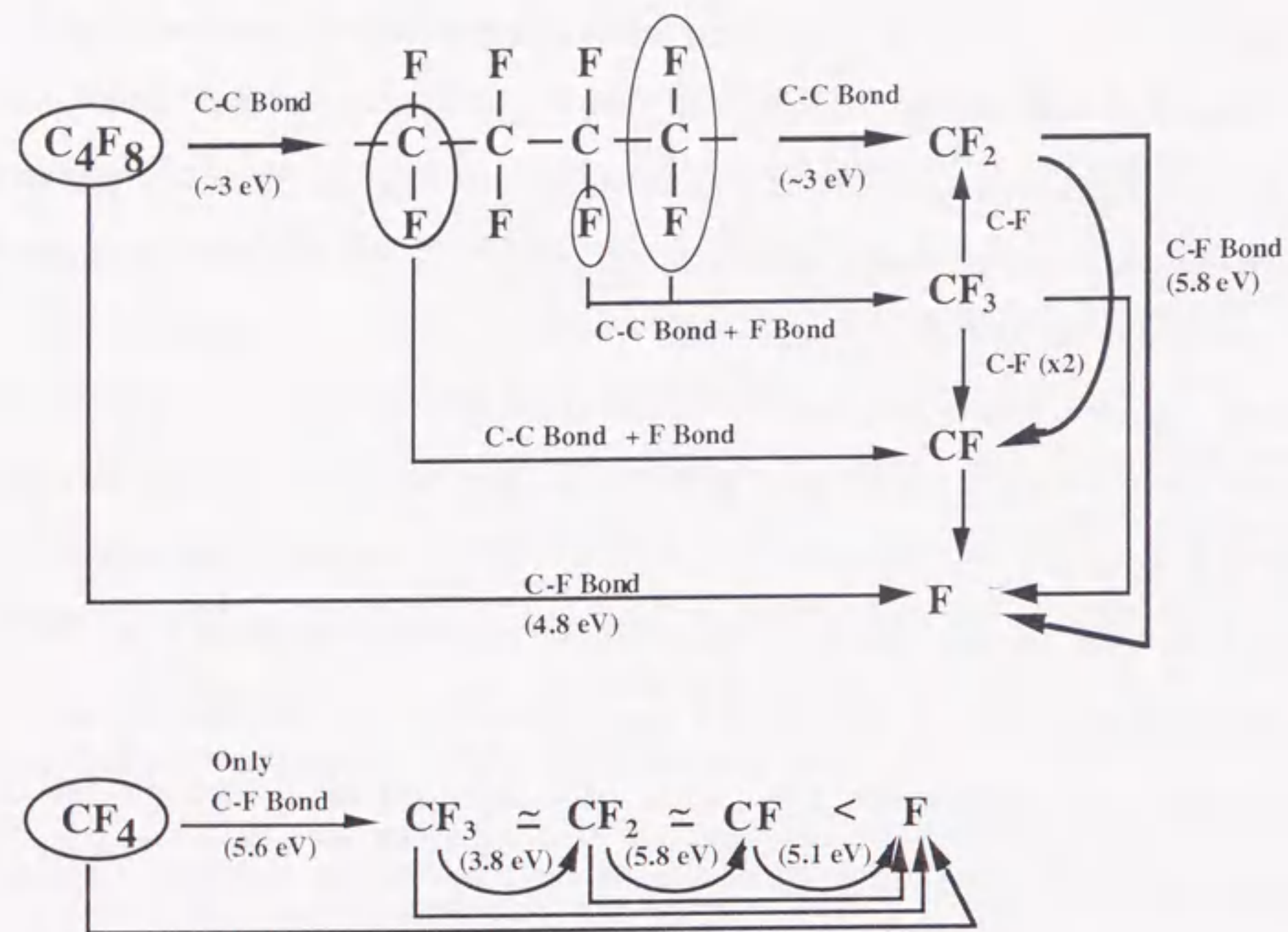
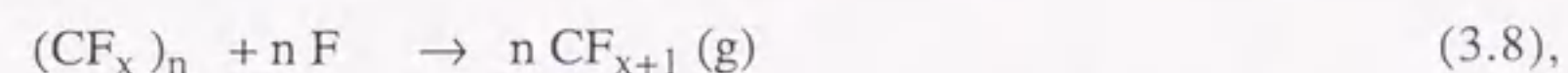
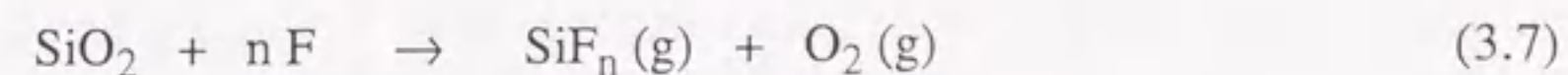


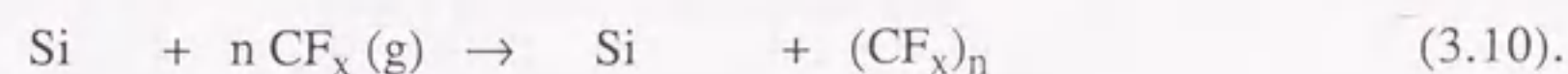
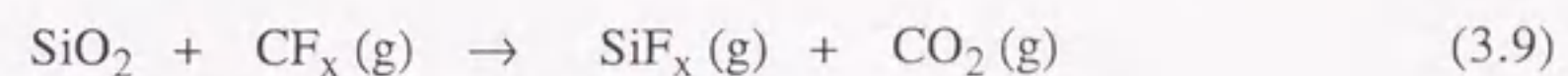
Fig. 3.7 Schematic diagram depicting dissociation mechanisms of the  $C_4F_8$  and  $CF_4$  molecule in ECR plasma.

### 3.4.2 Control of $CF_x/F$ Density ratios

Generally, it is believed that in selective  $SiO_2/Si$  etching process all of  $Si$ ,  $SiO_2$  and fluorocarbon polymer  $(CF_x)_n$  are etched by  $F$  atom through the reactions as follows,



and  $CF_x$  radicals ( $CF_x(g)$ ) etch the  $SiO_2$  under the ion-bombardment but principally some of  $CF_x(g)$  contribute to the deposition and form fluorocarbon polymer  $(CF_x)_n$  on the underlying  $Si$  as follows,



Therefore, it is considered that the ratio of  $CF_x$  density to  $F$  one ( $CF_x/F$ ) is very important factor indicating the selectivity of etching rate of  $SiO_2$  against that of  $Si$  in  $SiO_2/Si$  selective etching process using fluorocarbon gas plasma.

To summarize the above results, in Fig. 3.8 we have plotted the  $CF_2/F$  density ratio (a) and  $CF/F$  density ratio (b) as a function of input microwave power for the 300D-ECR plasma source. In both Figs. 3.8 (a) and (b), the density ratios for  $C_4F_8$  (curve (a)) and  $CF_4$  (curve (b)) ECR plasma are plotted along with curve (c) which represents the  $CF_x/F$  ( $x=1,2$ ) density ratio in the case of the C- ECR plasma source as a reference. Recently, it was reported that the  $CF_2/F$  and/or  $CF/F$  density ratio is predominately responsible for the selectivity of  $SiO_2/Si$  etching.[3,10] Control of  $SiO_2/Si$  etching selectivity is therefore determined by such ratios. In Fig. 3.8(a), it can be seen quite clearly that for  $C_4F_8$  300D-ECR plasma the  $CF_2/F$  and  $CF/F$  density ratios are larger than those for  $CF_4$  300D-ECR

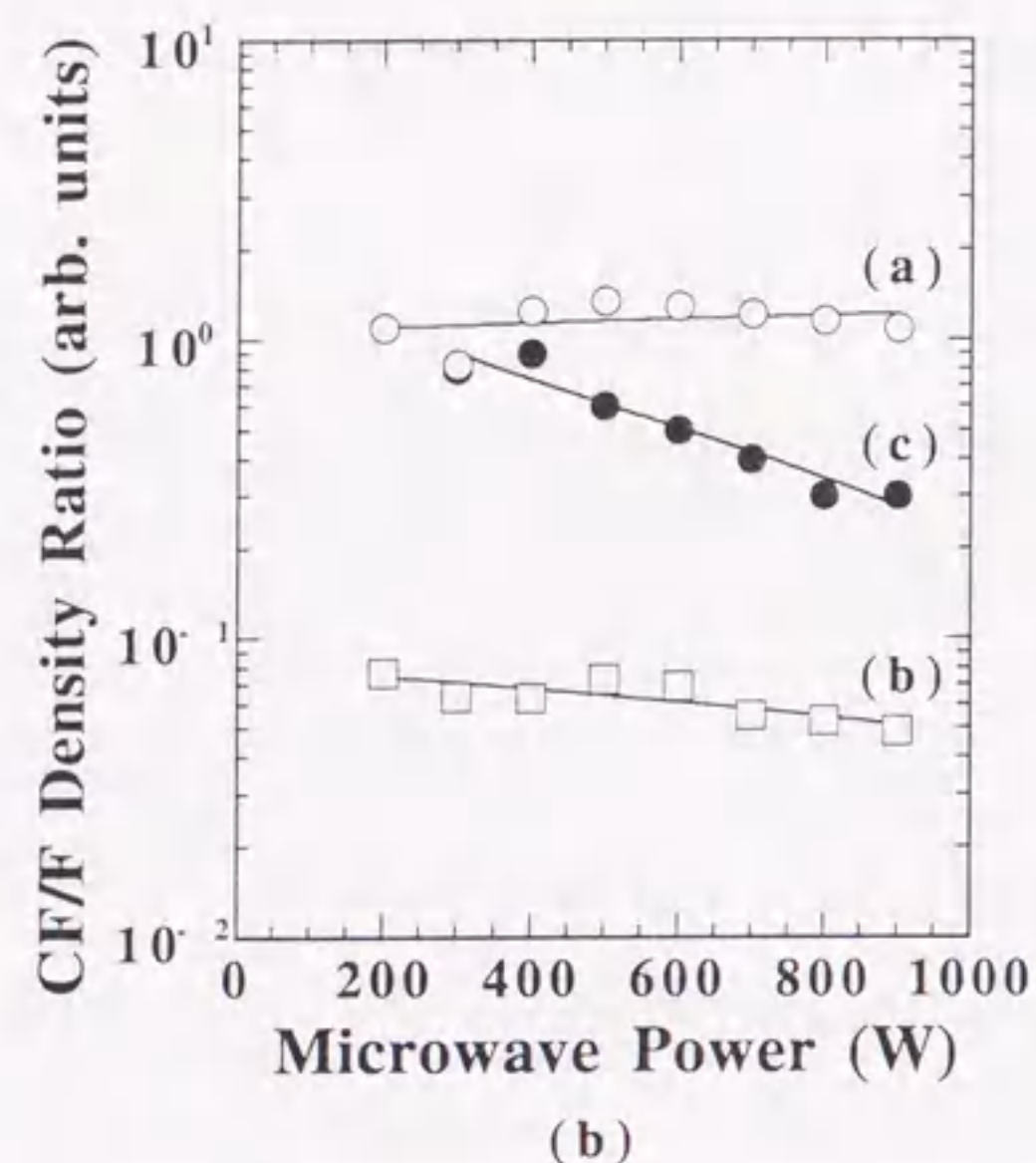
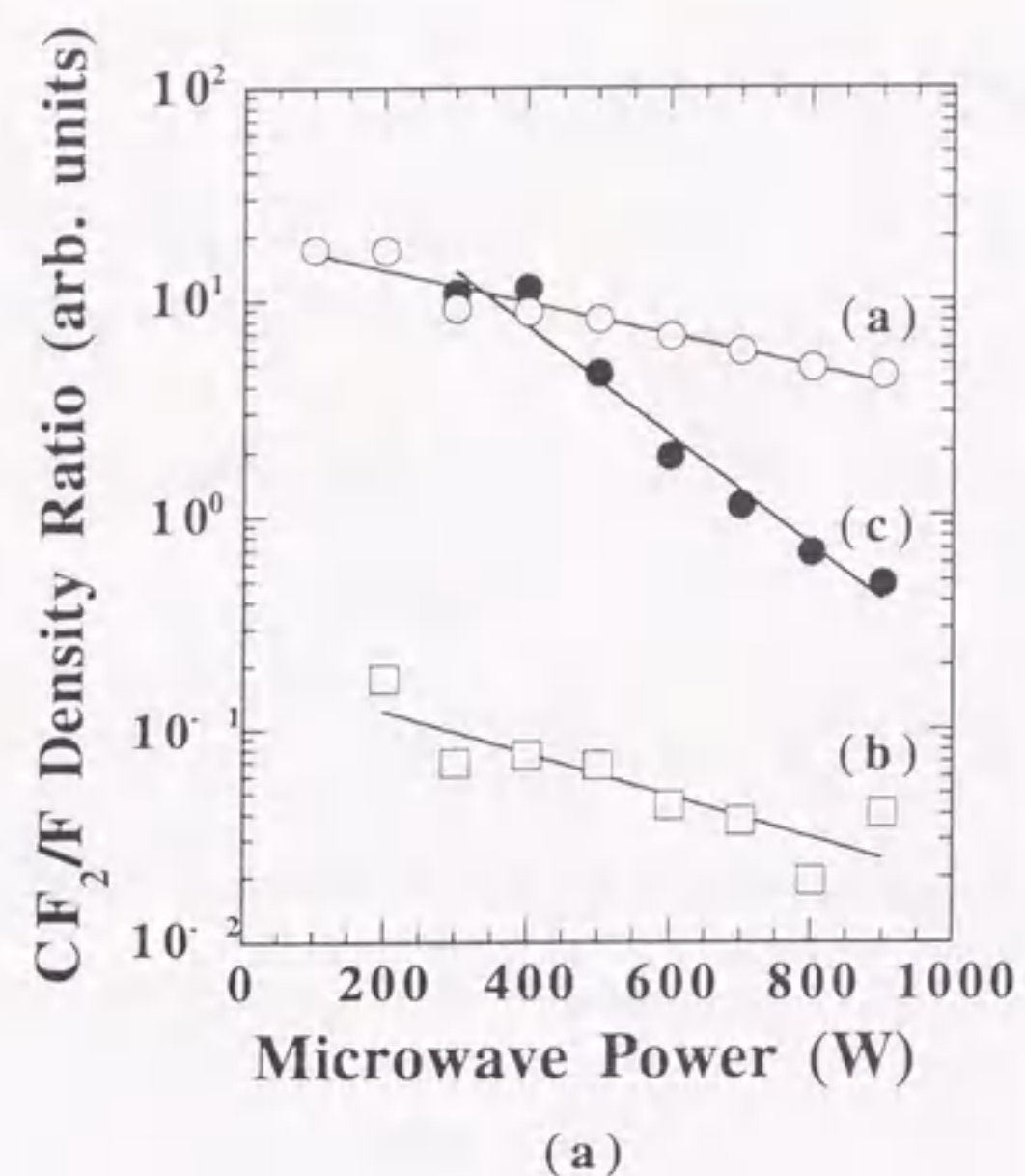


Fig. 3.8  $CF_2/F$  density ratio (a) and  $CF/F$  density ratio (b) as a function of input microwave power. In both (a) and (b) the density ratios for  $C_4F_8$  (curve (a)) and  $CF_4$  (curve (b)) ECR plasma are plotted along with curve (c) which represents the  $CF_x/F$  ( $x=1,2$ ) density ratio in the case of the C-ECR plasma source as a reference.

plasma. In the case of the C-ECR plasma source, the reduction of  $CF_2$  and  $CF$  radical densities and the increase of  $F$  atom density with increasing microwave power are leading to decrease of the etching selectivity. Since the etching rate of  $SiO_2$  on  $Si$  is mainly determined by the  $F$  atom density which increases linearly with input microwave power, it is necessary to maintain a high density of  $CF_x$  radicals in order to maintain high selectivity. On the basis of above results, a newly developed permanent magnet ECR plasma source which will allow superior control of etching selectivity at high etch rates using  $C_4F_8$  gas has been demonstrated. Moreover, etch selectivity will be obtained over a wide range of operating powers using this plasma source.

### 3.5 Summary

We have investigated changes in the densities of fluorocarbon radicals and  $F$  atoms in a size-scalable large-area permanent magnet and a conventional electromagnet ECR etching plasma source employing  $CF_4$  and  $C_4F_8$  gases using IRLAS and actinometric techniques. Dissociation kinetics associated with  $CF_4$  and  $C_4F_8$  gases were revealed. In the case of  $CF_4$  ECR plasma, the  $CF$  and  $CF_2$  radicals were produced by direct electron dissociation of the parent gas for both the 300D-ECR and C-ECR plasma sources. In the other case of  $C_4F_8$  300D-ECR plasma,  $CF$  radicals were found to be generated from electron dissociation of  $CF_2$  radicals. The decay time of radical densities in the afterglow of  $C_4F_8$  ECR plasma showed single exponential decays for both the 300D-ECR and C-ECR plasma sources. Decay times for the 300D-ECR source were 0.05 and 0.5s for the  $CF$  and  $CF_2$  radicals, respectively. Decay times for the C-ECR source were faster at 0.03 and 0.17s for the  $CF$  and  $CF_2$  radicals, respectively. Furthermore, in the 300D-ECR even at high input microwave power, high densities of  $CF_x$  ( $x=1,2$ ) radicals were obtained. This was in contrast to the increased rate of dissociation of  $CF_2$  ( $x=1,2$ ) radicals observed in the C-ECR plasma at high microwave power. A qualitative explanation of these differences was given in terms of particle confinement and diffusion which produces high-density plasma with relatively low



electron temperatures in the developed permanent magnet ECR plasma source. The high selectivity at high etch rates which can be realized in the 300D-ECR plasma source over a dynamic power range was also discussed.

## References

- [1] T. Fukusawa, A. Nakamura, H. Shindo and Y. Horike: Jpn. J. Appl. Phys. **33** (1994) 2139.
- [2] J. M. Cook, D. E. Ibbotson, P.D. Foo and D. L. Flamm: J. Vac. Sci. Technol. **A8** (1990) 1820.
- [3] S. Samukawa: Jpn. J. Appl. Phys. **33** (1994) 2133.
- [4] S. Arai, K. Tsujimoto and S. Tachi: Jpn. J. Appl. Phys. **31** (1992) 2011.
- [5] O. Joubert, G. S. Oehrlein and Y. Zhang: J. Vac. Sci. Technol. **A12** (1994) 658.
- [6] O. Joubert, G. S. Oehrlein and M. Surendra: J. Vac. Sci. Technol. **A12** (1994) 665.
- [7] K. Takahashi, M. Hori, K. Maruyama, S. Kishimoto and T. Goto: Jpn. J. Appl. Phys. **32** (1993) L694.
- [8] K. Takahashi, M. Hori and T. Goto: Jpn. J. Appl. Phys. **32** (1993) L1088.
- [9] K. Takahashi, M. Hori and T. Goto: Jpn. J. Appl. Phys. **33** (1994) 4745.
- [10] K. Miyata, M. Hori and T. Goto: J. Vac. Sci. Technol. **A14** (1996) 2343.
- [11] K. Maruyama, K. Ohkouchi, Y. Ohtsu and T. Goto: Jpn. J. Appl. Phys. **33** (1994) 4298.
- [12] N. Shida, T. Inoue, H. Kokai, Y. Sakamoto, W. Miyazawa, S. Den and Y. Hayashi: Jpn. J. Appl. Phys. **32** (1993) L1635.
- [13] W. Miyazawa, S. Tada, K. Ito, H. Saito, S. Den, Y. Hayashi, Y. Okamoto and Y. Sakamoto: Plasma Sources Sci. Technol. **5** (1996) 265.
- [14] J. Jenq, J. Ding, J. W. Taylor and N. Hershkowitz: Plasma Sources Sci. Technol. **3** (1994) 154.
- [15] K. Miyata, K. Takahashi, S. Kishimoto, M. Hori and T. Goto: Jpn. J. Appl. Phys. **34** (1995) L444.
- [16] Y. Hikosaka, M. Nakamura and H. Sugai: Jpn. J. Appl. Phys. **33** (1994) 3602.
- [17] J. W. Coburn and M. Chen: J. Appl. Phys. **51** (1980) 3134.
- [18] J. P. Booth, G. Hancock, N. D. Perry and M. J.: J. Vac. Sci. Technol. **A4** (1986) 1791.
- [19] K. Ninomiya, K. Suzuki, S. Nishimatsu and O. Okada: J. Appl. Phys. **66** (1989) 5251.
- [20] K. Kubota, H. Matsumoto, S. Shingubara, H. Shindo and Y. Horiike: Jpn. J. Appl. Phys. **34** (1995)
- [21] R. A. Gottscho and V. M. Donnelly: J. Appl. Phys. **56** (1984) 245.

## Chapter 4. Improvement of the Large-area Permanent Magnet Electron Cyclotron Resonance Plasma Source and Scale-up for 12-inch Wafer Processing

### 4.1 Introduction

In chapter one, early types of ECR plasma sources which use bulky coil magnets and required huge electric power were described. In order to solve these problems, large-area ECR plasma sources employing permanent magnets[1] and slot antennae[2,3] were reported. One such source is described in chapter 2. However, it has not been reported that highly dense ECR plasma sources with slot antennae are realized to meet the requirements for 12-inch wafer processing where the electron densities in excess of  $10^{11} \text{ cm}^{-3}$  and in good uniformity all over the wafer. One of the reasons why these sources have never been realized is that a slot antenna locally radiates microwave power which frequently generates the local breakdown in the case of scale-up from 8-inch to 12-inch.

This chapter describes an improved large-diameter ECR plasma source which employs a strip-bar antenna and utilizes strip transmission through a co-axial window to avoid local breakdown.[4] The diameter is 35cm which is suitable for 12-inch plasma processing. Characteristics of this source have been performed in oxygen plasma by using Langmuir probe diagnostics. Oxygen gas was chosen because firstly in view of practical point, it is usually used for assing of resist materials as a processing gas and for selective etching of  $\text{SiO}_2/\text{Si}$  as an additive gas. Secondly, oxygen plasma is involved in dissociation process which is different from the inert gas plasma such as Ar, and is very simple compare with the fluorocarbon plasma. Therefore, it enable to us to get better understanding of the plasma characteristics with dissociation kinetics. Electron densities of the order of  $10^{11} \text{ cm}^{-3}$  and electron temperature is around 3 eV have been successfully achieved in this plasma. The space potential with respect to the chamber walls is less than 20 eV. Uniformity of  $\pm 3.8\%$  ion current density over 30 cm has been demonstrated.

The targets which should be established for improvement and scale-up of the ECR plasma source for 12-inch wafer processing and the results are shown in Table 4.1.

Table 4.1 Targets and results of the ECR plasma source for 12-inch wafer processing.

	<b>Targets</b>	<b>Results</b>
<i>Electron Temperature ; <math>T_e</math></i>	< 5 eV	3 eV
<i>Electron Density ; <math>n_e</math></i>	> $10^{11} \text{ cm}^{-3}$	$1.4 \times 10^{11} \text{ cm}^{-3}$
<i>Non-uniformity across 12-inch of ion current</i>	< +/- 5 %	+/- 3.8 %
<i>Space Potential</i>	< 20 V	< 20 V
<i>Local Breakdown</i>	Non local breakdown	Co-axial window and Strip-bar antenna

### 4.2 Development of an Advanced Permanent Magnet Electron Cyclotron Resonance Plasma Source for 12-inch Wafer Processing

#### 4.2.1 Configuration

Figure 4.1 is a schematic diagram of the plasma production device. The plasma source itself is made of aluminum and mounted on a stainless steel chamber 35 cm in diameter and pumped by a 1500 l/s turbo molecular pump. Microwave power from a rectangular waveguide is introduced to the discharge region via a  $50\Omega$  co-axial  $\text{Al}_2\text{O}_3$  window which also provides a vacuum seal. The microwave is monitored continuously by a power monitor and the reflected power is maintained within 10% of the input power. The microwave launching system which couples the microwave power into the plasma consists of eight metal rods distributed at angles of  $45^\circ$  and  $90^\circ$ . A dielectric quartz plate is inserted between the metal bar and the metal ceiling of the plasma source. The plasma is characterized in three dimensions by employing two Langmuir probes 0.05 cm in diameter and 0.3 cm in length. All measurements are taken sufficiently downstream to avoid any effects of the magnetic field. The magnetic field value at the probe measurement position is less than 2.5 mT. Figure 4.2 shows photographs of the RSA source with the strip-bar antenna (a) and the experimental system (b).

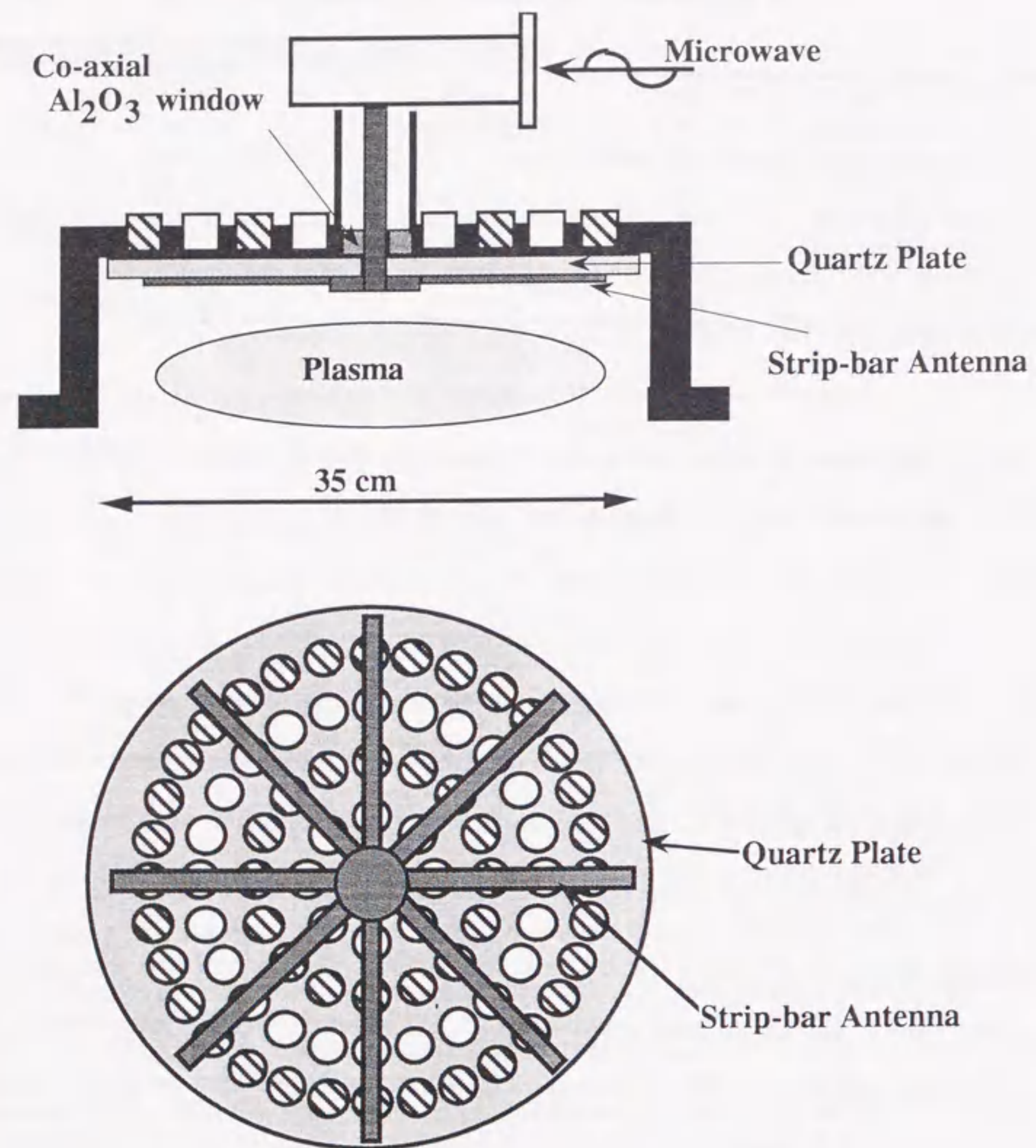
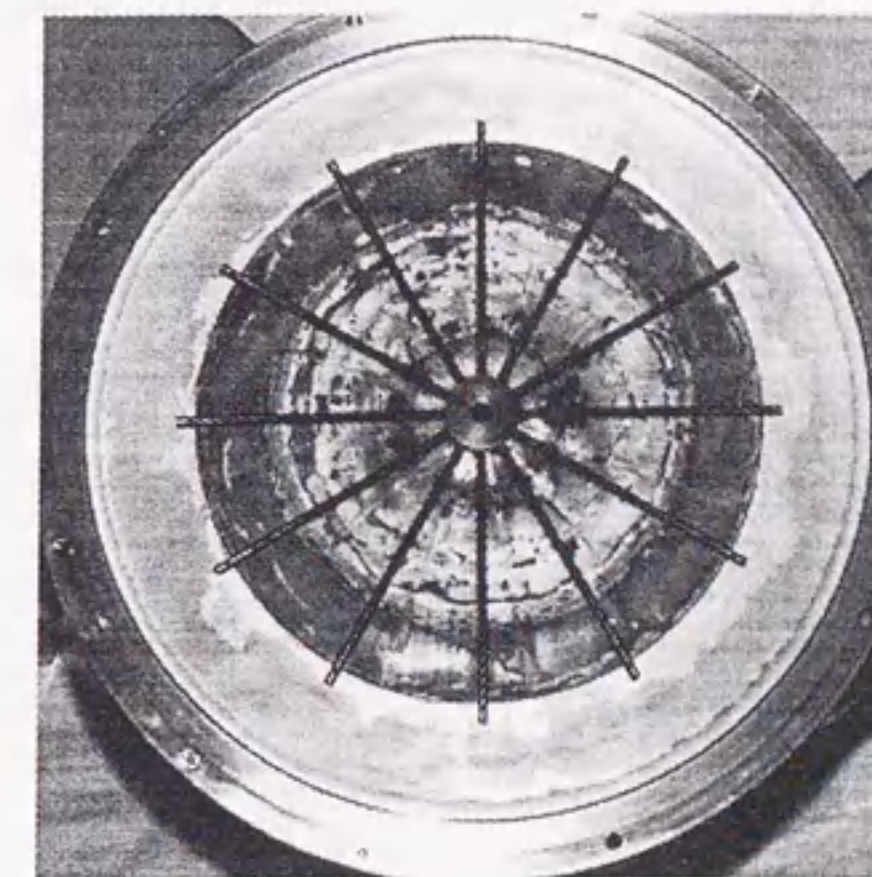
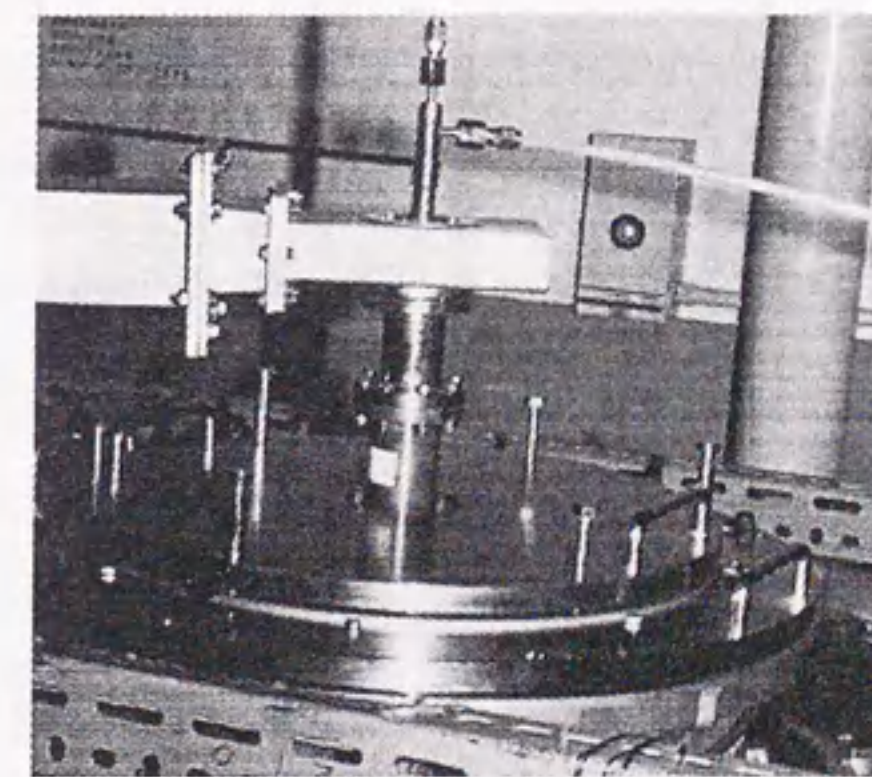


Fig. 4.1 A schematic diagram of the large-diameter permanent magnet ECR plasma source with a strip-bar antenna (RSA source).



(a)



(b)

Fig. 4.2 Photographs of the RSA source with the strip-bar antenna (a) and the experimental system (b).

A more detailed understanding of the strip-bar antenna and microwave launching can be obtained from Fig. 4.3. Microwave power is transmitted in the dielectric plate inserted between the strip-bar and source ceiling and can be approximated by a TEM mode. The labels  $E_t$  and  $E_l$  identify the transmission microwave electric field and the leak microwave electric field, respectively. The leak microwave radiates to the ECR zone provided by four rings of magnets and produces a plasma. We employed Sm-Co magnets which are suitable for high-temperature operation and generate an ECR zone (0.0875 T) in the discharge chamber 0.5 cm below the antenna. Magnetic field distributions have been measured in three dimensions. The magnetic field distribution 1.6 cm from the metal wall is shown in Fig. 4.4. A uniform plasma is obtained by controlling the size of the strip bar experimentally. To reduce contamination and protect both the strip-bar antenna and the chamber walls against plasma, all elements are coated with  $Al_2O_3$ .

#### 4.2.2 Characteristics

To demonstrate the performance of this plasma source, in Fig. 4.5, the radial profiles of the ion saturation current measured by a biased probe are plotted as a function of downstream position ( $L$ ). In Fig. 4.5(a) the pressure is 0.47 Pa and in (b) it is 1.33 Pa. An ion current density of the order of 15 mA/cm<sup>2</sup> was obtained at a pressure of 1.33 Pa. Moreover, we obtained an ion current density uniformity within 3.8% over 30 cm at  $L=10$  cm at a pressure of 0.47 Pa. From the ion saturation current an estimate of plasma parameters in an oxygen plasma was performed. An oxygen plasma, at a pressure of 0.47 Pa and with microwave power of 800 W was considered. Assuming that the dominant ions are molecular  $O_2^+$ , the oxygen plasma has the electron density of  $1.4 \times 10^{11}$  cm<sup>-3</sup>, an electron temperature of 3 eV and a space potential with respect to the metal chamber wall of less than 20 V.

Similar to the 300-D ECR plasma source described in chapter 2, uniform plasma production in the RSA source is explained in terms of charged particle dynamics in a static magnetic field. Figure 4.6 is a schematic diagram of the curved magnetic lines of force

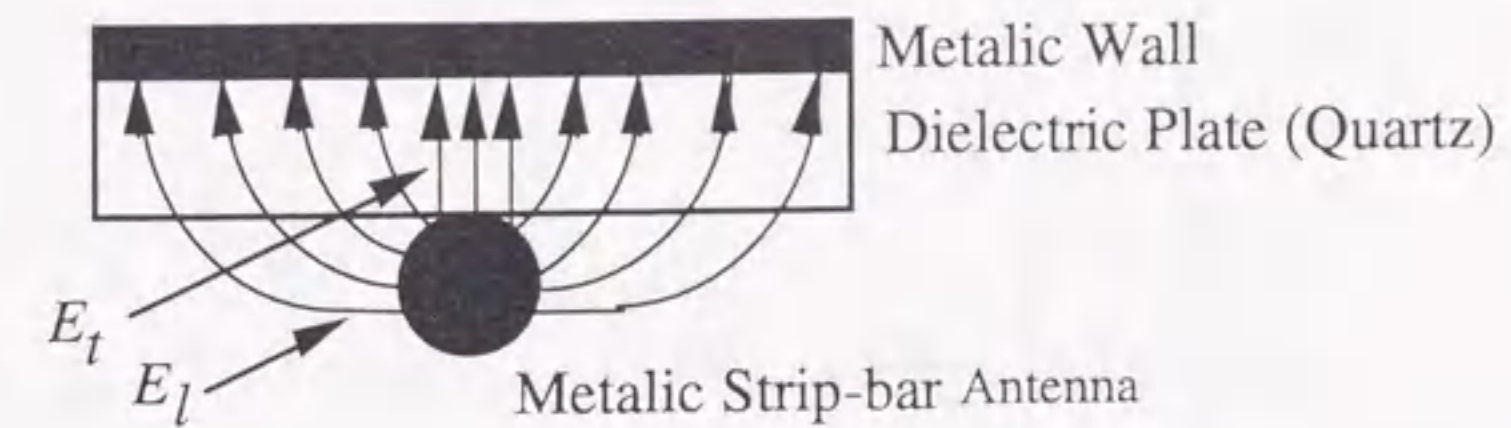


Fig. 4.3 A schematic illustration depicting microwave launching from the strip-bar antenna and transmission in the dielectric.

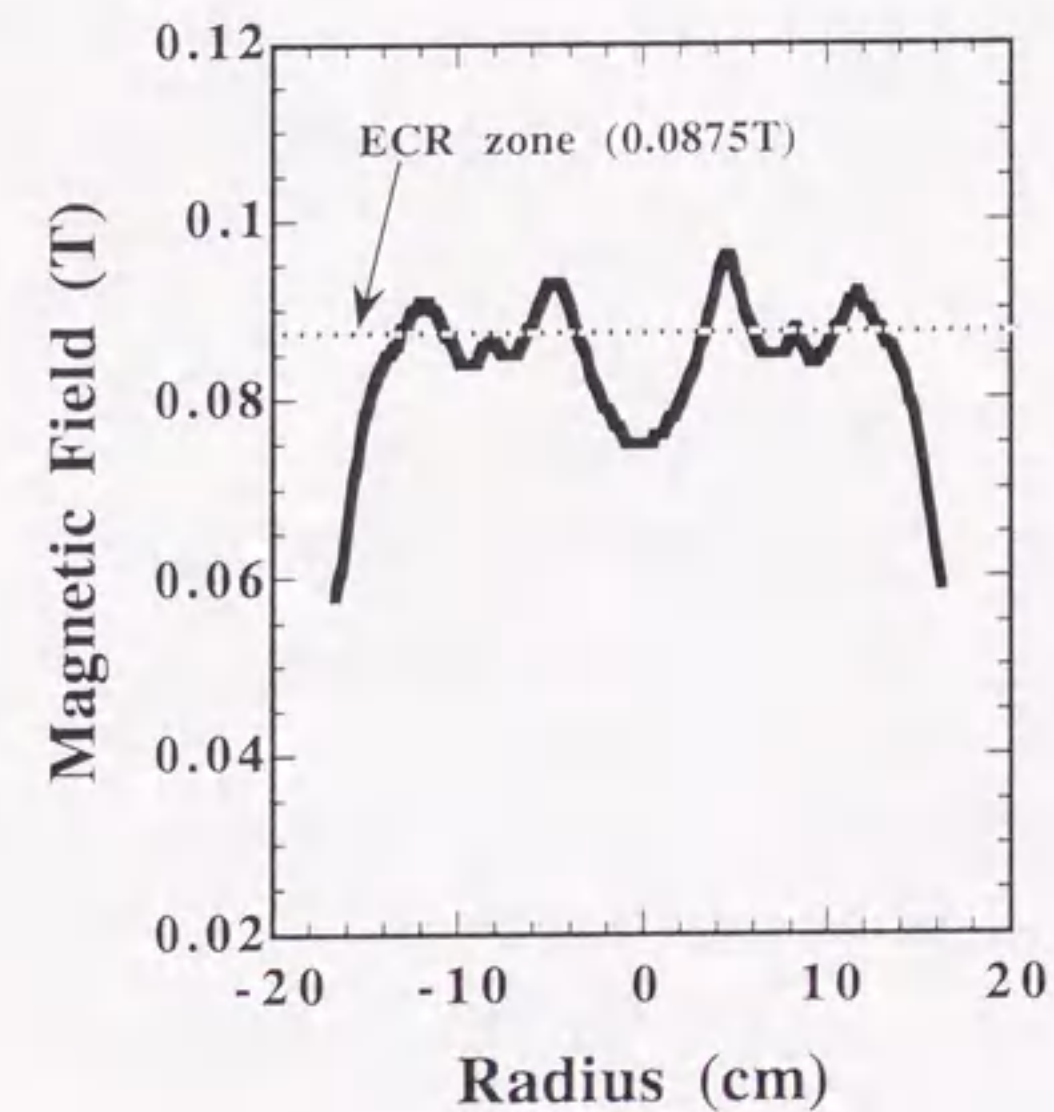


Fig. 4.4 The magnetic field distribution measured across the diameter of the source at 1.6 cm below the ceiling of the source.

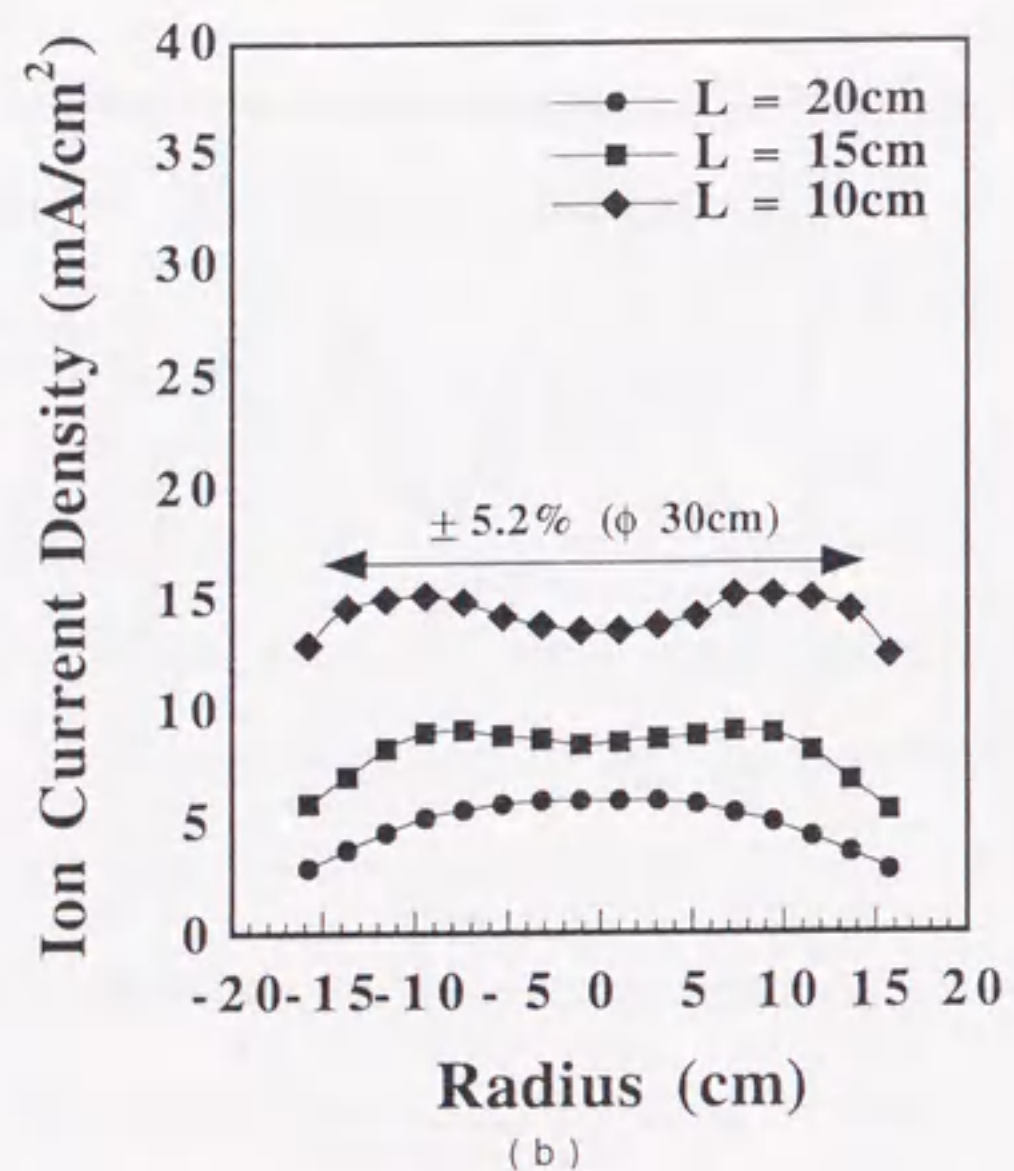
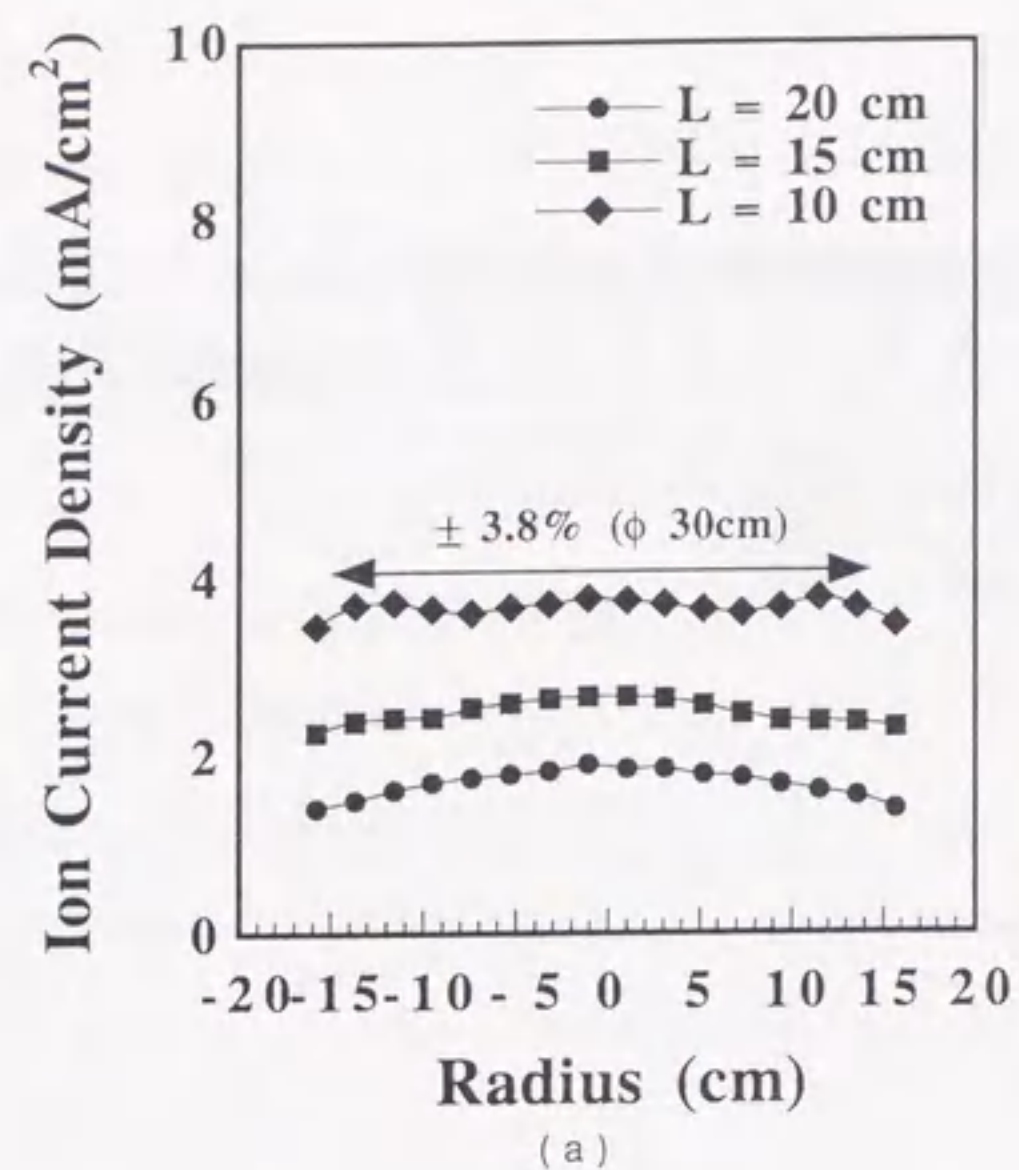


Fig. 4.5 The radial distribution of ion saturation current density at  $L = 10, 15$  and  $20$  cm for an oxygen plasma at (a)  $0.47$  Pa and (b)  $1.33$  Pa.

which run from the N to S poles of adjacent magnets. In this magnetic field, charged particles drift perpendicularly to curved magnetic lines of force  $B$  and the radius  $R$  due to the  $\nabla B$ , and the curvature drift[5], given by

$$v_{drift} = \frac{m R_c \times B}{q R_c^2 B^2} \left( v_{\parallel} + \frac{v_{\perp}^2}{2} \right) \quad (4.1)$$

where  $m$ ,  $q$ ,  $v_{\parallel}$ ,  $v_{\perp}$ ,  $R_c$  and  $B$  are the mass, the charge, the parallel and perpendicular velocities with respect to the magnetic line of force, the curvature radius and the magnetic field, respectively. The ions and electrons move in opposite directions, as is shown in Fig. 4.6. The plasma uniformity is determined by  $\nabla B$ , the curvature drifts of charged particles and downstream diffusion effects. If the electron mean free path is short compared with the distance between the metal bars of the strip-bar antenna, then an azimuthally uniform plasma is not obtained. Operation under conditions of short mean free path leads to charged particle collision with molecules and good uniformity is not obtained. For example, in the case of an oxygen plasma, we assume that the dominant ions are molecular  $O_2^+$ . Then the mean free path of  $O_2^+$  is given by

$$\lambda_{O_2^+} = \lambda_{O_2} = 1.5 \text{ cm}$$

(for  $300$  K and  $0.47$  Pa) and the electron mean free path  $\lambda_e$  is given by

$$\lambda_e = 4\sqrt{2}\lambda_{O_2} = 8.7 \text{ cm.}$$

Since it is desirable that the distance between the strip bars and the drift be equal to or shorter than the electron mean free path, the distance between antenna strips of the outermost channel should be approximately  $8.7$  cm. In the present plasma device, the distance is  $9$  cm

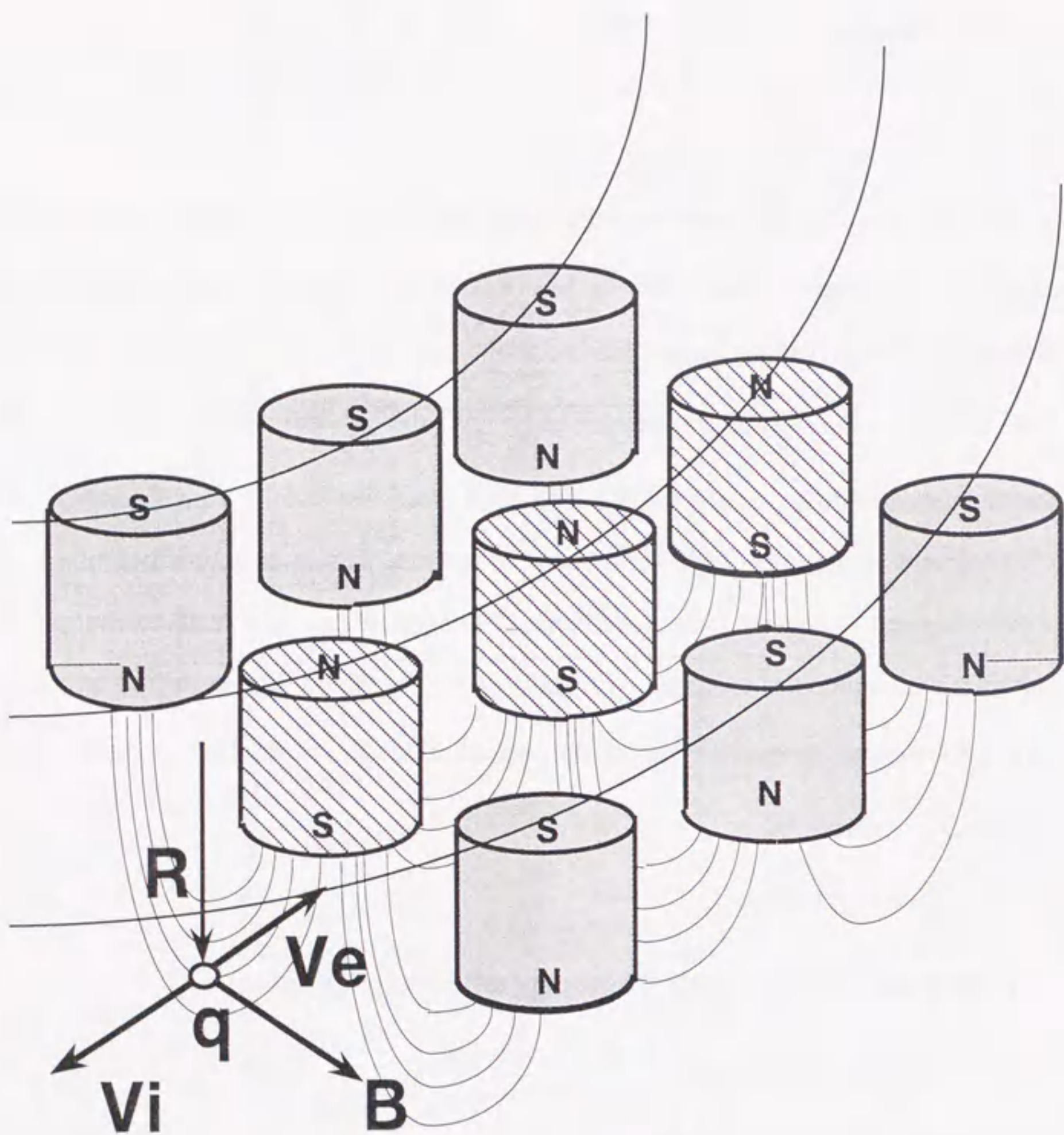


Fig. 4.6 A schematic illustration of the charged particle dynamics in the static magnetic field.

which is comparable with the estimated value above. This is the reason why the azimuthal uniformity is maintained. Therefore, under the experimental conditions described in Fig. 4.5(b) at 300K for 1.33 Pa, the electron mean free path becomes 3.1 cm, and as a result the plasma is less uniform. In this device, the plasma is produced near the bar antennae which supply microwave power to charged particles drifting in the radial direction. Therefore, by considering mean free paths within the plasma, we have designed a suitable strip-bar antenna, and as a result we achieved a good plasma uniformity.

#### 4.3 Summary

In conclusion, we have developed a large-diameter high-density permanent magnet ECR plasma source. A plasma density in excess of  $1.0 \times 10^{11} \text{ cm}^{-3}$  was successfully achieved by employing a strip-bar antenna. Charged particle diffusion under B and curvature drift in the downstream region leads to a density uniformity within  $\pm 3.8\%$  over a 30 cm diameter. In the case of an oxygen plasma, the plasma parameters were an electron density of  $1.4 \times 10^{11} \text{ cm}^{-3}$ , an electron temperature of 3 eV and a space potential with respect to the chamber wall of less than 20 V.

## References

- [1] M. Hagane, Y. Sakamoto, H. Kokai and Hayashi Y: *Proc. Int. Seminar on Reactive Plasma, Nagoya* (Division of Plasma Electronics, the Japan Society of Applied Physice) p 53 (1991).
- [2] N. Shida, T. Inoue, H. Kokai, Y. Sakamoto, W. Miyazawa, S. Den and Y. Hayashi Y *Japan.J. Appl. Phys.* **32** 1635 (1993).
- [3] N. Sato, S. Iizuka, Y. Nakagawa and T. Tsukada : *Appl. Phys. Lett.* **62** 1469 (1993).
- [4] W.Miyazawa, S.Tada, K.Ito, H.Sato, S.Den, Y.Hayashi, Y.Okamoto and Y.Sakamoto: *Plasma Sources Sci. Technol.* **5** (1996) 265-267.
- [5] Chen F. F.: *Introduction to Plasma Physics* (New York: Plenum), 1974, p.27.

## Chapter 5. Effect of Carbon Atoms on Selective SiO<sub>2</sub>/Si Etching with a Large-area Permanent Magnet Electron Cyclotron Resonance Plasma Source

### 5.1 Introduction

As outlined in chapter 1, the etch selectivity is determined by the plasma chemistry and plasma-material interaction processes, hence understanding the plasma chemistry and the kinetics involved is vital for achieving the required selectivity. For the selective etching of silicon dioxide (SiO<sub>2</sub>) over silicon (Si), a wide range of complex chemistries using various feed gases such as CHF<sub>3</sub>, CF<sub>4</sub>, C<sub>2</sub>F<sub>6</sub> and C<sub>4</sub>F<sub>8</sub> have been employed[1-8] both with and without additions of Ar, H<sub>2</sub> and O<sub>2</sub>. [8-10] Moreover, it has been shown that control of the fluorocarbon radical densities and fluorine (F) atom density will lead to higher selectivity.[1]

Further investigation of the C<sub>4</sub>F<sub>8</sub> ECR plasma kinetics which can be directly related to SiO<sub>2</sub>/Si etch selectivity needs to be carried out. Moreover, to the best of my knowledge, no direct measurement of the carbon atom density that could be related to the etch process has been made to date. It was shown recently by Zhang *et al.* that introducing extra carbon into the plasma by placing a thin piece of graphite on the wafer chuck increased the etch selectivity of SiO<sub>2</sub> over Si<sub>3</sub>N<sub>4</sub>. [12] It has also been shown by Bell *et al.* that gate oxide consumption increases as a result of carbon from the photoresist producing volatile C-O etching products.[13] Therefore, it is considered that carbon atoms play an important role in the etch process and maybe the main precursor defining etch selectivity and etch rate.

In this chapter, diagnostics of the fluorocarbon radical species along with carbon and fluorine atom densities in the RSA ECR etching plasma employing C<sub>4</sub>F<sub>8</sub> gas with the addition of CH<sub>4</sub> are described. To understand in more detail the effect of carbon and carbon products on the etch process of SiO<sub>2</sub> over Si, CH<sub>4</sub> was chosen because firstly, it is a source of carbon and hydrocarbon radicals similar to those species produced from the photoresist during etching, and second it provides hydrogen which increases fluorine associated reactions. Non-intrusive infrared diode laser absorption spectroscopy (IRLAS), actinometric

measurement techniques and hollow cathode absorption spectroscopy are used in studying the kinetic processes associated with etching plasma chemistry. In particular, the control of the carbon atom to fluorine atom ratio by addition of  $\text{CH}_4$  which results in higher selectivity in the etching of  $\text{SiO}_2$  over Si is discussed. The objective of this paper is not to elucidate as to the origin of the plasma characteristics but rather to study their effect if any on the etch process of  $\text{SiO}_2$  over Si. Hence, the main discussion in this paper is concerned with, diagnostics of the fluorocarbon radical species along with carbon and fluorine atom densities in a high density ECR etching plasma employing  $\text{C}_4\text{F}_8$  gas to which  $\text{CH}_4$  is added in order to understand in more detail the effect of carbon (C) and carbon products on etch process of  $\text{SiO}_2$  over Si.

## 5.2 Experimental

### 5.2.1 Experimental Set-up

The ECR plasma source (Nichimen Electronic Technology Corporation, RSA) has been described in detail in the previous chapter. The techniques used to measure the absolute densities of ground state  $\text{CF}_x$  ( $x=1-3$ ) and fluorine species are IRLAS and actinometry, respectively. Prior to measurements being made, the surfaces of the chamber walls were aged by exposure to fluorocarbon plasma. In all experiments, the microwave input power is 900 W, the pressure and gas flow rate were maintained constant at 0.4 Pa and 15 sccm, respectively. All the measurement results discussed here were obtained at a position 20 cm downstream. Etching of  $\text{SiO}_2$  on Si wafers was carried out 10 cm downstream at room temperature. In order to avoid carbon or carbon products other than those produced in the gas phase, a simple Si mask was used. No resist material was present during the etching process. An radio frequency bias of 400 kHz and a  $V_{\text{DC}}$  of -150 V was applied to the wafer.

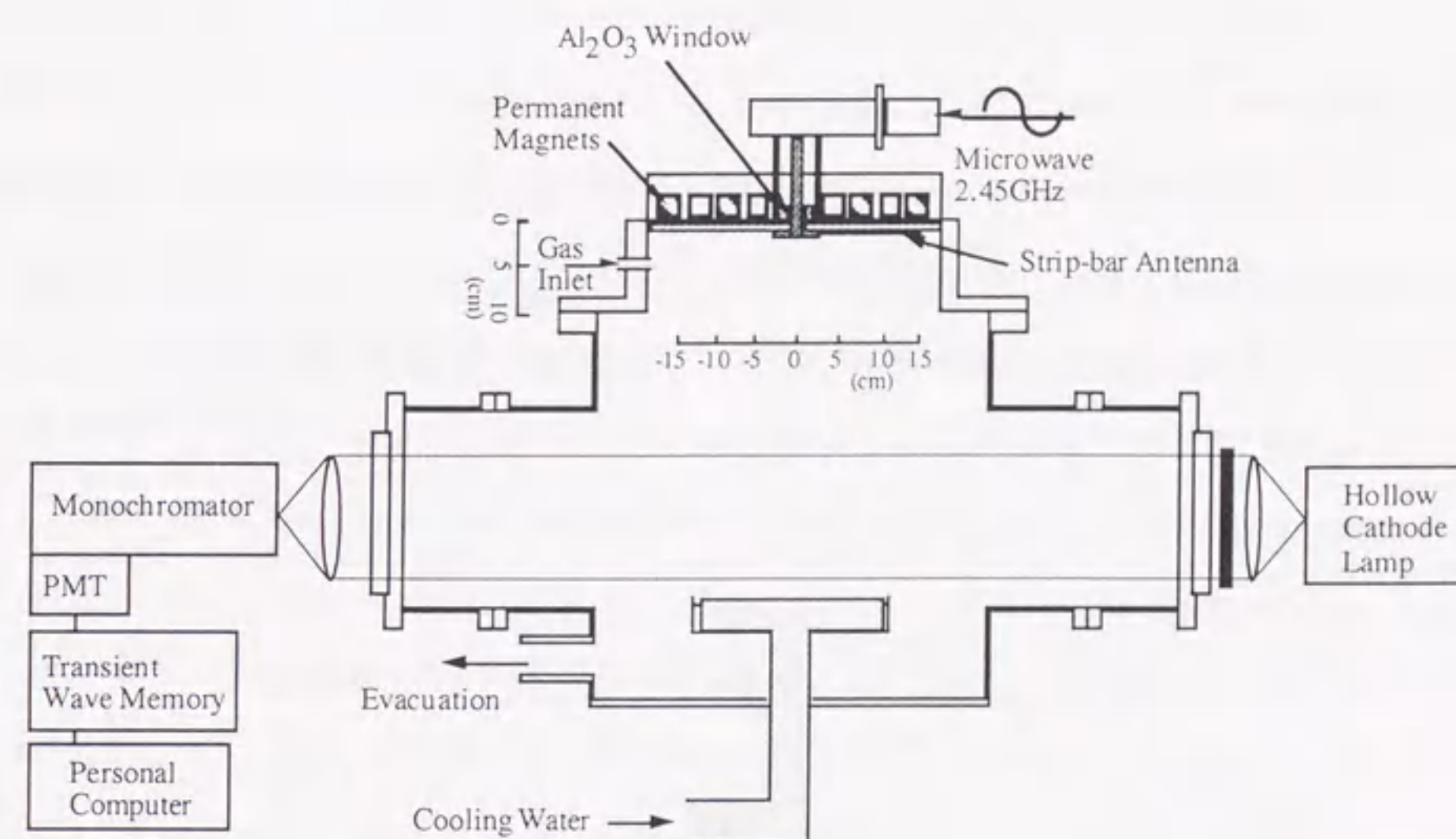


Fig. 5.1. Schematic diagram of the experimental setup.



### 5.2.2 Hollow Cathode Lamp Absorption Spectroscopy for Measurement of C Atom Density

An estimate of the carbon atom density was obtained using a hollow cathode spectroscopy.[14] Carbon atom absorption of the ultra violet light from the hollow cathode lamp at 296.7 nm was selected by a monochromator and detected using a photomultiplier tube. A schematic diagram of the experimental setup is shown in Fig. 5.1. In calculating the absolute carbon density, the following assumptions are made: (1) the absorption length is equal to the chamber diameter, (2) carbon atoms do not go through collisions and recombine at the chamber walls and the temperature of C atoms is assumed to be ~400K. Each data point is the average value of 500 readings and the measurement signal sensitivity is within  $\pm 0.5\%$  of the total transmission. In this chapter, relative dependence of carbon atom density is discussed because only one Einstein's A coefficient which was evaluated theoretically has been reported. This value is too small to discuss the absolute density. Probably, the Einstein's A coefficient has a large error value and not exact to be used here.

### 5.3 Diagnostics of CF<sub>x</sub> radicals and fluorine atom density in C<sub>4</sub>F<sub>8</sub> plasma

To understand the effect on fluorocarbon radicals of CH<sub>4</sub> addition to the ECR plasma, diagnostics of fluorocarbon radicals and the fluorine atom density in C<sub>4</sub>F<sub>8</sub> plasma were undertaken. In Fig. 5.2(a), the CF<sub>x</sub> (x=1-3) radical densities measured by IRLAS and the fluorine atom density calculated from eqn. (3.3) described in Chapter 3 are shown as a function of CH<sub>4</sub> gas percentage. It can be seen from this figure that for a pure C<sub>4</sub>F<sub>8</sub> plasma, the dominant species is CF<sub>2</sub> radicals which have a density of the order of 10<sup>13</sup> cm<sup>-3</sup>, followed by fluorine atoms, CF<sub>3</sub> and CF radicals which have a density an order of magnitude lower at 10<sup>12</sup> cm<sup>-3</sup>. The CF<sub>2</sub>, CF<sub>3</sub> radical and fluorine atom densities all decrease with increasing CH<sub>4</sub> gas addition. The decrease of CF<sub>2</sub> and CF<sub>3</sub> is due to both dilution by CH<sub>4</sub> gas addition and reactions of CF<sub>x</sub>(x=2,3) radicals with H which is readily produced by dissociation of CH<sub>4</sub>. [15] The rapid decrease of the fluorine atom density is caused by both

gas phase reactions with CH<sub>x</sub>(x=1-4) and fluorine scavenging with H. To compare the relative dependence of the CF<sub>x</sub> (x=1-3) radical densities on CH<sub>4</sub> gas percentage in Fig. 5.2(b), the normalized densities of CF<sub>x</sub> (x=1-3) radicals are plotted as a function of CH<sub>4</sub> gas addition. Both CF<sub>2</sub> and CF<sub>3</sub> radical densities decrease slowly up to 20% after which they display a rapid decrease with increasing CH<sub>4</sub> gas. Similar results have been reported recently by Doh *et al.* [8] for H<sub>2</sub> addition to a C<sub>4</sub>F<sub>8</sub> ECR plasma. Therefore, the H radical produced by dissociation of the CH<sub>4</sub> gas will play an important role in determining the plasma chemistry. On the other hand, the CF radical increases up to 40% of CH<sub>4</sub> gas addition and then decreases rapidly. It is possible to explain this increase in CF radicals by considering the production and extinction processes of CF radicals through reactions of CF<sub>x</sub>(x=1-3) radicals with H, for example[9]



which has a large reaction rate constant. The most probable source for the increase in CF radicals is, therefore, the reaction of H with CF<sub>2</sub> and CF<sub>3</sub>. However, it should also be noted that for a CH<sub>4</sub> percentage of 40%, the density of CF is greater than the sum of densities of CF<sub>2</sub> and CF<sub>3</sub>. This suggests that some other production mechanisms also exist, for example direct electron impact dissociation.

At present selective etching of SiO<sub>2</sub> over Si is considered to be performed by depositing a fluoropolymer on the underlying Si, and research has been concerned with identifying the main gas precursors for this fluoropolymer deposition. Various evidence has been put forward in support of both CF and CF<sub>2</sub> radical species as being the main precursor.[1,16] However, the main precursor species still remains very much a debated point, which is compounded by the fact that carbon atoms may also play a significant role[12,13], but to date very little data has been presented. The objective of this paper is not to elucidate as to the origin of the plasma characteristics but rather to study their effect if any

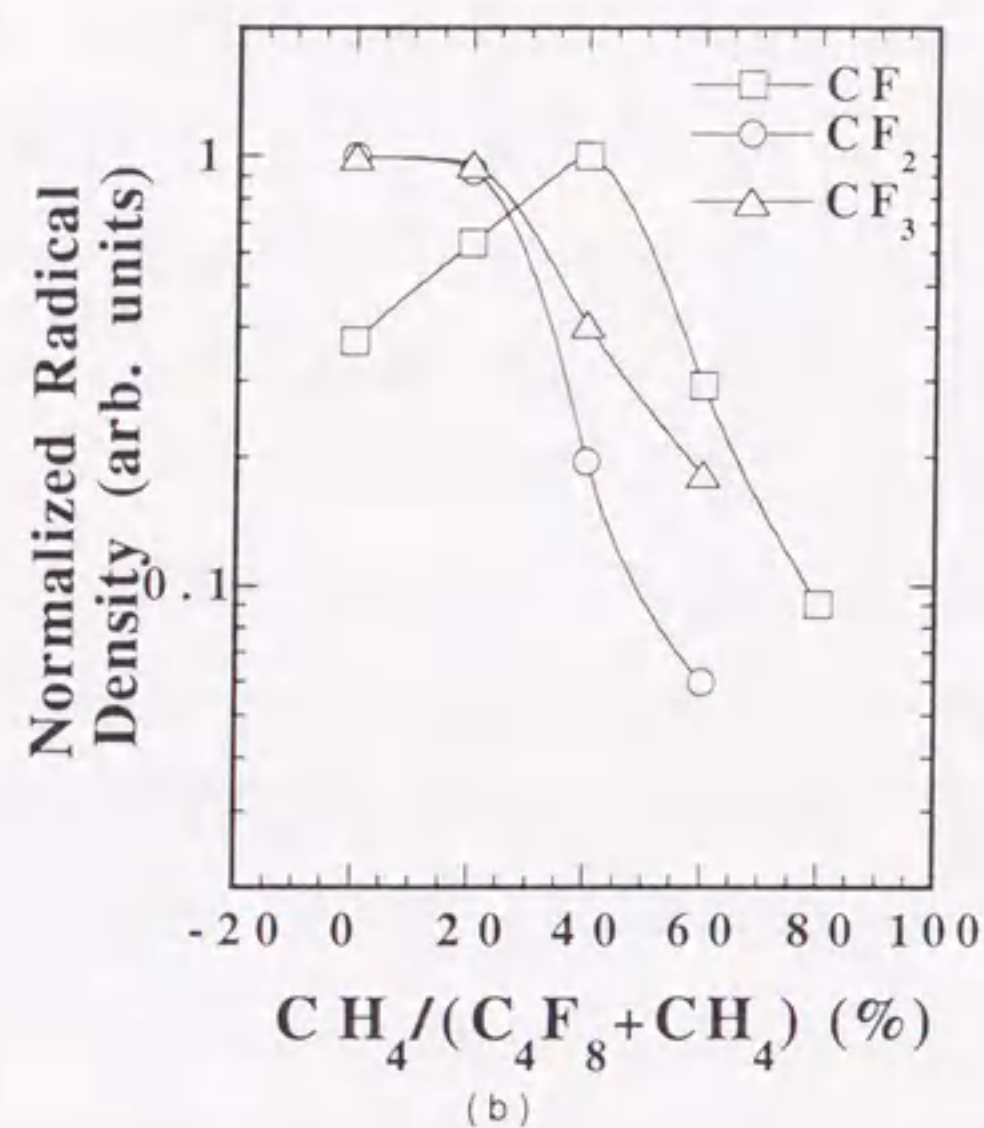
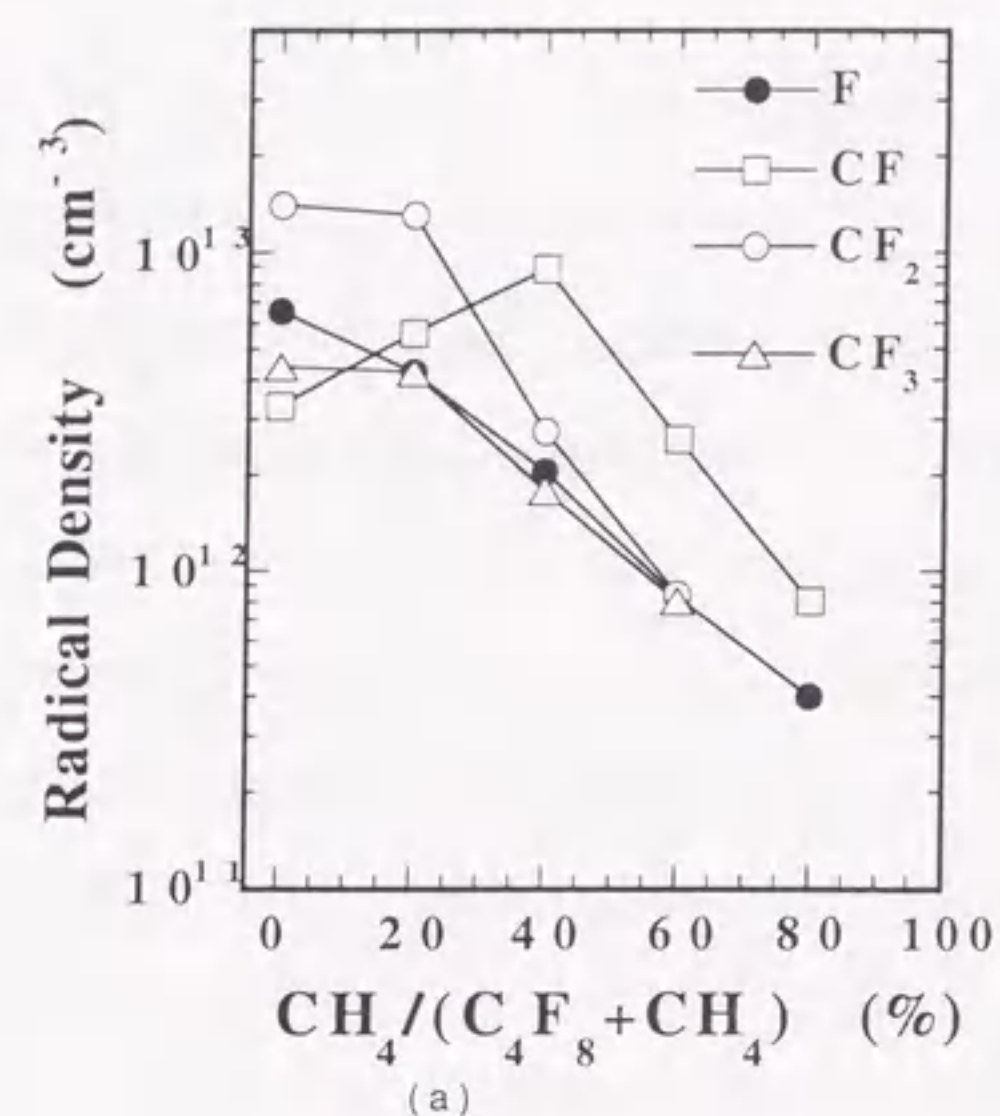


Fig. 5.2. Absolute  $CF_x(x=1-3)$  radical densities and fluorine atom density (a) and normalized  $CF_x(x=1-3)$  radical densities (b) in  $C_4F_8$  plasma as a function of  $CH_4$  gas percentage. The input microwave power is 900 W, pressure 0.4 Pa and position downstream is 20 cm.

on the etch process of  $SiO_2$  on Si. Hence, the main discussion in this paper is concerned with diagnostics of the fluorocarbon radical species along with carbon and fluorine atom densities in a high density ECR etching plasma employing  $C_4F_8$  gas to which  $CH_4$  is added in order to understand in more detail the effect of carbon and carbon products on the etch process of  $SiO_2$  over Si. To understand the precursor chemistry involved in fluorocarbon etch gases, and as a means of comparison with etching results, in Fig. 5.3, the  $CF_x(x=1-3)/F$  ratios are plotted as a function of  $CH_4$  percentage.

#### 5.4 Measurement of the carbon atom density in a $C_4F_8$ ECR etching plasma.

The most interesting point to note about the addition of  $CH_4$  to  $C_4F_8$  ECR plasma is that it has enabled us to measure for the first time the carbon atom density in an etching plasma. Measurements were carried out by hollow cathode absorption spectroscopy. The measured results are shown in Fig. 5.4(a). Although these results do not represent absolute densities, they do allow us to make some very interesting observations. The first point to note is that only above 20% of  $CH_4$  are there enough carbon atoms to register a signal. The second point is that the carbon atom density increases linearly up to  $CH_4$  gas addition above 80%. As the plasma chemistry approaches 100%  $CH_4$ , the carbon atom density decreases again below measurable levels. The fact that for both pure  $C_4F_8$  and  $CH_4$  plasma the carbon atom density falls below the measurable limit implies that the main production mechanism of carbon atoms is not that of electron impact dissociation. Therefore, it is more probable that the carbon atoms are produced by gas phase reactions such as



The reaction rate constants of reaction (5.3) for  $x=1-3$  are of the order of  $10^{11} \text{ cm}^3/\text{s}$  which is quite rapid.[9] Moreover, an increase in the carbon atom density with increasing  $CH_4$  and

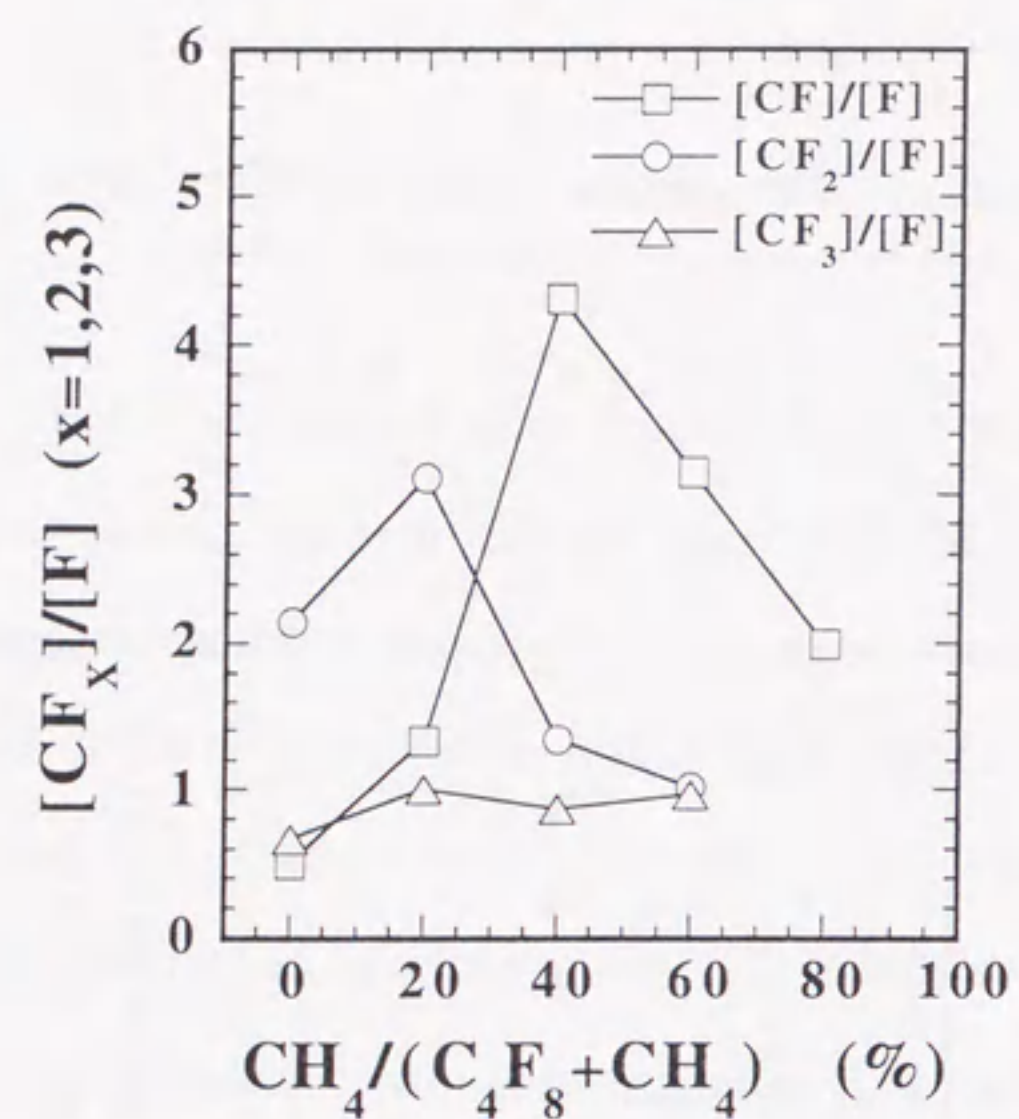


Fig. 5.3. The  $CF_x$  (x=1-3)/flourine ratios in  $C_4F_8$  plasma plotted as a function of  $CH_4$  percentage. The input microwave power is 900 W, pressure 0.4 Pa and position downstream is 20 cm.

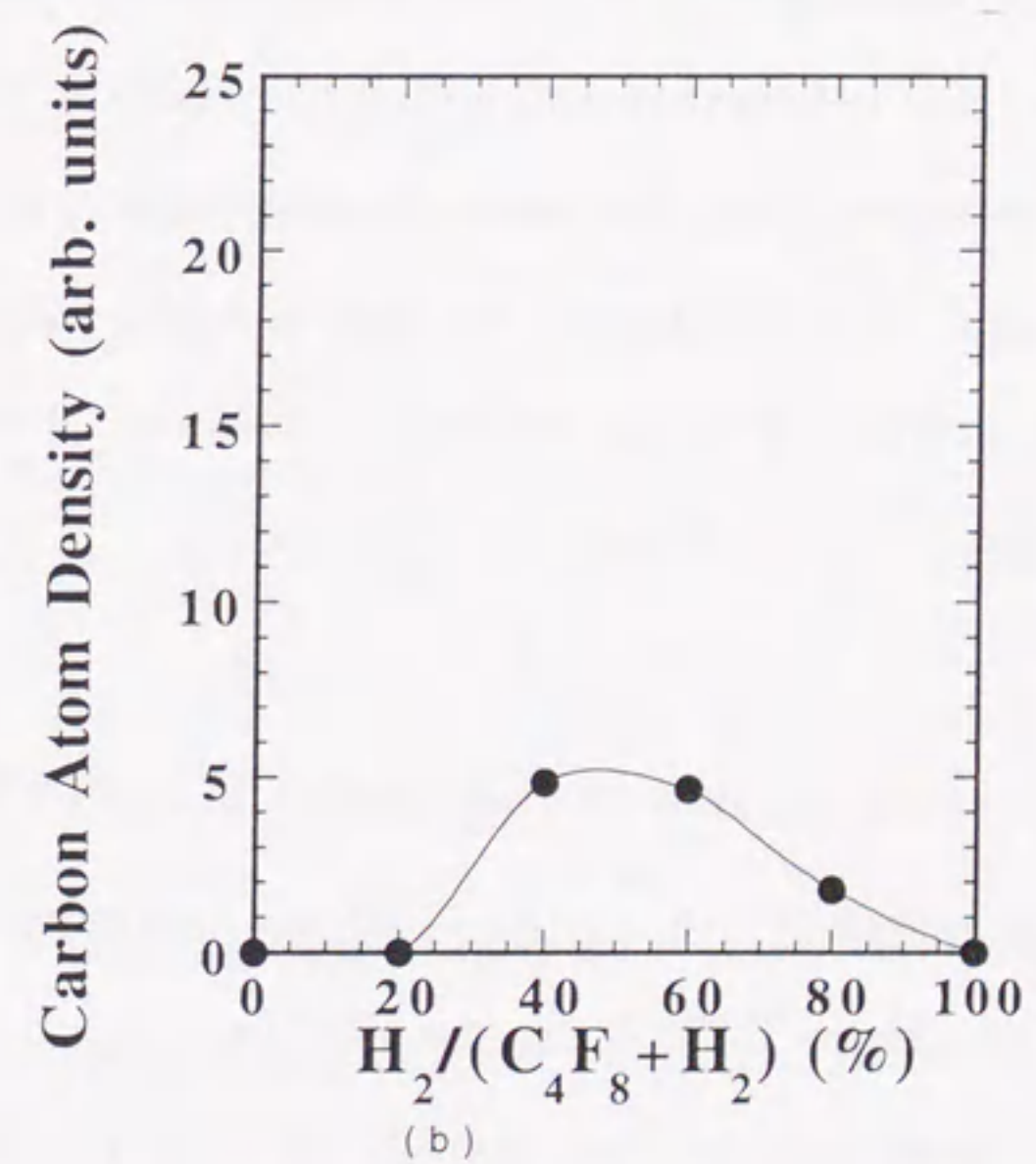
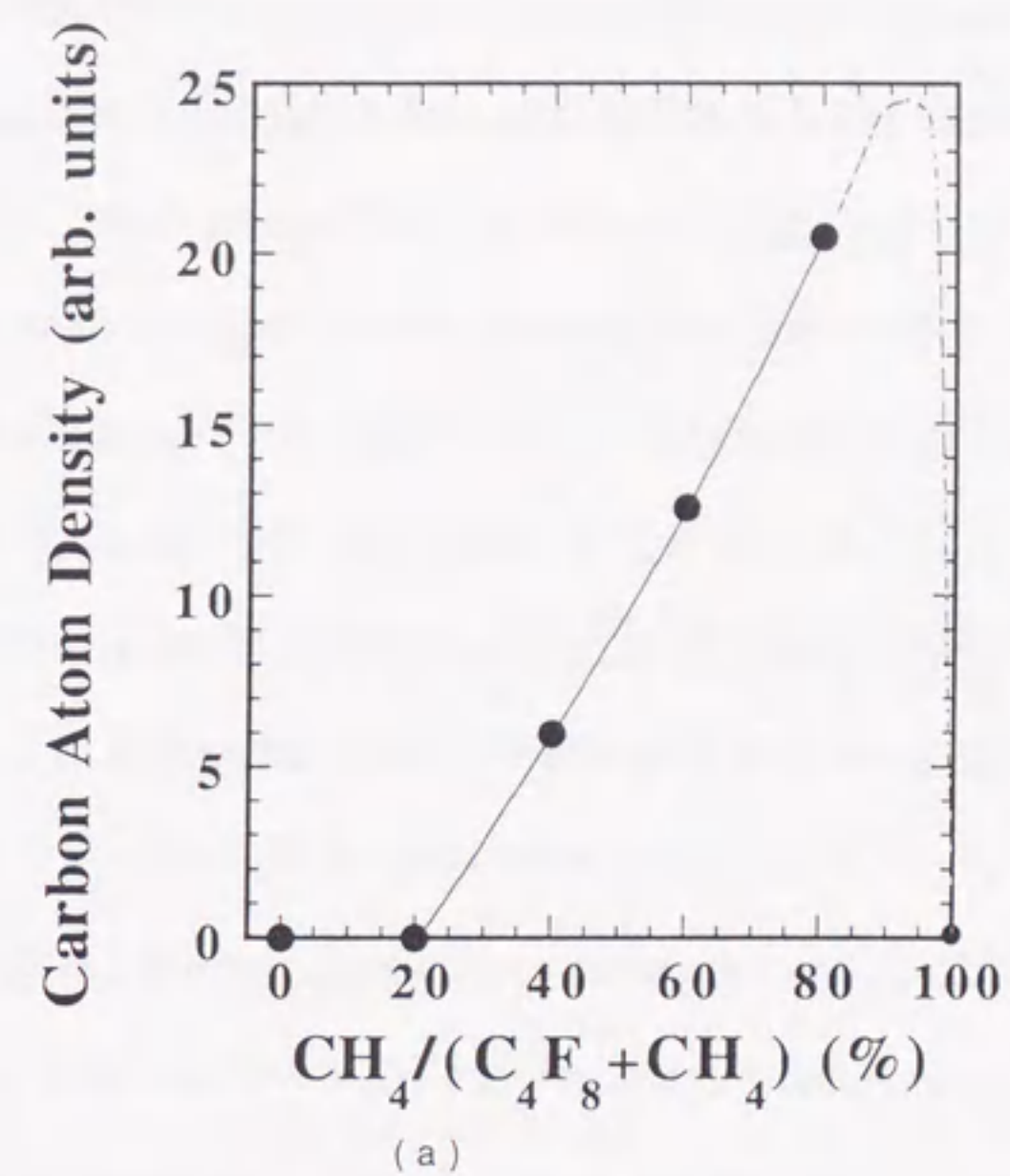


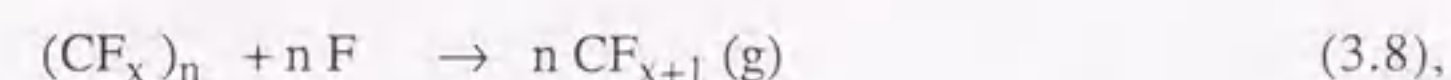
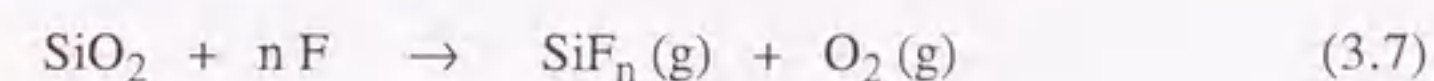
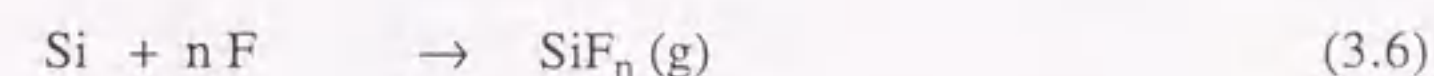
Fig. 5.4. Characteristics of the carbon atom density in  $C_4F_8$  plasma plotted as a function of  $CH_4$  percentage (a) and  $H_2$  percentage (b). The input microwave power is 900 W, pressure 0.4 Pa and position downstream is 20 cm.

decreasing fluorine atom density suggests that the process is driven by CH<sub>4</sub> addition. This is consistent with results by Takahashi *et al.* who showed that addition of H<sub>2</sub> to a CHF<sub>3</sub> plasma resulted in the deposition of carbon-rich fluorocarbon films in ECR plasma.[9] There has also been a lot of work carried out in analyzing the effect of H<sub>2</sub> addition to the etching gas chemistry.[9,12] It has been shown that by H<sub>2</sub> addition, the CF<sub>x</sub>/F ratio can be controlled and it is suggested that this is responsible for enhanced selectivity. Due to the difficulty in measuring the carbon atom density, the effects of carbon atoms have not figured strongly in these discussions. As a comparison with the results in Fig. 5.4(a), the carbon atom density in a C<sub>4</sub>F<sub>8</sub> ECR plasma as a function of H<sub>2</sub> addition is plotted in Fig. 5.4(b). Compared to CH<sub>4</sub> addition, the maximum carbon atom density has decreased by a factor of 4. This is further evidence that the process is CH<sub>4</sub> driven and that reaction (5.3) plays an important role in the production of carbon atoms and H for reaction with F. However, it can be seen quite clearly that addition of H<sub>2</sub> results in a significant increase in the carbon atom density which may play an important role in the etch processes and can therefore not be omitted from the discussion. The initial increase in carbon atom density with increasing H<sub>2</sub> addition is considered to occur through reactions given in eqn. (5.2). These reaction processes reach a maximum at around 50% of H<sub>2</sub> addition and then decrease due to the decreasing parent gas.

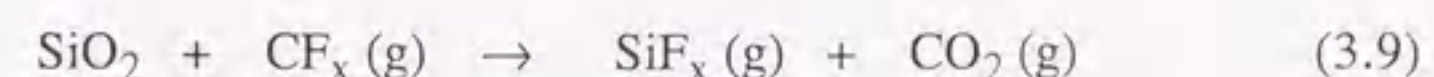
### 5.5 Etch Rate and Selectivity of SiO<sub>2</sub> and Si in C<sub>4</sub>F<sub>8</sub>/CH<sub>4</sub> ECR plasma.

The data presented thus far is in part qualitative which makes exact identification and understanding of the kinetics difficult. On the other hand, actual SiO<sub>2</sub>/Si etching is very quantitative and combined with the above characteristics may provide an intuitive insight as to the actual kinetics involved. In Fig. 5.5, the etch rate of SiO<sub>2</sub> and Si as a function of CH<sub>4</sub> percentage are plotted. The etch rate of both SiO<sub>2</sub> and Si decrease with increasing CH<sub>4</sub>. Above a CH<sub>4</sub> percentage of 60%, no etching of Si occurs. The effect of this can be seen more clearly in Fig. 5.6 where the etch selectivity as a function of CH<sub>4</sub> percentage is plotted.

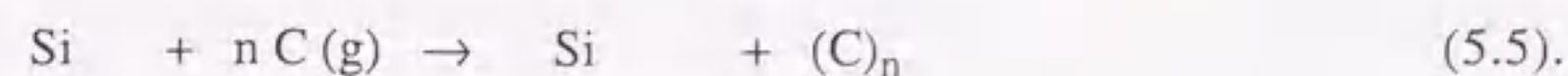
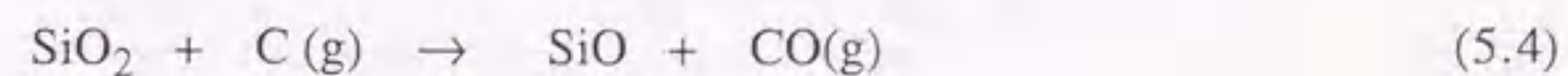
Above 60% due to zero Si etching, the selectivity goes to infinity. What is even more interesting is that as shown in Fig. 5.5, the carbon atom to fluorine atom ratio (C/F) follows a similar trend to that of the selectivity. From the results presented in Fig's 5.5 and 5.6, there is a direct correlation between the carbon atom density and etch selectivity. This result is consistent with results by Goto *et al.*[16,17] who observed the formation of carbon rich fluorocarbon films on Si surfaces that resulted in highly selective SiO<sub>2</sub> etching. It was described in Chapter 3 that in selective SiO<sub>2</sub>/Si etching process all of Si, SiO<sub>2</sub> and fluorocarbon polymer (CF<sub>x</sub>)<sub>n</sub> are etched by F atom through the reactions as follows,



and CF<sub>x</sub> radicals (CF<sub>x</sub>(g)) etch the SiO<sub>2</sub> but deposit and form fluorocarbon polymer (CF<sub>x</sub>)<sub>n</sub> on the underlying Si as follows,



On the other hand, it is considered that carbon atom works as precursor of carbon film which is most difficult material to be etched, and it is given as follows,



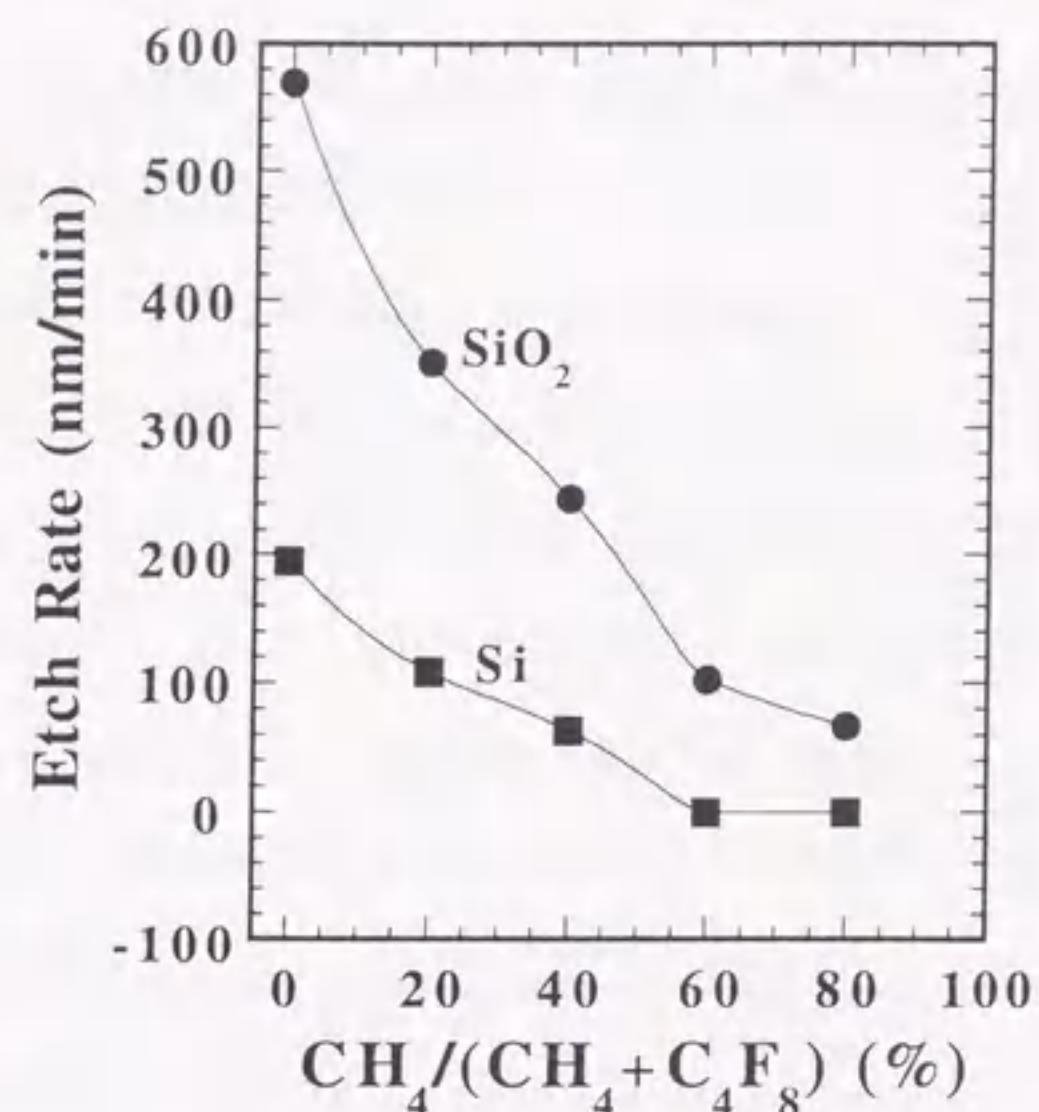


Fig. 5.5. Etch rate of SiO<sub>2</sub> over Si plotted as a function of CH<sub>4</sub> percentage. The input microwave power is 900 W, pressure 0.4 Pa and position downstream is 10 cm.

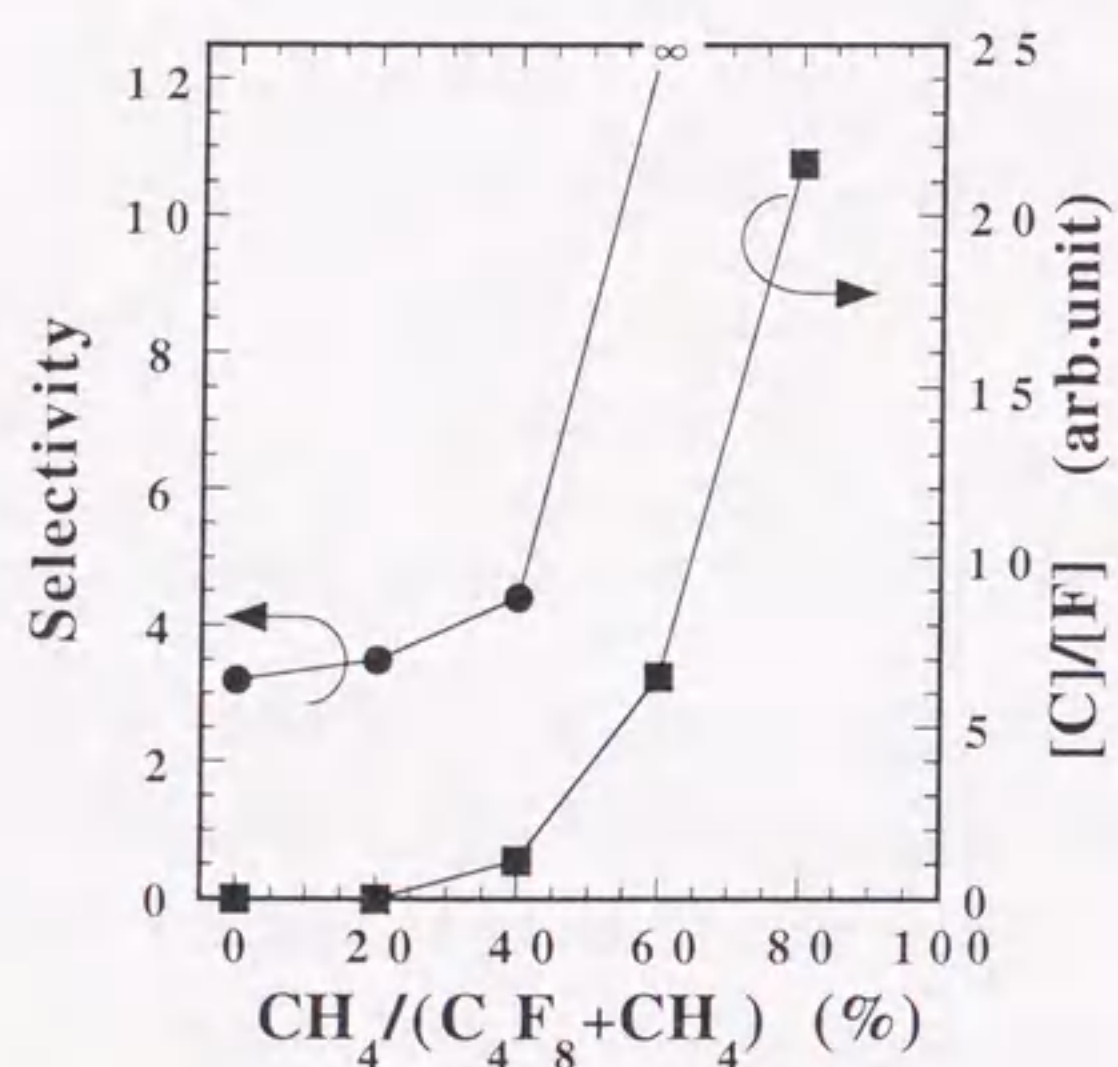


Fig.5.6. Etch selectivity and carbon atom to fluorine atom density ratio(C/F) as a function of CH<sub>4</sub> percentage.

It is therefore considered that the formation of a carbon rich fluorocarbon film will be enhanced by means of the high carbon density in C<sub>4</sub>F<sub>8</sub> plasma with the addition of CH<sub>4</sub>. These reactions of carbon atoms may be a key factor in the selective etch process. No correlation can be seen between etch selectivity and the CF<sub>x</sub> (x= 1-3)/F ratios which were plotted in Fig. 5.3. This suggests that the carbon atom plays an important role in the etch process and may be the main precursor involved in attaining good etch selectivity. This result is of particular importance for processing applications in which photoresists are used. In such applications, carbon from the photoresist and the plasma chemistry may be the limiting factor for process resolution. While this is only a preliminary investigation, it certainly places importance on quantifying the carbon atom density, if a more complete understanding of sub-0.25μm etch processes is to be achieved. Lastly, it should be noted that little attention was paid to optimizing the process conditions. Hence, although the etching rate of SiO<sub>2</sub> is low when the selectivity to Si goes to infinity, with further investigation and optimization higher etch rates are expected.

## 5.6 Summary

We have investigated changes in the densities of fluorocarbon radicals and fluorine atoms in a size-scalable large-area compact permanent magnet ECR etching plasma source employing C<sub>4</sub>F<sub>8</sub> gas adding with CH<sub>4</sub> gas which was chosen mainly because it is a source of carbon atoms similar to those produced from the photoresist. It was seen using IRLAS that for a pure C<sub>4</sub>F<sub>8</sub> plasma, the dominant species is CF<sub>2</sub> radicals which have a density of the order of 10<sup>13</sup> cm<sup>-3</sup>, followed by fluorine atoms, CF<sub>3</sub> and CF radicals which have a density an order of magnitude lower at 10<sup>12</sup> cm<sup>-3</sup>. The dissociation kinetics of the different fluorocarbon radical species were found to display different dependencies on increasing CH<sub>4</sub> gas addition. Hollow cathode absorption spectroscopy was used to estimate the carbon atom density, for the first time in an etching plasma. The carbon atom density increases linearly with CH<sub>4</sub> gas addition between 20 to 80% and the dissociation process is believed to be CH<sub>4</sub>

driven. Actual SiO<sub>2</sub>/Si etching revealed that the etch rate of both SiO<sub>2</sub> and Si decreased with increasing CH<sub>4</sub>. Moreover, above 60% due to zero Si etching the selectivity goes to infinity. It was also shown that the carbon atom to fluorine atom ratio follows a similar trend to that of the selectivity indicating a direct correlation between the carbon atom density and etch selectivity.

## References

- [1] S. Samukawa: Jpn. J. Appl. Phys. 33, 2133 (1994).
- [2] S. Arai, K. Tsujimoto and S. Tachi: Jpn. J. Appl. Phys. 31, 2011 (1992).
- [3] O. Joubert, G. S. Oehrlein and Y. Zhang: J. Vac. Sci. Technol. A 12, 658 (1994).
- [4] O. Joubert, G. S. Oehrlein and M. Surendra: J. Vac. Sci. Technol. A 12, 665 (1994).
- [5] K. Takahashi, M. Hori and T. Goto: Jpn. J. Appl. Phys. 33, 4745 (1994).
- [6] K. Miyata, K. Takahashi, S. Kishimoto, M. Hori and T. Goto: Jpn. J. Appl. Phys. 34, L444 (1995).
- [7] K. Miyata, M. Hori and T. Goto: J. Vac. Sci. Technol. A 14, 2343 (1996).
- [8] H. Doh, J. Kim, S. Lee and K. Whang: J. Vac. Sci. Technol. A 14, 2827 (1996).
- [9] K. Takahashi, M. Hori and T. Goto: J. Vac. Sci. Technol. A 14, 2011 (1996).
- [10] K. Takahashi, M. Hori and T. Goto: J. Vac. Sci. Technol. A 14, 2004 (1996).
- [11] S. Den, T. Kuno, M. Ito, M. Hori, T. Goto, Y. Hayashi and Y. Sakamoto: Jpn. J. Appl. Phys. 35, 6528 (1996).
- [12] Y. Zhang, G. S. Oehrlein and F. H. Bell: J. Vac. Sci. Technol. A 14, 2127 (1996).
- [13] F. H. Bell and O. Joubert: J. Vac. Sci. Technol. B 14, 3437 (1996).
- [14] H. Ito, M. Ikeda, M. Ito, M. Hori, T. Goto, T. Takeo and H. Hattori: submitted to Jpn. J. Appl. Phys..
- [15] K. Tachibana: Jpn. J. Appl. Phys. 33, 4329 (1994).
- [16] K. Takahashi, M. Hori, M. Inayoshi and T. Goto: Jpn. J. Appl. Phys. 35, 3635 (1996).
- [17] T. Goto and M. Hori: Jpn. J. Appl. Phys. 35, 6521 (1996).

## Chapter 6. Development and Characterization of a Compact Radical Source Using Permanent Magnet Microwave Plasma

### 6.1 Introduction

Advances in the design and development of compact plasma sources have led to their use in a wide variety of processing applications.[1-4] Future plasma processing making the best use of radical species requires a plasma source with high radical and low ion densities, a dynamic operating pressure range and enhanced control of plasma parameters. Applications include substrate surface cleaning[5] in which hydrogen plasma is used for substrate cleaning prior to growth processes such as atomic layer epitaxy, molecular beam epitaxy and chemical beam epitaxy, also in etching[6] and as an assist in thin film deposition.[7] Microwave plasma is attractive since it is associated with low electron and ion temperatures that minimize damage. It is also operational over a wide pressure range even with reactive gases.

Recently, a compact radical source using permanent magnet microwave plasma has been successfully used as a source of hydrogen radicals during the high pressure chemical vapor deposition(CVD) of diamond.[8,9] Due to the compact source design, preferential injection of hydrogen radicals near the substrate was possible. This provided the necessary hydrogen flux to produce the diamond phase. Reactive oxygen plasma is also used in a wide variety of microelectronic applications such as etching, thin film deposition and resist ashing.[10-12] More recently oxygen plasma has been used in the formation of ultra-thin SiO<sub>2</sub> films at low temperatures.[13] Unlike previous high temperature thermal processing the use and control of the activated radical species in oxygen plasma allow high quality SiO<sub>2</sub> films ~100 Å thick to be grown at a low temperature.[14] In understanding such plasma-material interaction processes, it is necessary that the radical density is quantified and that its interaction with the chamber surroundings be understood. It has been shown empirically that the material surrounding the discharge can determine the loss rate of plasma species and hence density of radical species.[15,16]

In this chapter, the development and characterization of a compact microwave plasma source are described. Plasma production with microwave powers of up to 500 W is possible, however unlike other high power microwave sources, the discharge zone is inside the vacuum chamber. This allows for very high densities of active radical species to be delivered very close to the substrate. Oxygen atom densities of up to 10<sup>16</sup> cm<sup>-3</sup> have been measured. The plasma source is also specifically designed to allow a wide operation range. Operational pressure range from 0.1 to 100 Pa with an input microwave power range from 100 to 500 W. From an application point of view, initial characterization of reactive oxygen plasma is presented. Emission spectroscopy is used to identify the plasma species present and their dependence on plasma operation parameters. To estimate the absolute density of radicals in a plasma source, actinometric and laser-induced fluorescence(LIF) techniques are often employed.[17,18] However, actinometry only provides a qualitative measurement while LIF analysis is complex. To overcome these problems, development of titration measurement techniques are of interest in providing a simple means of quantitative radical measurements. In the present study, titration using NO<sub>2</sub> gas is used independently to correlate the oxygen atom density with the plasma operating conditions. In particular, measurement of the oxygen atom dependence on chamber wall material is discussed.

### 6.2 Configuration

A compact microwave source operational over a pressure range of 0.1 to 100 Pa has been designed and developed. A cross sectional view of the compact plasma source is shown in Fig. 6.1 with details of the main components and dimensions. Figure 6.2 shows photographs of the source (a) and when it is mounted to the chamber (b). The source is variable in overall length and allows application to a 114 mm conflat flange. The outer diameter of the discharge zone is 57 mm. The source is constructed from stainless steel and all components are ultra high vacuum compatible. Microwave from a rectangular waveguide is converted to a coaxial mode and propagates along a water cooled co-axial line to the discharge zone. Microwave powers of up to 500 W can be coupled into to the discharge zone via a disk antenna. Optimum coupling of the microwave to the discharge zone is provided by

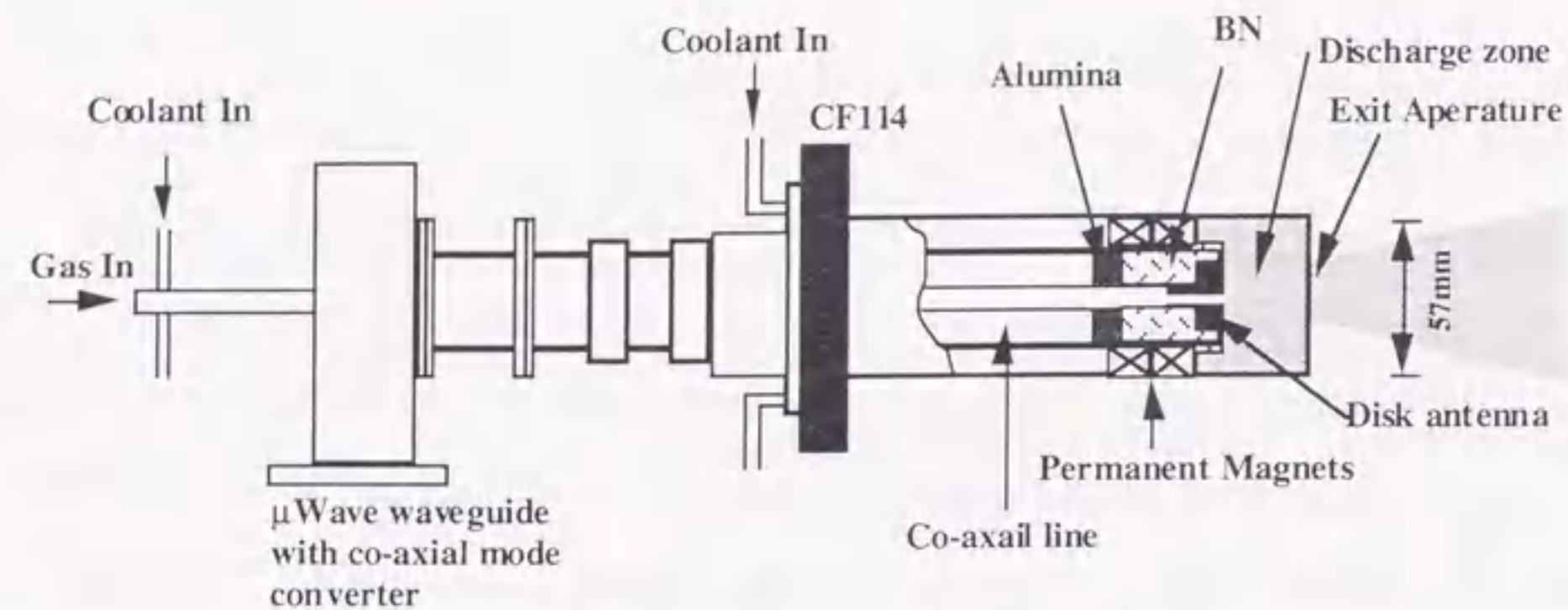


Figure 6.1 Schematic diagram of the compact microwave plasma source.

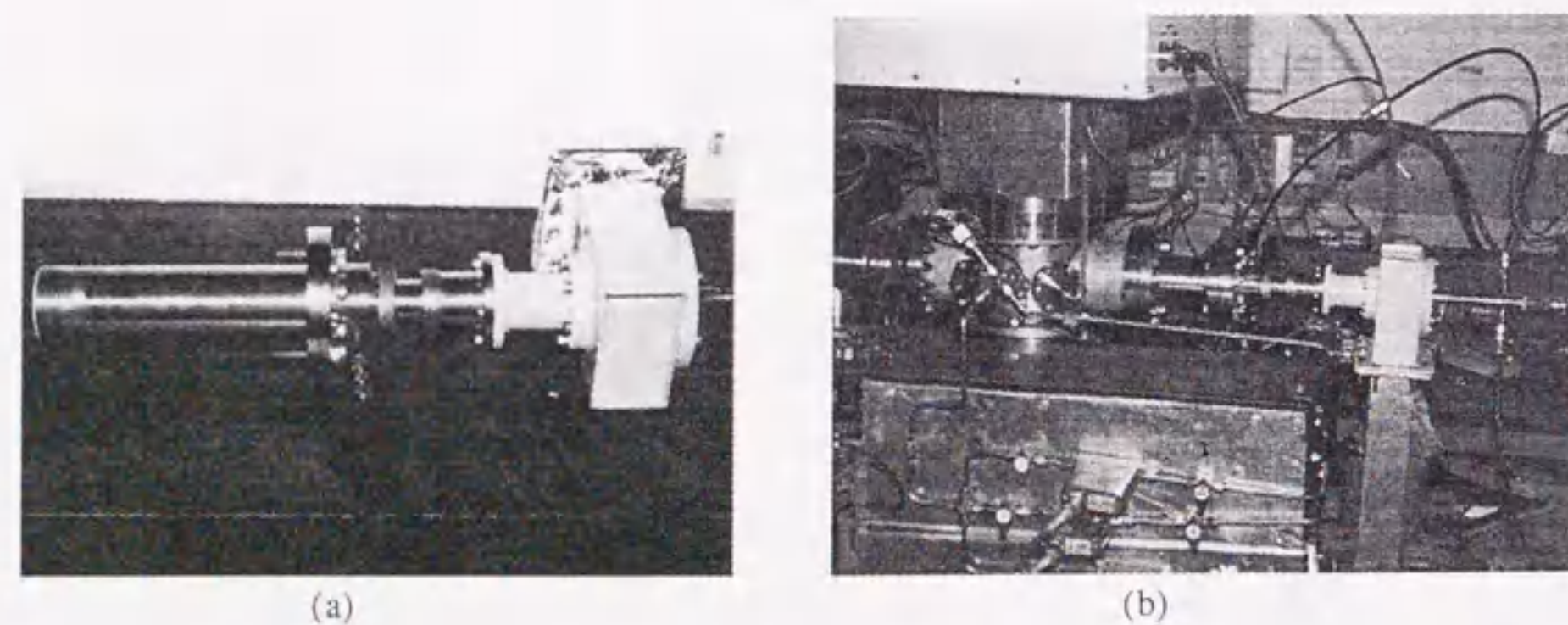


Figure 6.2 Photographs of the source (a) and when it is mounted to the chamber (b).

adjustment of a 3-stub tuner(not shown) and the reflected power is maintained within 10 % of the input value. The discharge zone which is 29 mm in length and 50 mm in diameter is defined by boron nitride. It contains a 2 mm hole to allow introduction of the gas, which is fed from the rear. An interchangeable exit aperture is fitted at the front and provides control of the pressure in discharge zone independently of chamber pressure. For low pressure operation, a magnetic field provided by two ring-shaped water cooled Sm-Co permanent magnets are employed. A permanent magnet arrangement placed in front of the exit aperture provides a trap for electrons which prevents dissociation due to plasma electrons in the downstream region.

The microwave plasma source was mounted on a stainless steel chamber 160 mm in diameter 280 mm in height, pumped by a 200 l/s turbomolecular pump. The chamber wall is covered with a Teflon liner. All measurements were taken 80 mm downstream of the discharge zone. A Langmuir probe was used to analyze plasma parameters in the low pressure regime, optical emission spectroscopy identified the plasma species present and titration measurements using  $\text{NO}_2$  gas allowed quantification of the O atom densities. In particular, the effect of chamber wall material on the O atom density was investigated.

### 6.3 Characterization

Argon (Ar) plasma was initially characterized using single Langmuir probe diagnostics. All measurements were carried out on-axis downstream from the source in order to reduce perturbations associated with operating a Langmuir probe in a magnetic field. Cleaning by electron bombardment was performed before each measurement. The electron density ( $n_e$ ) and electron temperature ( $T_e$ ) of Ar plasma as a function of discharge pressure are plotted in Fig. 6.3. The input microwave power was maintained constant at 190 W, the position downstream was 30 mm. Over the pressure range investigated, in contrast to ECR plasma  $n_e$  increases with increasing pressure while  $T_e$  decreases with increasing pressure. The decrease in  $T_e$  is explained by diffusion of the plasma (decreasing mean free path) at the



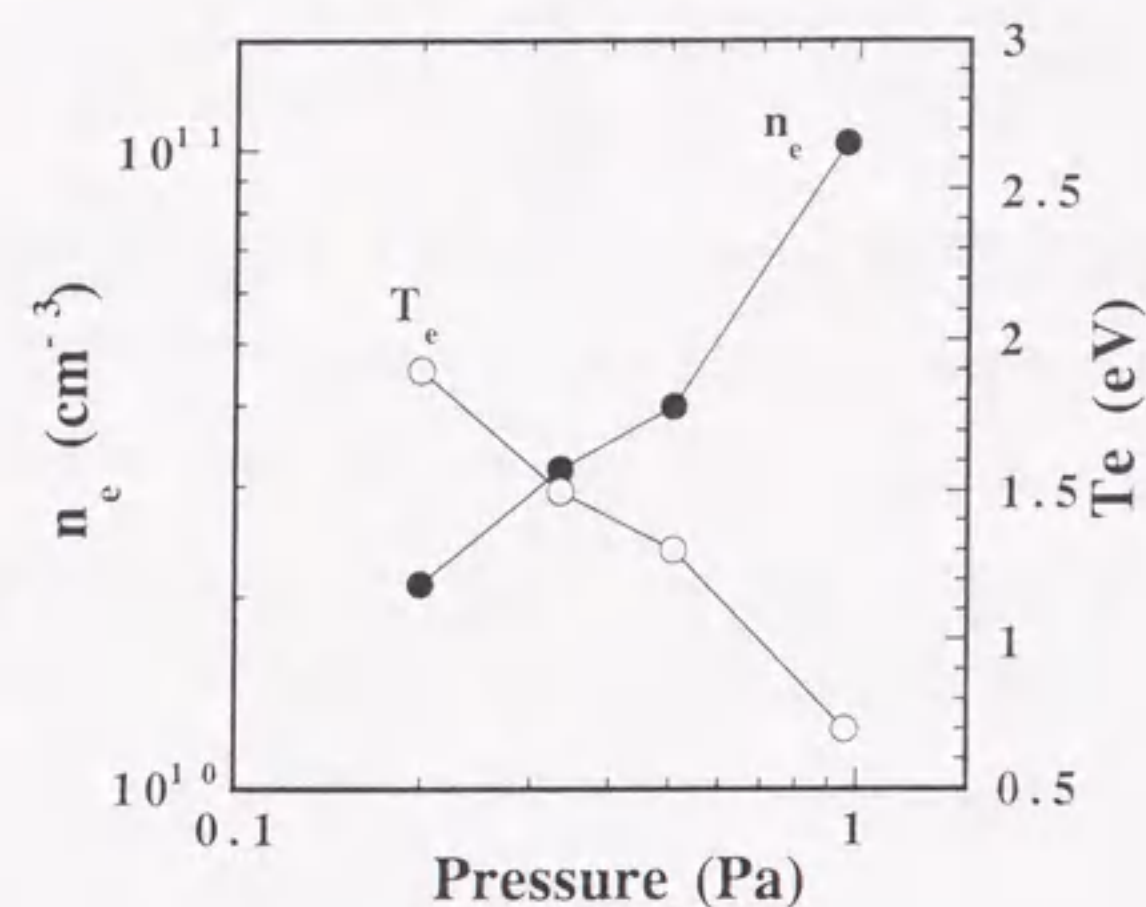


Figure 6.3 The electron density ( $n_e$ ) and electron temperature ( $T_e$ ) of argon plasma as a function of discharge pressure. The input microwave power was 190 W, the position downstream was 30 mm.

higher pressures which results in lower average electron energies hence the decrease in  $T_e$ . A plasma potential of lower than 8 V has also been recorded.

To obtain more information about the plasma chemistry, in particular, at high operational pressures, optical emission spectroscopy was performed. Figure 6.4 shows typical emission spectra obtained from oxygen microwave plasma. The spectrum in Fig. 6.4 (a) was obtained from oxygen plasma at 10.6 Pa and an input microwave power of 200 W. The spectrum is dominated the oxygen radical ( $\text{O}^*$ ) emission line at 777.6 nm that corresponds to a transition from the  $3p^5P$  state to the  $3s^5S$  state. Ionic emission bands ( $\text{O}_2^+$ ) at 562 nm, 490 nm and 410 nm from  $^4\Sigma_g^- \rightarrow ^4\Pi_u$  transitions are also observed. This spectrum is typical of microwave oxygen plasma and has been well documented.[19,20] Increasing the pressure up to 16.0 Pa, we see that the spectrum is still dominated by the 777.6 nm emission but also a new emission peak at 759 nm that is assigned to molecular oxygen transitions from  $^1\Sigma_g^+ \rightarrow X^3\Pi_g^-$  recently observed also by T. T. Chau *et al.* at pressures above 9.3 Pa also in a microwave plasma.[20] From these results, it can be seen that the plasma chemistry is, therefore, controlled by the different reaction processes in the different pressure regimes. Up to approximately 10 Pa, the dominant processes are electron impact ionization and dissociation. At pressures above 10 Pa, ionization processes are suppressed due to decreasing mean free path and plasma temperatures. This can be seen also in Fig. 6.5 where the emission intensities of  $\text{O}^*$  at 777.6 nm and  $\text{O}_2^+$  at 562 nm are plotted as a function of (a) pressure and (b) power.

From Fig. 6.5(a), it can be seen that the emission intensity of  $\text{O}_2^+$  decreases exponentially with increasing pressure. The emission intensity of  $\text{O}^*$  initially increases up to a pressure of 8 Pa and then decreases exponentially with increasing pressure. Chau *et al.* have attributed this decrease to be due to the decreasing mean free path giving rise to the following reactions[20]

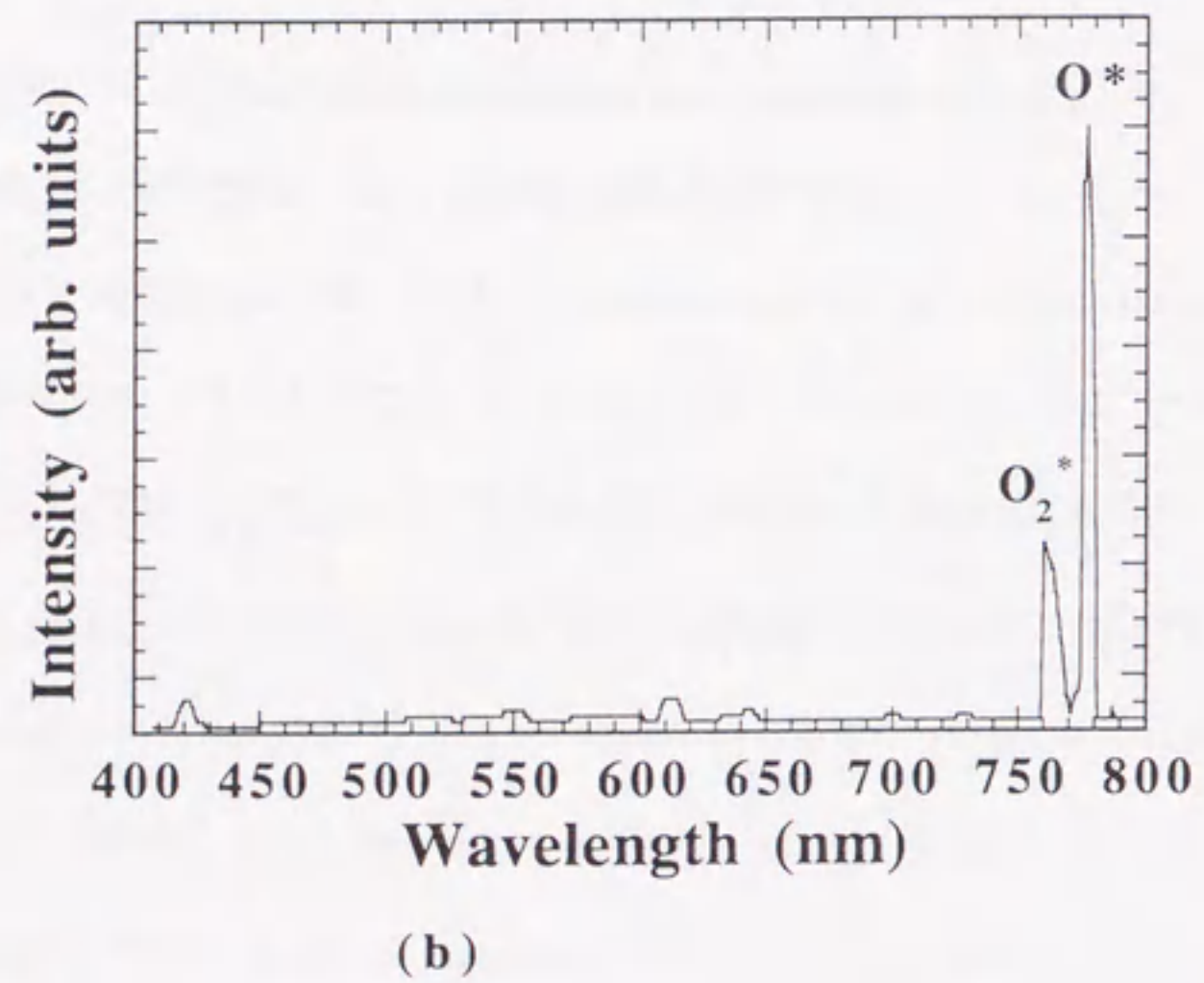
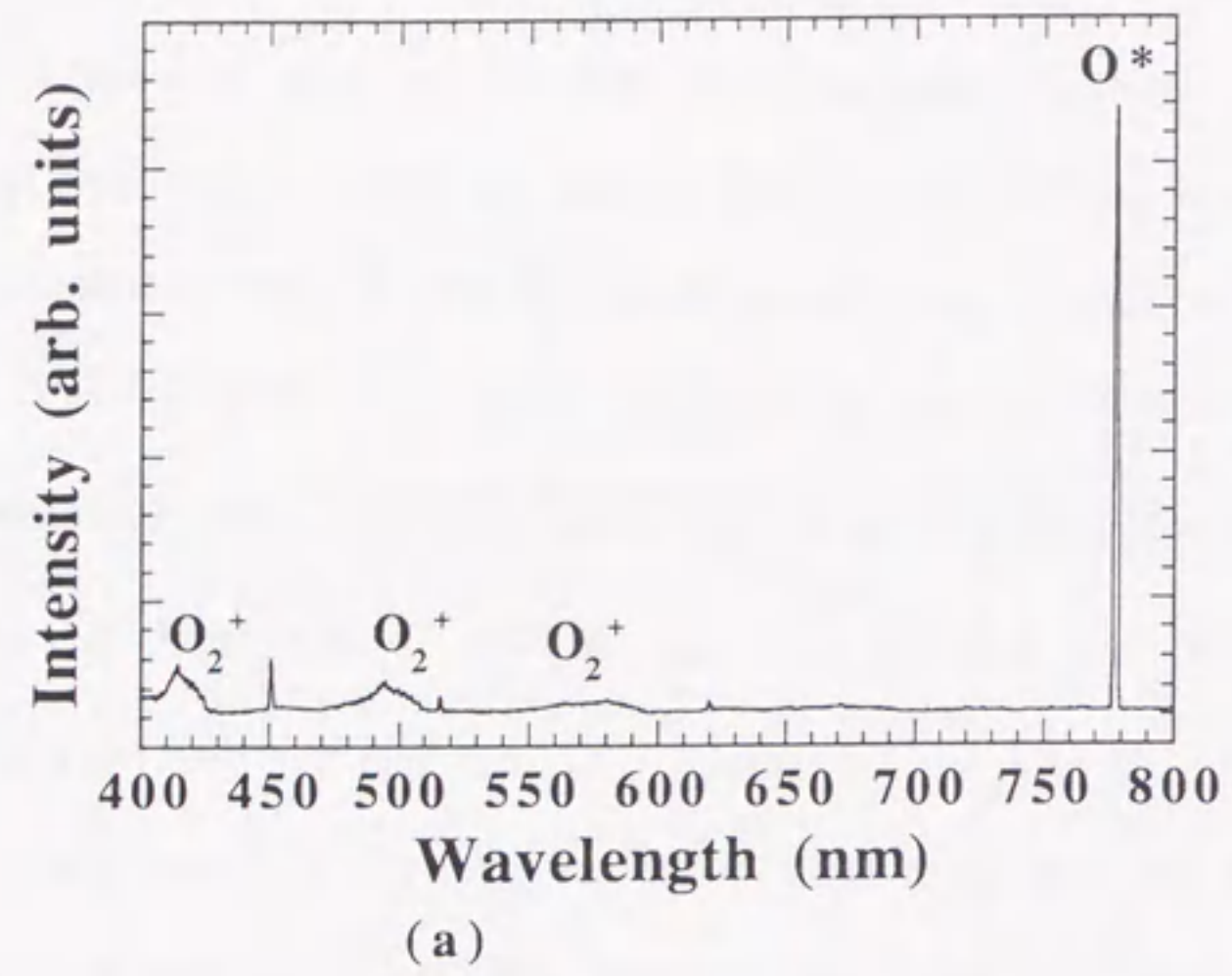


Figure 6.4 Typical emission spectra obtained from oxygen microwave plasma (a) at 10.6 Pa and (b) 16 Pa for an input microwave power of 200 W.

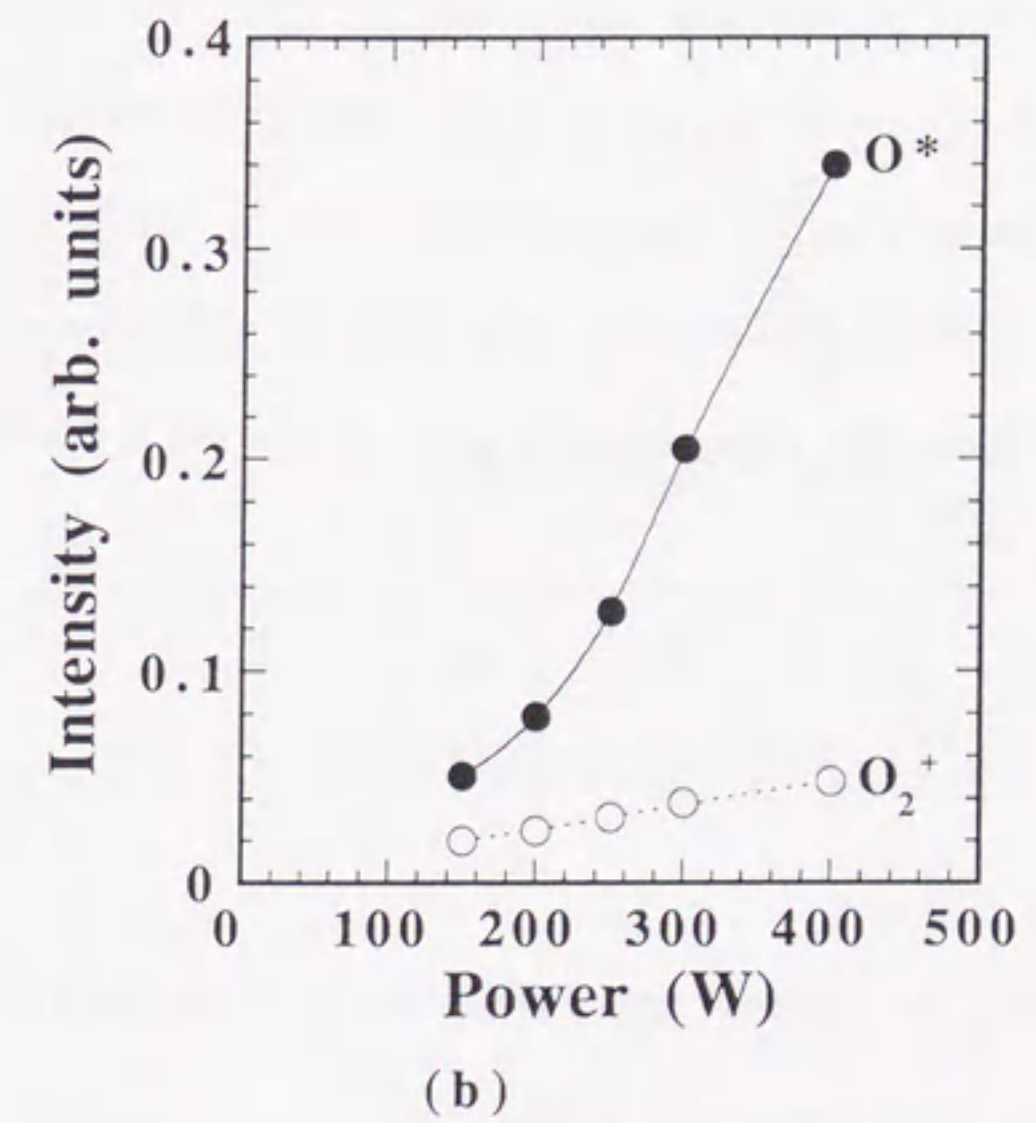
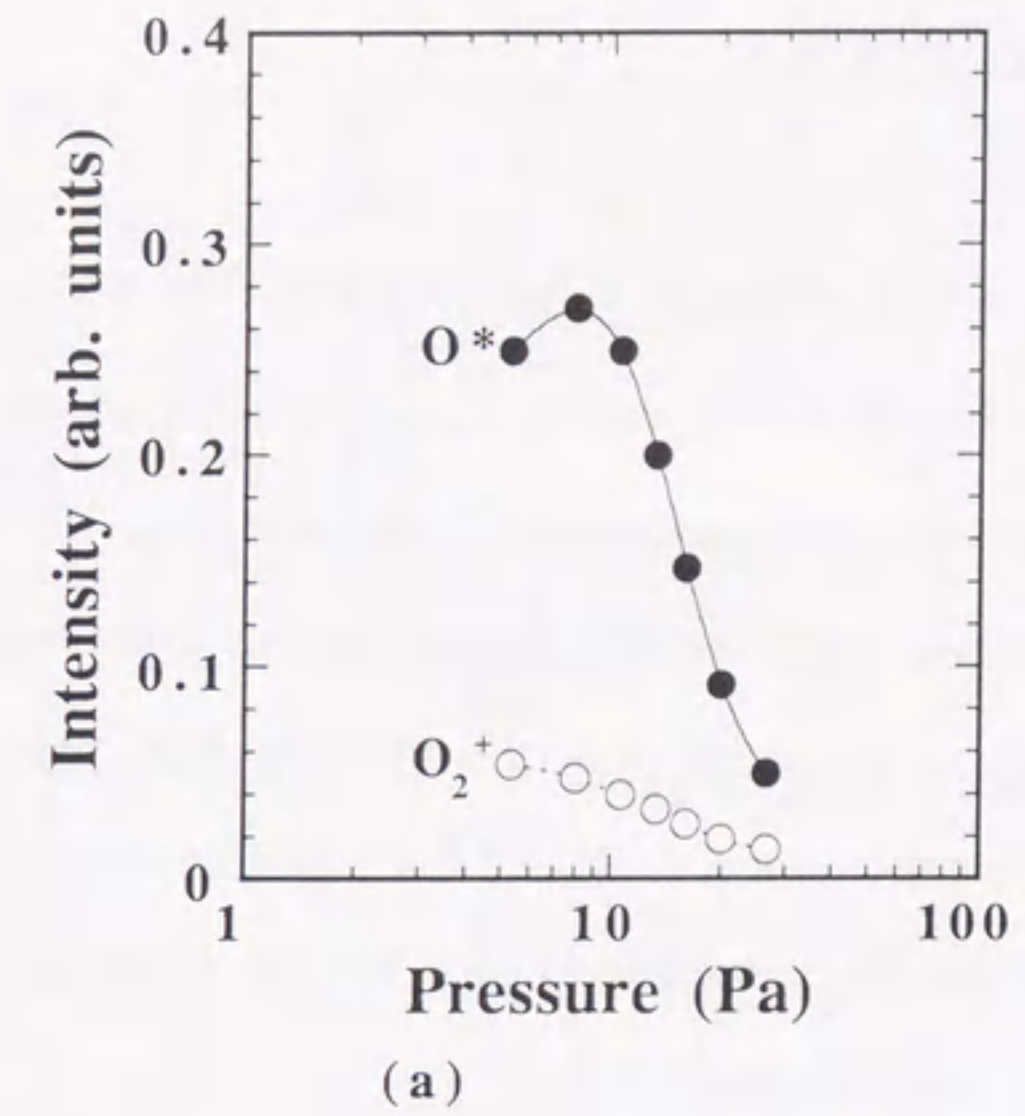
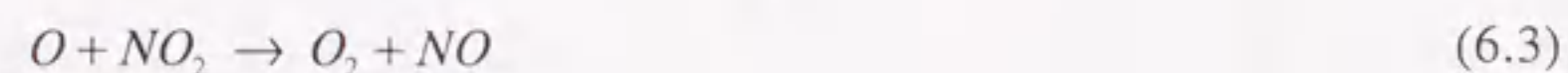


Figure 6.5 Emission intensity of the oxygen radical species at 777.6 nm and the ionic species at 562 nm as a function of (a) pressure at a microwave power of 300 W and (b) power at a pressure of 10.6 Pa.



hence the reason  $O_2^*$  is only observed at high pressures. The emission intensities of  $O^*$  at 777.6 nm and  $O_2^+$  at 562 nm versus power are shown in Fig. 6.4(b). It can be seen that although both increase with increasing power, the rate of increase is different which suggests that increasing the microwave power results mainly in direct dissociation of  $O_2$  rather than in ionization. This result is consistent with the fact that high operational pressures are associated with low electron temperatures and high electron density. Increased ionization requires an increase in electron temperature which was not evident from ion current density measurements in the pressure range of 10 Pa.

Although emission spectroscopy provides information on the plasma chemistry, the emission intensity does not provide any information regarding the density of plasma species. Quantification of radical densities is vital in understanding processing mechanisms such as oxidation rate. A particularly useful technique which can be used in the quantification of O atom density is titration. An estimate of the atom density in oxygen plasma can be obtained by adding  $NO_2$  gas to the oxygen plasma. This gives rise to the following reactions.[21]



Therefore, by monitoring the dependence of  $NO_2$  emission versus  $NO_2$  partial pressure, an estimate of the O atom density can be obtained.

Figure 6.6 shows the  $NO_2$  emission intensity versus  $NO_2$  partial pressure. The oxygen plasma pressure was 16.6 Pa. Although the overall pressure in the chamber is increasing, saturation of the ion current density in this pressure range suggests minimum change in the oxygen plasma characteristics. The emission line investigated was 548 nm which corresponds to approximately the center of the broadband emission due to  $NO_2^*$

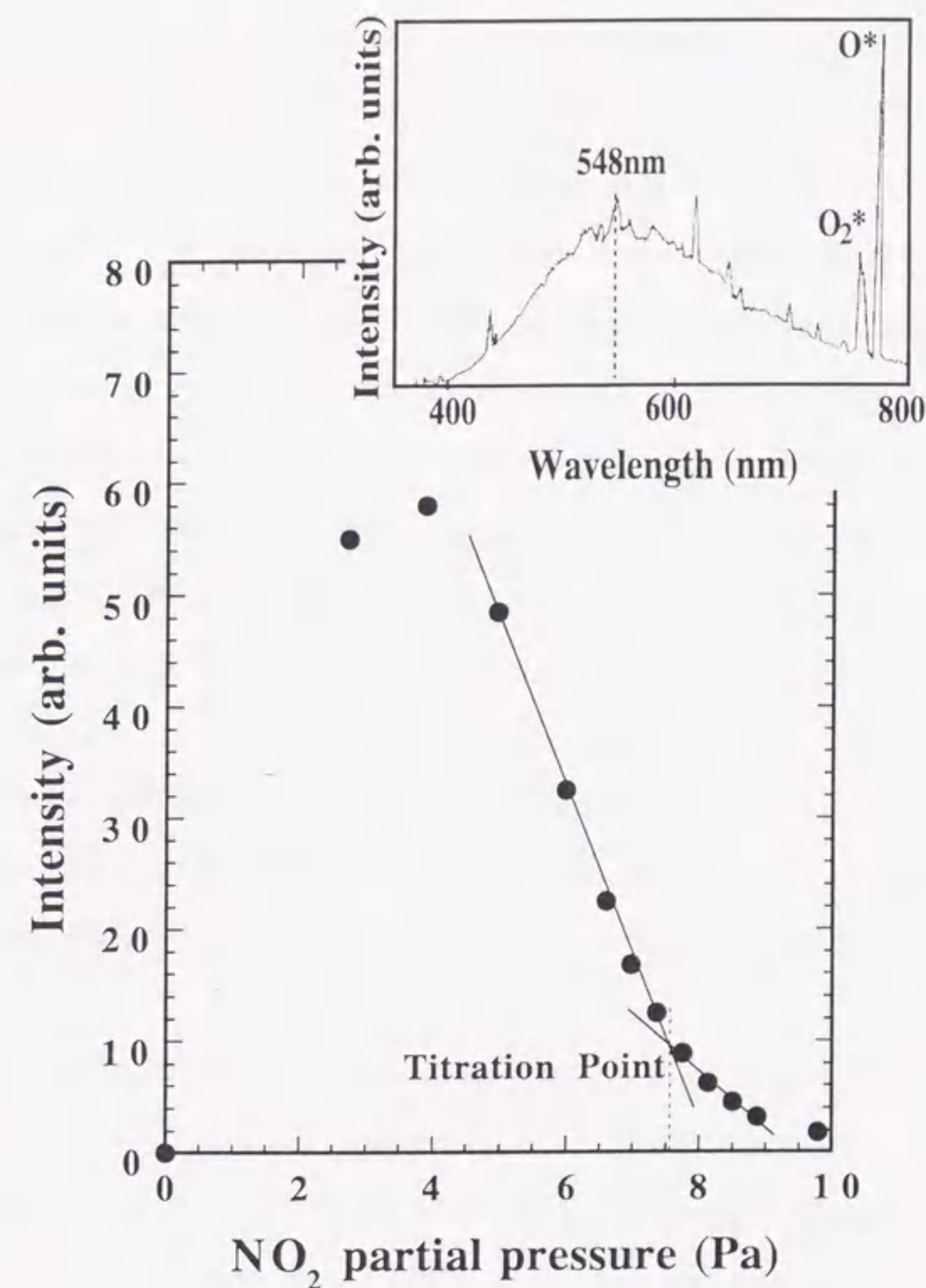


Figure 6.6  $NO_2$  emission intensity at 548 nm versus  $NO_2$  partial pressure. The oxygen plasma pressure was 16.6 Pa. The titration point and hence atom density is defined by the partial pressure value at the intersection of the two lines. The inset shows the total emission spectrum with  $NO_2$  added.

shown in the inset in Fig. 6.6. The titration point corresponds to the value 10 on the arbitrary y-scale and is determined in this case by the measurement system. The actual titration point may be lower but this at least gives us a means by which to estimate the minimum oxygen atom density. Moreover, it was confirmed that  $\text{NO}_2^*$  emission was not observed in Ar plasma. This implies that due to the effect of the permanent magnet electron trap, the electron excitation of  $\text{NO}_2$  is negligible.

Typical oxygen atom density and dissociation rate results obtained using this technique are shown in Fig. 6.7 and Fig. 6.8 as a function of power and pressure, respectively. In Fig. 6.7, it can be seen that the oxygen atom density at a pressure of 16.6 Pa increases linearly with increasing power from  $1.4 \times 10^{15} \text{ cm}^{-3}$  at 200 W to  $1.9 \times 10^{15} \text{ cm}^{-3}$  at 300 W. As expected, the dissociation rate also increases from 17.5 % at 200 W to 24 % at 300 W. These values are almost an order of magnitude greater than those reported by Brockhaus *et al.*[22] also in a microwave plasma. The difference can be explained by noting that first, in our case, the measurement position was 8 cm whereas Brockhaus *et al.* made measurements 22.5 cm downstream[22]. Second, the presence of permanent magnets in our microwave source will give rise to electron confinement and subsequent excitation and dissociation.

In Fig. 6.8, the oxygen atom density measured at a power of 200 W is plotted versus pressure both with and without the Teflon chamber liner. The first point to note is that at low pressure (2.7 Pa), the oxygen atom density is the same for both the Teflon lined chamber walls and the bare stainless steel walls. It can be seen that the oxygen atom density increases linearly with increasing the pressure up to 100 Pa in the presence of both Teflon and stainless steel, but the increasing rate of Teflon is higher. At 100 Pa, the oxygen atom density in the case stainless steel is  $5.0 \times 10^{15} \text{ cm}^{-3}$  which is increased to  $6.5 \times 10^{15} \text{ cm}^{-3}$  when the Teflon liner is inserted. From these experimental results and conditions, it can be deduced as follows. At low pressures, the main removal mechanism in the present system is through the pumping mechanism. Therefore, effect of the wall material is small. To increase the pressure up to 100 Pa, the gate valve above the turbomolecular pump requires closing. This reduces the effective pumping speed which results in loss mechanisms

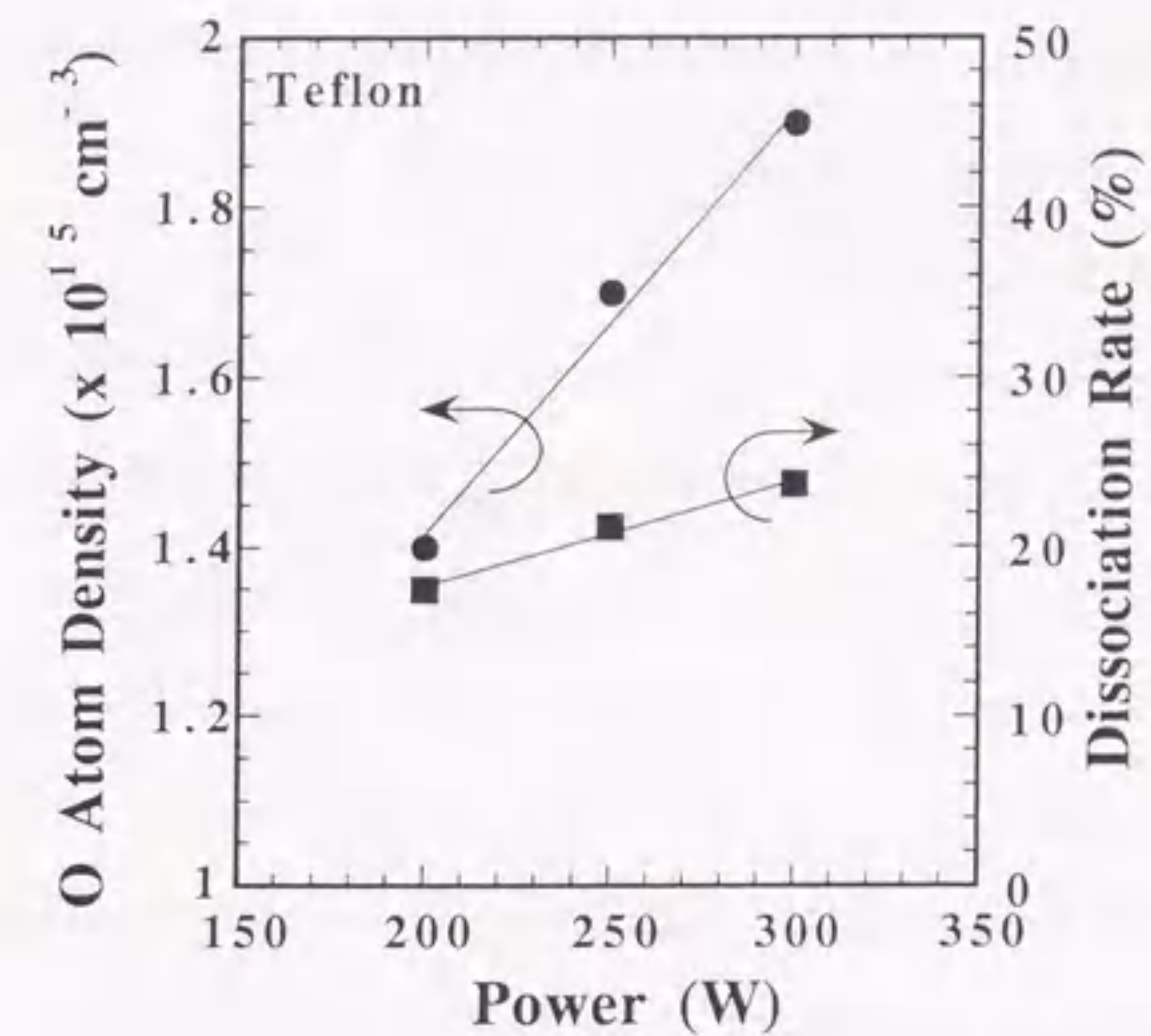


Figure 6.7 Oxygen atom density and dissociation fraction as a function of power at a pressure of 16.6 Pa. The chamber walls are lined with Teflon.

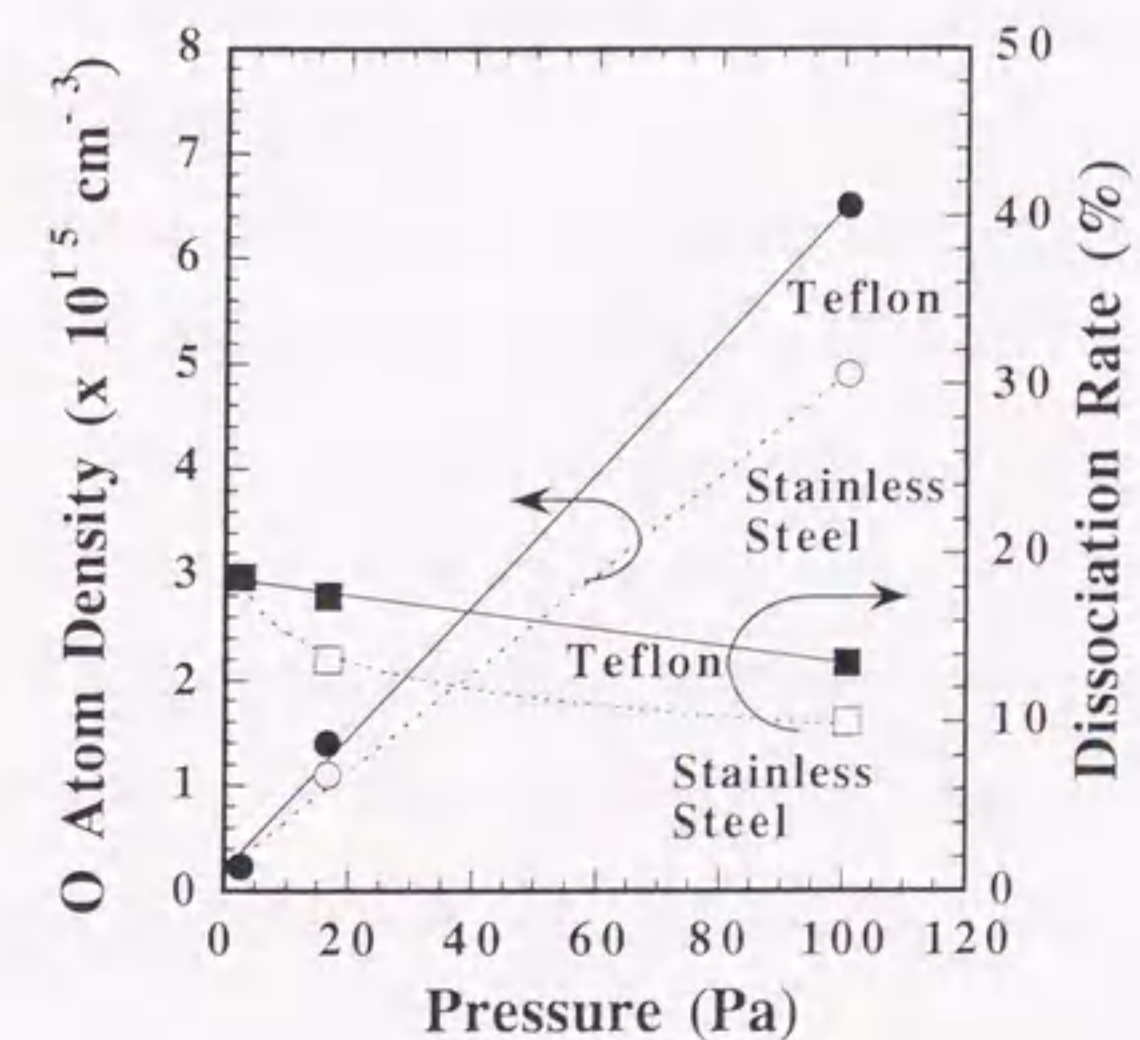


Figure 6.8 Oxygen atom density and dissociation fraction as a function of pressure at a power of 200 W when the chamber walls are stainless steel and Teflon.

to the chamber walls at high pressures. Using a Teflon liner at high pressures provides a 30 % increase in oxygen atom density due to the lower recombination coefficient of Teflon compared to stainless steel.[21] Moreover, as the input power is maintained constant, it implies the dissociation rate for both materials decreases with increasing pressure, the rate being slower in the case of Teflon.

The compact microwave plasma source described above is useful not only as a source of oxygen radicals but also for H, OH, N and  $CF_x$  radical production. It is presently being employed as a remote source of H and OH radical species in the synthesis of diamond films by chemical vapor deposition. It is also being used as a plasma source for in-situ pre-cleaning of semiconductor surfaces. This in-situ pre-clean process is essential in providing a clean surface for processing and in insuring that the process conditions remain constant. Other applications include, controlling the  $CF_x$  radical species for Si and  $SiO_2$  etching and in clarifying the role of  $CF_x$  radical species in surface reaction processes.

#### 6.4 Summary

A new compact microwave plasma radical source has been developed and outlined. The source is novel in that up to 500 W of microwave power can be delivered to the compact discharge zone and can be conveniently brought close to the processing substrate. Plasma production is also possible over a wide pressure range. Measured plasma parameters include electron densities in excess of  $10^{11} \text{ cm}^{-3}$  and low plasma potential ( $< 10 \text{ V}$ ). By emission spectroscopy, atomic oxygen radicals were found to be the main excited species. Titration using  $NO_2$  gas was employed to correlate the oxygen atom density with the plasma operating conditions. At 300 W and a  $O_2$  partial pressure of 16.6 Pa, oxygen atom densities in excess of  $1.9 \times 10^{15} \text{ cm}^{-3}$  have been measured. Dissociation rates of  $O_2$  are approximately 20 %. At higher pressures, oxygen atom density of up to  $6.5 \times 10^{15} \text{ cm}^{-3}$  have been recorded. Chamber wall materials were seen to determine the oxygen atom density at a high pressure. Using a Teflon liner at high pressures provides a 30 % increase in oxygen atom density compared to stainless steel. The application of this compact microwave plasma radical

source, as a remote high density source of active plasma species, is providing us with the control necessary to understand complex plasma-material interaction processes, and will lead to further development of plasma processing techniques of advanced materials.

## References

- [1] J. Asmussen, R. Fritz, L. Mahoney, G. Fournier and G. Demaggio: *Rev. Sci. Instrum.* **61** (1989) 282.
- [2] Z. Sitar, M. J. Paisley, D. K. Smith and R. F. Davis: *Rev. Sci. Instrum.* **61** (1990) 2407.
- [3] P. O'Keeffe, S. Komuro, S. Den, T. Morikawa and Y. Aoyagi: *Jpn. J. Appl. Phys.* **30** (1991) 3164.
- [4] P. O'Keeffe, C. O'Morain, S. Den, Y. Hayashi, S. Komuro and T. Morikawa: *Rev. Sci. Instrum.* **61** (1989) 282.
- [5] A. Takamori, S. Sugata, K. Asakawa, E. Miyauchi and H. Hashimoto: *Jpn. J. Appl. Phys.* **26** (1987) L142.
- [6] K. Takahashi, M. Hori, M. Inayoshi and T. Goto: *Jpn. J. Appl. Phys.* **35** (1996) L635.
- [7] K. Morikawa, Y. Enomoto, S. Kubo and T. Murakami: *Jpn. J. Appl. Phys.* **27** (1988) 3635.
- [8] M. Ikeda, M. Hori, T. Goto, M. Inayoshi, K. Yamada, M. Hiramatsu and M. Nawata: *Jpn. J. Appl. Phys.* **34** (1995) 2484.
- [9] M. Ikeda, E. Mizuno, M. Hori, T. Goto, M. Inayoshi, K. Yamada, M. Hiramatsu and M. Nawata: *Jpn. J. Appl. Phys.* **35** (1996) 4826.
- [10] V. M. Donnelly, D. L. Flamm, W. C. Dautremont-Smith and D. J. Werder: *J. Appl. Phys.* **55** (1984) 242.
- [11] P. O'Keeffe, S. Komuro, S. Den, T. Morikawa and Y. Aoyagi: *Jpn. J. Appl. Phys.* **30** (1991) L834.
- [12] Z. Yu, G. Collins, S. Hattori, D. Sugimoto and M. Saita: *Appl. Phys. Lett.* **59** (1991) 1194.
- [13] T. Fuyuki, S. Muanaka and H. Matsunami: private communication.
- [14] J. Battey and E. Tierney: *J. Appl. Phys.* **60** (1990) 1336.
- [15] A. Donnelly, M. P. Hughes, J. Geddes and H. B. Gilbody: *Meas. Sci. Technol.* **3** (1992) 528.
- [16] L. S. Yu-Jahnes, W. T. Brogan, A. C. Anderson and M. J. Cima: *Rev. Sci. Instrum.* **63** (1992) 4149.
- [17] R. E. Walkup, K. L. Saenger, and G. S. Selwyn: *J. Chem. Phys.* **84** (1986) 2668.
- [18] G. Hancock and M. J. Toogood: *Appl. Phys. Lett.* **60** (1992) 35.
- [19] S. Kimura, E. Murakami, K. Miyake, T. Warabisaka, H. Sunami and T. Tokunuma: *J. Electrochem. Soc.* **132** (1985) 1460.
- [20] T. T. Chau and K. C. Kao: *J. Vac. Sci. Technol. B* **14** (1996) 527.
- [21] Y. Hatanaka and S. Wickramnayaka: *J. Jpn. Soc. Appl. Phys.* **35** (1992) 894.
- [22] A. Brockhaus, Y. Yuan, St. Behle and J. Engemann: *J. Vac. Sci. Technol. A*, **14** (1996) 1882.

## Chapter 7. Conclusions

### 7.1 Overall Summary

This thesis describes the development and characterization of ECR plasma sources designed specifically for semiconductor processing, in particular etching. The first large-area ECR source, the 300D-ECR, developed in this study was simple and compact in design. Extensive characterization using Langmuir probe diagnostics, and emission spectroscopy was employed to assess performance. IRLAS measurements that reveal the kinetics associated with different source gases and source design was used for the first time in evaluating a ULSI production tool. Based on the experience gained from the above experimental investigations an advanced ECR plasma source, the RSA ECR was designed and commissioned for 12-inch wafer processing. Initial characterization using IRLAS and actinometric techniques of the kinetics of the plasma species present in fluorocarbon etching gases was carried out. Furthermore, for the first time, the carbon density was measured using hollow cathode absorption spectroscopy and correlation with actual etching result is leading to clearer identification as to the etch mechanism. Finally, a remote compact plasma source was developed and characterized. Titration techniques were used to estimate the density of radical species. It is envisaged that application of remote plasma sources may provide more control over etching and deposition process in the future. A summary of each chapter is outlined below.

In chapter 1, some of the features of low pressure high density plasma sources are reviewed. Problems that needed to be overcome in the development of high density large-area ECR plasma sources for etching applications are identified and the objectives and composition of this thesis are outlined.

In chapter 2, an ECR plasma source (300D-ECR) of 20 cm in diameter was described. The magnetic field was generated by permanent magnets and whistler mode launching of the microwaves was applied to produce a high density plasma. Typical characteristics include a plasma density of  $4.3 \times 10^{11} \text{ cm}^{-3}$ , maximum ion current density of

approximately  $11.5 \text{ mA/cm}^2$  with a non-uniformity of ion current density of  $\pm 3.5\%$  over 20 cm and  $\pm 1.8\%$  over 16 cm. The electron temperature is around 3 eV, and the plasma potential is around 17 V with the uniformity within  $\pm 1\%$  over 20 cm diameter. No impurities generated from the chamber wall material were detected and no damage was observed after the continuous operation for 100 hr with a microwave power of 600 W.

In chapter 3, in order to monitor the performance of the developed permanent magnet ECR source the changes in the densities of fluorocarbon radicals and F atoms in etching plasma employing  $\text{CF}_4$  and  $\text{C}_4\text{F}_8$  gases using IRLAS and actinometric techniques were investigated. Results from the 300D-ECR and a conventional electromagnet (C-ECR) ECR plasma were compared and the dissociation kinetics associated with  $\text{CF}_4$  and  $\text{C}_4\text{F}_8$  gases were revealed. In  $\text{CF}_4$  ECR plasma the CF and  $\text{CF}_2$  radicals were produced by direct electron dissociation of the parent gas for both plasma sources. In the case of  $\text{C}_4\text{F}_8$  plasma, CF radicals were found to be generated from electron dissociation of  $\text{CF}_2$  radicals in the developed 300D-ECR plasma source.

The decay time of radical densities in the afterglow of  $\text{C}_4\text{F}_8$  ECR plasma showed single exponential decays for both the 300D-ECR and C-ECR plasma sources. Decay times for the 300D-ECR source were 0.05 and 0.5s for the CF and  $\text{CF}_2$  radicals, respectively. Decay times for the C-ECR source were faster at 0.03 and 0.17s for the CF and  $\text{CF}_2$  radicals, respectively. A qualitative explanation of the differences between these sources was given in terms of particle confinement and diffusion which produce high-density plasma with relatively low electron temperatures in the developed permanent magnet ECR plasma source. The high selectivity at high etch rates which can be realized in the 300D-ECR plasma source over a dynamic power range was also discussed.

In chapter 4, an advanced large-diameter high-density permanent magnet ECR plasma source (RSA) was described. A plasma density in excess of  $1.0 \times 10^{11} \text{ cm}^{-3}$  was achieved by employing a strip-bar antenna. A density uniformity within  $\pm 3.8\%$  over a 30 cm

diameter was achieved. Typical plasma parameters were an electron density of  $1.4 \times 10^{11} \text{ cm}^{-3}$ , an electron temperature of 3 eV and space potential with respect to the chamber wall of less than 20 V.

The changes in the densities of fluorocarbon radicals and fluorine atoms in the RSA ECR etching plasma source employing  $\text{C}_4\text{F}_8$  gas with  $\text{CH}_4$  addition are investigated in chapter 5.  $\text{CH}_4$  was chosen because, it is a source of carbon and hydrocarbon radicals similar to those species produced from the photoresist during etching. Using IRLAS, the dominant species in a pure  $\text{C}_4\text{F}_8$  plasma is  $\text{CF}_2$  radicals. The dissociation kinetics of the different fluorocarbon radical species were found to display different dependencies on increasing  $\text{CH}_4$  gas addition. Hollow cathode absorption spectroscopy was used to estimate the carbon atom density, for the first time in an etching plasma. The carbon atom density increases linearly with  $\text{CH}_4$  gas addition between 20 to 80% and the dissociation process is believed to be  $\text{CH}_4$  driven. Actual  $\text{SiO}_2/\text{Si}$  etching revealed that the etch rate of both  $\text{SiO}_2$  and Si decreased with increasing  $\text{CH}_4$ . Moreover, above 60%  $\text{CH}_4$  addition due to zero Si etching the selectivity goes to infinity. It was also shown that the carbon atom to fluorine atom ratio follows a similar trend to that of the selectivity indicating a direct correlation between the carbon atom density and etch selectivity. Therefore, carbon atoms and hydrocarbon radicals produced from the photoresist during etching may play a very important role, because the 99% surface of wafer in DRAM device is covered with photoresist materials.

In chapter 6, a new compact microwave plasma source for the remote plasma injection was outlined. The compact cavity size is approximately 6cm in diameter and can therefore be incorporated into any existing processing system. Similar to both the 300D-ECR and the RSA ECR plasma sources this source also employs permanent magnets. The source is novel in that up to 500 W of microwave power can be delivered to the compact discharge zone and can be conveniently brought close to the processing substrate. Measured plasma parameters include, electron densities in excess of  $10^{11} \text{ cm}^{-3}$  and low plasma potential (< 10 V). Atomic oxygen radicals were found to be the main excited species and titration using

$\text{NO}_2$  gas was employed to correlate the oxygen atom density with the plasma operating conditions. At 300 W and a  $\text{O}_2$  partial pressure of 16.6 Pa oxygen atom densities in excess of  $1.9 \times 10^{15} \text{ cm}^{-3}$  have been measured. Dissociation rates of  $\text{O}_2$  are approximately 20 % . At higher pressures oxygen atom density of up to  $6.5 \times 10^{15} \text{ cm}^{-3}$  have been recorded. Chamber wall materials were seen to determine the oxygen atom density at high pressure. Using a Teflon liner at high pressures provides a 30 % increase in oxygen atom density compared to stainless steel. Future applications include, substrate surface cleaning with hydrogen plasma, as a source of hydrogen and methane in diamond CVD and as a source of oxygen in resist ashing and thin film deposition.

## 7.2 Future Prospects

It was mentioned in chapter one that in evaluating ECR plasma sources a very important factor is how well the ion energy distribution function (IEDF) can be controlled. It was also mentioned that although the precise mechanisms responsible for etching are still not clarified it is clear that ions play an important role. It also has been shown that charge build-up effects on patterned wafers, due to accelerated ions, can be remedied if control of the plasma potential is achieved.[1] It is therefore important to measure the IEDF and also find a means to control it. In the thesis effects of the IEDF in etching are not considered.

We are presently looking at two methods to control the ion energy distribution function (IEDF). The first method is controlling the magnetic field in the downstream region. To demonstrate the control that can be achieved by varying the magnet position, ion energy analysis was carried out using a planar retarding field energy analyzer positioned 50mm downstream of a prototype ECR source.[2] The effect of magnet position on the IEDF can be seen clearly in Fig.7.1, where the IEDF for magnet positions of 0mm, 0.75mm and 3.0mm are plotted. Changing the magnet position by from 0mm to 3mm results in decreasing the average ion energy ( $E_{av}$ ) from 16 eV to 8 eV. Such results are consistent with Langmuir probe diagnostics where a decrease in plasma potential was recorded with increasing the magnet position. An interesting point to note is that for certain magnet



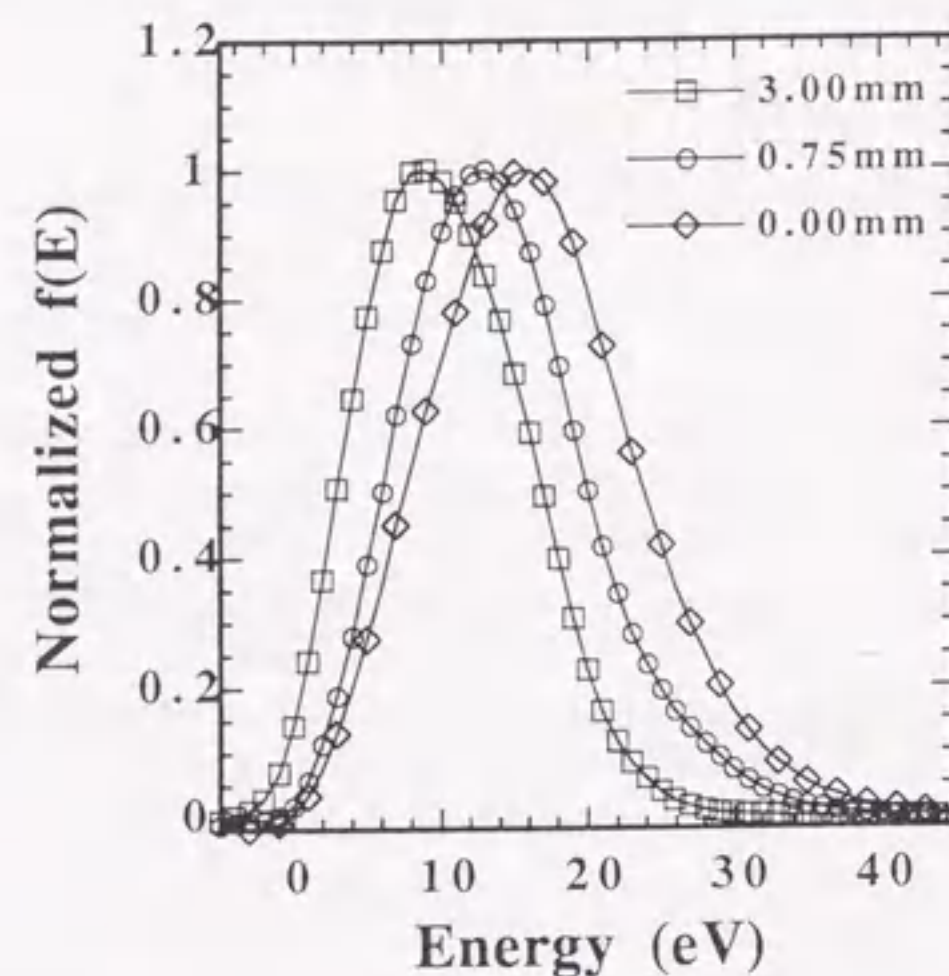


Fig. 7.1 Ion energy distribution functions of nitrogen plasma vs. magnet position. Input microwave power, 100 W; discharge pressure, 0.078 Pa.

configurations it is possible to control the ion energy while at the same time maintaining a high plasma density. The plasma density is dependent not only the downstream magnetic field but also conditions within the discharge zone in particular at the point of microwave absorption. The ion energy downstream is explained in terms of charged particle diffusion (ambipolar diffusion) in the downstream region only. Moving the magnet position from 0mm to 3mm increases the downstream magnetic field which increases the effective confinement of charged particles. This increase in confinement was correlated with an decrease in the downstream space potential gradient measured by Langmuir probe diagnostics. Therefore, the decrease in energy of ions extracted by ambipolar diffusion is caused by the decrease in downstream space potential gradient. Similar results have been obtained in large area ECR systems employing downstream sub coils to control the magnetic field.[3,4] The second method is using electrostatic grids. Control of the IEDF can be easily achieved by application of an electrostatic grid. Insulating the source from the chamber and fitting it with an electrostatic grid allows control of the ion energy as shown in Fig. 7.2. These are preliminary results taken from a compact ECR source and applying such techniques to the RSA ECR source will require further development. This thesis has been mainly concerned with the development of a production worthy plasma etch system for next-generation device processing. In terms of characterization, the main emphasis has been placed on, quantifying the basic plasma characteristics, quantifying the densities of radical species and studying the effect of such characteristics on the etch process. Future IEDF characterization combined with today's knowledge of the etch process is necessary if feature sizes of  $0.1\mu\text{m}$  are to be realized.

It was seen in chapter 5 that the carbon atom density was qualified and in very good correlation with actual etch selectivity results. This suggests that carbon may be the main precursor involved in achieving high selectivity. Despite the fact that very good selectivity was achieved, the etch rate was low. In the future, the aim will be to have high selectivity but with an etch rate of  $1\mu\text{m}/\text{min}$ . Moreover, in order to avoid carbon or carbon products other than those produced in the gas phase a simple Si mask was used. No resist material

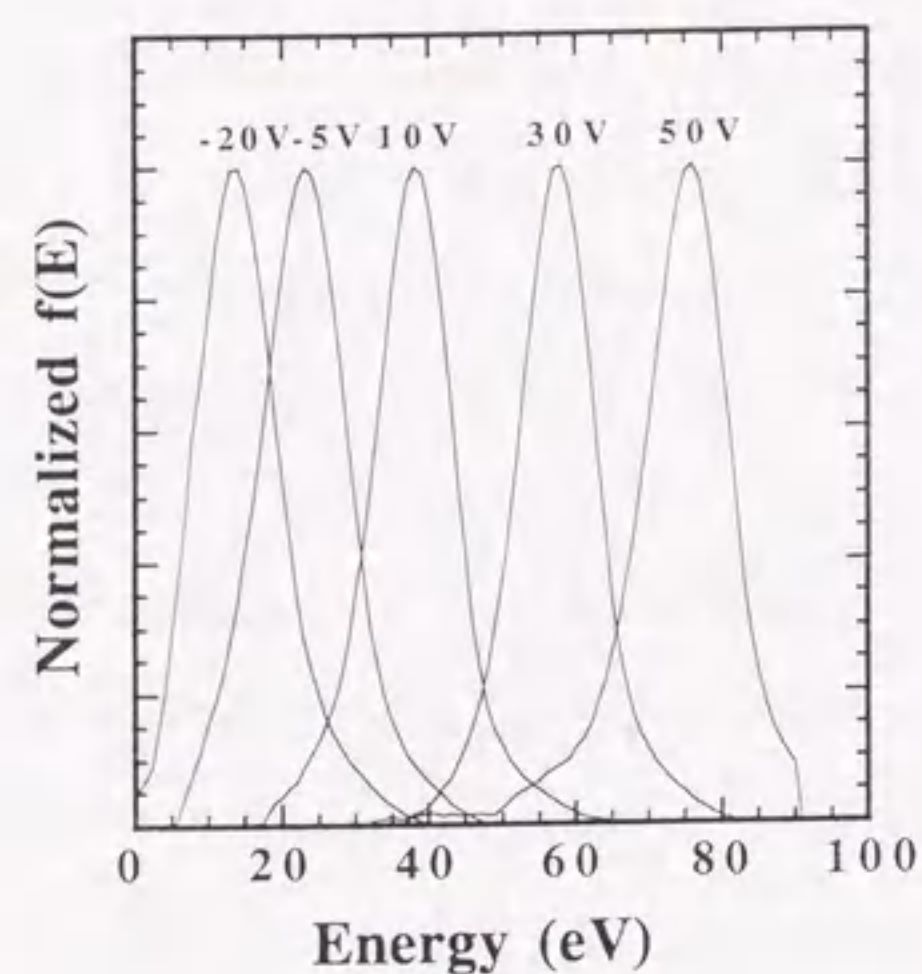


Fig. 7.2 Control of the ion energy distribution function using a biased electrostatic grid.

was present during the etching process. The etch experiments were not carried out on actual line and space resist patterned wafers. It is of course imperative that good etch characteristics are reproduced uniformly across the wafer in real etch applications. The last point that needs to be addressed with regard to etching is that of damage to both the bulk and surface. Both electrical and microscopic techniques are available for such characterization. Acceptance in the field of ULSI processing will require that such effects are quantified.

A compact microwave plasma source as a remote high density source of active plasma species that could lead to the further development of plasma processing techniques of advanced materials was described. The developed source has a high radical density that allows a specific radical to be selectively injected (RIT, radical injection technique) into a processing plasma. This technique will allow clearer identification of the role specific species play in the process of interest. Hence, further plasma characterization of process gases combined with actual application to different processes will be needed to evaluate this particular source and the technique of RIT.

Finally, every effort has been done but further effort must be continued to meet the requirements in development not only of superior plasma source but also process system for next-generation device production. The one who succeeds in perfectly controlling the plasma process will play a leading role in next-generation device industry. As rapid technology development and its quick delivery are required, scientific evaluation and development of equipment for future device fabrication are essential. The author must touch upon the cost because of his standpoint as one of members in equipment maker. If the scientific evaluation and development technology in each plasma process such as that in this work are established, overall cost reduction of process system can be achieved by drastically downsizing of the system, improving system reliability and simplifying operation and maintenance procedure not only in semiconductor device process but also in display panel or film fabrication process in which larger and larger substrate will be used. The author would like to make further effort in order to realize highly advanced plasma source and process system employing this technology with reasonable price. At the same time, he would like to ask industries to actively adopt these plasma sources and systems employing this technology.

## References

- [1] N. Fujiwara, T. Maruyama, M. Yoneda, K. Tsukamoto and T. Banjo, *Jpn J Appl. Phys.*, 33 (1994) 2164.
- [2] P. O'Keeffe, C. O'Morain, S. Den, Y. Hayashi, S. Komuro, and T. Morikawa, *Rev. Sci. Instrum.*, 66 (1995) 5252.
- [3] M. Matsuoka and K. Ono, *J. Vac. Sci. Technol. A*6 (1988) 25.
- [4] W. M. Holber and J. Forster, *J. Vac. Sci. Technol. A*, 8 (1990) 3720.

## Acknowledgments

I first and foremost express my sincere thanks to my research advisor, Pr. Toshio Goto, Department of Quantum Engineering, Nagoya University, for his advice, supervision and encouragement throughout the entire course of this research. I also sincerely thank my vice-advisor, Pr. Takashi Mizutani, for his valuable suggestion and comments to preparing this thesis, and to my vice-advisor, Associate Pr. Masaru Hori, Department of Quantum Engineering, Nagoya University, for his continuous encouragement, advice, supervision and discussion through this work. At the same time, I am greatly indebted to Professors in Department of Quantum Engineering, Nagoya University, for their creating the problem-free atmosphere of research.

I thank deeply to Pr. Akihiro Kono, Center for Cooperative Research in Advanced Science & Technology, Nagoya University, for his advice and encouragement, Associate Pr. Masakazu Mori, Associate Pr. Hideo Takeuchi, Assistant Pr. Masafumi Ito and Research Associate Norihiko Nishizawa, Department of Quantum Engineering, Nagoya University, and Dr. M. Meyyappan (NASA, USA) for their valuable discussions and advice.

I must thank to Dr. Yuichi Sakamoto (vice-president of NETEC, Ltd.) for his valuable advice, suggestion and cooperation, Mr. Sigekazu Tada (NETEC) and several other NETEC members for their cooperation.

I would like to thank to Dr. Kunimasa Takahashi (Matsushita Electric Industrial Co., Ltd.), Dr. Koji Maruyama (Tokyo Electron Ltd.) and Dr. Masanobu Ikeda, for their good advice, Mr. Yasuo Yamamoto, Mr. Muneto Inayoshi, Mr. Ryoichi Nozawa, Mr. Koji Miyata, Mr. Tatsusi Kuno and several other students in Pr. Goto's Lab. for their discussions and assistance.

I must of course thank to our president Dr. Norikimi Irie, managing director Mr. Yuzo Hayasi (Irie Koken Co., Ltd.), for providing me with this opportunity and encouraging me on time to time. At the same time, I owe a great deal to Mr. Chuji Yosida (president of Vacuum Device Co., Ltd. (VD)), Mr. Hiroaki Isozaki (VD), Mr. Toshiro Katagiri (president of Katagiri Engineering Co., Ltd) and Mr. Yoshinobu Hanasaka (president of Hanasaka Seisakusho), for their tight cooperation.

I thank to Mr. Hideo Soma, Mr. Yoshimasa Sato, Mr. Shinji Nonogaki, Mr. Harunobu Muto, Mr. Hironori Saito, Mr. Koji Yamakawa, Mss. Xue-Ying Jia and Mrs. Taeko Senzaki in R&D Lab. of Irie Koken for their continuous assistance. Looking back over the past nine years, there has been one person in particular to whom I am deeply indebted, Dr. Patrick J. O'Keeffe, with whom I have shared both troubles and joys.

Since twenty years ago at the start of my research and development work, there have been countless people who have contributed to and helped me along the way. Although small repayment, I would like to thank sincerely to Pr. Goro Ohira, Pr. Osamu Izumi and Pr. Shuji Hanada in Tohoku University, Pr. Akihiko Nagata (Akita University), Pr. Susumu Namba (Nagasaki Industrial University), Pr. Takuo Sugano (Toyo University and Nano-electronics, RIKEN), Dr. Yoshinobu Aoyagi (RIKEN), Associate Pr. Shuji Komuro (Toyo University) and Dr. Taiji Hoshiya (Japan Atomic Energy Research Institute).

Finally, I would like to express my thanks to my late parents, my wife Sachiko and my three children, Nariaki, Hideaki and Misa, for their encouragement.

### List of papers

#### 1. Original Papers

Title	Journal	Authors
1. Large-area Electron Cyclotron Resonance Plasma Source with Permanent Magnets	Jpn. J. Appl. Phys. vol.32, No.11A, pp. L1635-L1637, November (1993)	N.Shida, T.Inoue, T.Kokai, Y.Sakamoto, W.Miyazawa, <u>S.Den</u> and Y.Hayashi
2. A Large-area ECR Processing Plasma	Plasma Sources Sci. Technol. vol. 5, pp. 265-267, January (1996)	W.Miyazawa, S.Tada, K.Ito, <u>S.Den</u> , Y.Hayashi, Y.Okamoto and Y.Sakamoto
3. Diagnostics of Fluorocarbon Radicals in a Large-Area Permanent Magnet Electron Cyclotron Resonance Etching Plasma	Jpn.J.Appl.Phys. Vol.35, No.12B, pp.6528-6533 December (1996)	S.Den, T.Kuno, M.Ito, M.Hori, T.Goto, Y.Hayashi and Y.Sakamoto
4. Development and Characterization of a New Compact Microwave Radical Beam Source	Jpn.J.Appl.Phys. Vol.36, No.7B, pp.4588-4592 July (1997)	S.Den, P.O'Keeffe, Y.Hayashi, M.Ito, M.Hori and T.Goto
5. Influence on Selective SiO <sub>2</sub> /Si Etching of Carbon Atoms Produced by CH <sub>4</sub> Addition to a C <sub>4</sub> F <sub>8</sub> Permanent Magnet Electron Cyclotron Resonance Etching Plasma	J. Vac.Sic.Technol.A Vol.15, No.6, pp.2880-2884, November/December (1997)	S.Den, T.Kuno, M.Ito, M.Hori, T.Goto, P.O'Keeffe, Y.Hayashi and Y.Sakamoto

## 2. International Conference

Title	Conference	Authors
1. Measurement of Radical Densities Associated with C <sub>4</sub> F <sub>8</sub> Plasma from a Large Area ECR Plasma Source	48th Annual Gaseous Electronics Conference October 9-13,1995 Berkeley,CA	S.Den, T.Kuno K.Takahashi, M.Ito M.Hori, Y.Hayashi Y.Sakamoto and T.Goto
2. Diagnostics of Fluorocarbon Radicals in a Compact Permanent Magnet ECR Etching Plasma	MicroProcess'96 The 9th International MicroProcess Conference, July 8-11,1996 Kitakyushu International Conference Center, Kitakyushu	S.Den, T.Kuno, M.Ito M.Hori, T.Goto Y.Hayashi and Y.Sakamoto
3. Diagnostics of a Newly Developed 300mm Homogeneous Permanent Magnet ECR Plasma	43rd National Symposium October 14-18,1996 Pennsylvania Convention Center, Philadelphia, Pennsylvania	S.Den, T.Kuno, M.Hori M.Ito, T.Goto and Y.Sakamoto
4. Development and Characterization of a Microwave Radical Beam Source	3rd International Conference on Reactive Plasmas and 14th Symposium on Plasma Processing, January 21-24, 1997, Nara-ken New Public Hall Nara, Nara	S.Den, P.O'Keeffe Y.Hayashi, M.Ito M.Hori and T.Goto

## Other Related Publications:

P. O'Keeffe, S. Komuro, S. Den, T. Morikawa and Y. Aoyagi: Jpn. J. Appl. Phys. **30** (1991) 3164.

*"Development and Applications of a Compact Electron Cyclotron Resonance Source"*

C. O'Morain, P. O'Keeffe, S. Den and Y. Hayashi: Meas. Sci. Technol. **4** (1993) 1484.

*"Large-diameter plasma profile monitoring system using Faraday cup and Langmuir probe arrays"*

P. O'Keeffe, C. O'Morain, S. Den, Y. Hayashi, S. Komuro and T. Morikawa: Rev. Sci. Instrum. **66** (1995) 5252.

*"Characterization and in-situ monitoring of a novel compact ECR plasma source"*

P. O'Keeffe, H. Mutoh, S. Den, Y. Hayashi, S. Komuro and T. Morikawa: Thin Solid Films 281-282 (1996) 102-104

*"Energy selective ECR plasma for controlled surface reaction processes"*

